

**ATTACHMENT 3**

**Westinghouse Electric Company LLC LTR-SGMP-09-108 NP-Attachment, "Response to  
NRC Request for Additional Information on H\*;  
Model 44F and Model 51F Steam Generators" (Non-Proprietary)**

**VIRGINIA ELECTRIC AND POWER COMPANY  
(DOMINION)  
SURRY POWER STATION UNITS 1 AND 2**

Westinghouse Electric Company

**Response to  
NRC Request for Additional Information on H\*;  
Model 44F and Model 51F Steam Generators**

August 27, 2009

---

Westinghouse Electric Company LLC  
P.O. Box 158  
Madison, PA 15663

© 2009 Westinghouse Electric Company LLC  
All Rights Reserved

**Response to  
NRC Request for Additional Information on H\*;  
Model 44F and Model 51F Steam Generators**

**References:**

1. L-2009-151, "Turkey Point Units 3 and 4, Docket Nos. 50-250 and 50-251, License Amendment Request No. 197 for H\*: Alternate Repair Criteria for Steam Generator Tubesheet Expansion Region," FPL, July 23, 2009.
2. 09-455, "Virginia Electric and Power Company (Dominion), Surry Power Station Units 1 and 2, Proposed License Amendment Request, Permanent Alternate Repair Criteria for Steam Generator Tube Repair for Units 1 and 2," Virginia Electric and Power Company, July 28, 2009.
3. E-mail from Jason Paige (NRC) to Bob Tomonto (FPL), "RAI Questions RE Turkey Point's H\* LAR," August 17, 2009.
4. E-mail from Karen Cotton (NRC) to Gary D. Miller (Generation -6), "Surry Clarifications Regarding H\* PARC," August 14, 2009.
5. WCAP-17091-P, "H\*: Alternate Repair Criteria for the Tubesheet Expansion Region in Steam Generators with Hydraulically Expanded Tubes (Model 44F)," Westinghouse Electric Company LLC, June 2009.
6. WCAP-17092-P, "H\*: Alternate Repair Criteria for the Tubesheet Expansion Region in Steam Generators with Hydraulically Expanded Tubes (Model 51F)," Westinghouse Electric Company LLC, June 2009.
7. LTR-SGMP-09-100, "Responses to NRC Request for Additional Information on H\*; Model F and Model D5 Steam Generators," Westinghouse Electric Company LLC, July 29, 2009.
8. LTR-SGMP-09-109, "Response to NRC Request for Additional Information on H\*; RAI#4; Model F and Model D5 Steam Generators," Westinghouse Electric Company LLC, August 25, 2009.

**Introduction**

In response to formal requests for technical specification amendments, References 1, and 2 the USNRC requested additional information via e-mail in References 3 and 4. This document provides responses to NRC RAI on the Turkey Point and Surry requests for a permanent license amendment to implement H\*. These plants represent the Model 44F and Model 51F steam generators for which the H\* technical justification is provided in Reference 5 and 6. The RAIs included in References 3 and 4 duplicate most of the prior RAIs received by Model F and Model D5 plants (Reference 7). The single new question is RAI 16 received only by Turkey Point (Reference 3). Several other RAIs to which responses were provided in Reference 7 were omitted from References 3 and 4. The responses to the current RAIs are the same as the responses provided in LTR-SGMP-09-100 (Reference 3), except that model-specific values have been changed where necessary to reflect the proper values for the Model 44F and Model 51F SGs. The NRC questions are repeated verbatim for each of the plants that received formal or draft RAI in the tables preceding the response to each question. The current NRC RAIs are specific to WCAP-17091-P (Model 44F H\*) and WCAP-17092-P (Model 51F H\*); however, generic responses may include information as well for the Model F and Model D5 SGs.

<b>RAI</b>	<i>Turkey Point</i>	<i>1. Reference 1, Page 6-21, Table 6-6. This table contains a number of undefined parameters and some apparent inconsistencies with Table 5-2 on page 5-6. Please define the input parameters in Table 6-6.</i>
	<i>Surry</i>	<i>1. Reference 1, Page 6-21, Table 6-6. This table contains a number of undefined parameters and some apparent inconsistencies with Table 5-2 on page 5-6. Please define the input parameters in Table 6-6.</i>

## Response:

Table 6-6 in WCAP-17091-P and WCAP-17092-P is provided principally as a reference to provide a bridge to the source of basic design data maintained by Westinghouse and as a historical reference from prior H\* reports. Although many of the entries in Table 6-6 are not used in the H\* analysis, the table was provided to show traceability to the principal sources of the design data, the Westinghouse Power Capability Working Group (PCWG) sheets and the Systems Standards 1.3F and 1.3, which provide transient response data for component design. The references to Point Beach Unit 1 in WCAP-17091-P and to Surry in WCAP-17092-P reflect that these plants are the limiting plants for the Model 44F and Model 51F SGs that are candidates for application of H\*.

Updated Tables 6-6 for the Model 44F and Model 51F are provided as Tables RAI1-2 and RAI1-3. The references in the tables have been updated from those contained in Revision 0 of WCAP-17091-P and WCAP-17092-P.

**Table RAI1-1**  
**Updated Table 6-6 of WCAP-17071-P: Summary of H\* Millstone Unit 3 Analysis**  
**Mean Input Properties**

Plant Name	Pont Beach 1		
Plant Alpha	WEP		
Plant Analysis Type	Hot Leg		
SG Type	44F		

Input	Value	Unit	Reference
<b>Accident and Normal Temperature Inputs</b>			
a,c,e			
NOP T <sub>hot</sub>		°F	PCWG-06-9
NOP T <sub>low</sub>		°F	PCWG-06-9
SLB TS ΔT		°F	1.3F
SLB CH ΔT		°F	1.3F
Shell ΔT		°F	1.3F
SLB Primary ΔT		°F	1.3F
SLB Secondary ΔT		°F	1.3F
Secondary Shell ΔT Hi		°F	PCWG-06-9
Secondary Shell ΔT Low		°F	PCWG-06-9
Cold Leg ΔT		°F	PCWG-06-9
Hot Standby Temperature		°F	PCWG-06-9
<b>Operating Pressure Input</b>			
Faulted SLB Primary Pressure	2560.0	psig	1.3F, Rev. 0
Normal Primary Pressure	2235.0	psig	PCWG-07-49
Cold Leg ΔP		psig	PCWG-07-49
NOP Secondary Pressure – Low		psig	PCWG-07-49
NOP Secondary Pressure – Hi		psig	PCWG-07-49
Faulted SLB Secondary Pressure	0.0	psig	1.3F, Rev. 0

Notes. 1. The value for Faulted SLB Primary Pressure used in the H\* analysis is 2235 psi. The value of 2235 psig for peak primary-secondary pressure differential differs from the value provided in Table 5-3 (2240 psia) reported in WCAP-17091-P. The value reported in Table 5-3 should be 2235 psig.

**Table RAI1-2**  
**Updated Table 6-6 of WCAP-17072-P: Summary of H\* Byron Unit 2 Analysis**  
**Mean Input Properties**

<b>Plant Name</b>	Surry 1 and 2		
<b>Plant Alpha</b>	VPA		
<b>Plant Analysis Type</b>	Hot Leg		
<b>SG Type</b>	51F		
<b>Input</b>	<b>Value</b>	<b>Unit</b>	<b>Reference</b>
<b>Accident and Normal Temperature Inputs</b>			
		a,c,e	
NOP T <sub>hot</sub>		°F	PCWG-07-49
NOP T <sub>low</sub>		°F	PCWG-07-49
SLB TS ΔT		°F	1.3F, Rev. 0
SLB CH ΔT		°F	1.3F, Rev. 0
Shell ΔT		°F	1.3F, Rev. 0
SLB Primary ΔT		°F	1.3F, Rev. 0
SLB Secondary ΔT		°F	1.3F, Rev. 0
Secondary Shell ΔT Hi		°F	PCWG-07-49
Secondary Shell ΔT Low		°F	PCWG-07-49
Cold Leg ΔT		°F	PCWG-07-49
Hot Standby Temperature*		°F	PCWG-07-49
<b>Operating Pressure Input</b>			
		a,c,e	
Faulted SLB Primary Pressure	[ ]	psig	1.3F, Rev. 0
Normal Primary Pressure	2235	psig	PCWG-07-49
Cold Leg ΔP		psig	PCWG-07-49
NOP Secondary Pressure – Low		psig	PCWG-07-49
NOP Secondary Pressure – Hi		psig	PCWG-07-49
Faulted SLB Secondary Pressure	0.0	psig	1.3F, Rev. 0

Much of the data provided in Table 6-6 is not utilized in the final H\* analysis. Table RAI1-3 provides a summary of whether the data is utilized in the reference analysis of H\* and in which analysis model it is used (See Figure 1-1 in the respective reports). It is emphasized that changes made in Tables RAI1-1 and RAI1-2 do not affect the H\* results provided in References 5 and 6 of this document.

Table RAI1-3

## Utilization of Data from Table 6-6

Input	Where Used
<b>Accident and Normal Temperature Inputs</b>	
NOP T <sub>hot</sub>	H* Integrator Spreadsheet
NOP T <sub>low</sub>	H* Integrator Spreadsheet
SLB TS $\Delta T$	Not Used
SLB CH $\Delta T$	Not Used
Shell $\Delta T$	Not Used
SLB Primary $\Delta T$	Not Used
SLB Secondary $\Delta T$	Not Used
Secondary Shell $\Delta T$ Hi	H* Integrator Spreadsheet; same as Secondary Fluid Temperature at NOP High T <sub>avg</sub> Conditions
Secondary Shell $\Delta T$ Low	H* Integrator Spreadsheet; same as Secondary Fluid Temperature at NOP Low T <sub>avg</sub> Conditions
Cold Leg $\Delta T$	Not Used
Hot Standby Temperature	H* Integrator Spreadsheet
<b>Operating Pressure Input</b>	
Faulted SLB Primary Pressure	H* Integrator Spreadsheet
Normal Primary Pressure	H* Integrator Spreadsheet
Cold Leg $\Delta P$	Not Used
NOP Secondary Pressure – Low	H* Integrator Spreadsheet
NOP Secondary Pressure – Hi	H* Integrator Spreadsheet

The definitions of the entries in the Table 6-6 of WCAP-17091-P and WCAP17092-P are presented below. Also, discussion is provided regarding the consistency of the values in Table 6-6 of the respective reports with Tables 5-1 through 5-6 of the reports.

### **NOP $T_{hot}$**

The steam generator hot leg temperature at high  $T_{avg}$  normal operating conditions at 100% power (considered to be the same as the reactor vessel outlet temperature).

Model 44F: [ ]<sup>a,c,e</sup> °F at the inlet of the tubes at high  $T_{avg}$  normal operating conditions at 100% power for Point Beach Unit 1 is consistent with the value provided in Table 5-1 (WCAP-17091-P).

Model 51F: [ ]<sup>a,c,e</sup> °F at the inlet of the tubes at high  $T_{avg}$  normal operating conditions at 100% power Surry Units 1 and 2 is consistent with the value provided in Table 5-1 (WCAP-17092-P).

### **NOP $T_{low}$**

The steam generator hot leg temperature at the inlet of the tubes at low  $T_{avg}$  normal operating conditions at 100% power (considered to be the same as the reactor vessel outlet temperature).

Model 44F: [ ]<sup>a,c,e</sup> °F is consistent with the value provided in Table 5-1.

Model 51F: [ ]<sup>a,c,e</sup> °F is consistent with the value provided in Table 5-1.

### **SLB TS $\Delta T$**

Model 44F: [ ]<sup>a,c,e</sup> °F, ([ ]<sup>a,c,e</sup> °F - 70°F) = [ ]<sup>a,c,e</sup> °F: The steam generator hot and cold leg temperature difference that occurs during a postulated steam line break event during the maximum pressure difference across the tubesheet of 2235 psi between the steady-state tubesheet metal temperature and the ambient temperature surrounding the steam generator (assumed to be 70°F). The value of [ ]<sup>a,c,e</sup> °F is not used in the analysis.

Model 51F: [ ]<sup>a,c,e</sup> °F, ([ ]<sup>a,c,e</sup> °F - 70°F) = [ ]<sup>a,c,e</sup> °F: The steam generator hot and cold leg temperature difference that occurs during a postulated steam line break event during the maximum pressure difference across the tubesheet of [ ]<sup>a,c,e</sup> psi between the steady-state tubesheet metal temperature and the ambient temperature surrounding the steam generator (assumed to be 70°F). The value of [ ]<sup>a,c,e</sup> °F is not used in the H\* analysis.

### **SLB CH $\Delta T$**

Model 44F: [ ]<sup>a,c,e</sup> °F, [ ]<sup>a,c,e</sup> °F: The steam generator hot and cold leg temperature difference that occurs during a postulated steam line break event during the maximum pressure difference across the tubesheet of 2235 psi between the steady-state

channelhead metal temperature and the ambient temperature surrounding the steam generator (assumed to be 70°F). The value of [ ]<sup>a,c,e</sup> °F is not used in the H\* analysis.

Model 51F: [ ]<sup>a,c,e</sup> °F, ([ ]<sup>a,c,e</sup> °F): The steam generator hot and cold leg temperature difference that occurs during a postulated steam line break event during the maximum pressure difference across the tubesheet of 2560 psi between the steady-state channelhead metal temperature and the ambient temperature surrounding the steam generator (assumed to be 70°F). The value of [ ]<sup>a,c,e</sup> °F is not used in the H\* analysis.

### Shell ΔT

Model 44F: ([ ]<sup>a,c,e</sup> °F - 70°F) = [ ]<sup>a,c,e</sup> °F: The steam generator secondary side temperature difference that occurs during a postulated steam line break event during the maximum pressure difference across the tubesheet of 2235 psi between the steady-state secondary side shell metal temperature and the ambient temperature surrounding the steam generator (assumed to be 70°F). The [ ]<sup>a,c,e</sup> °F value is not used in the H\* analysis.

Model 51F: ([ ]<sup>a,c,e</sup> °F - 70°F) = [ ]<sup>a,c,e</sup> °F. The steam generator secondary side temperature difference that occurs during a postulated steam line break event during the maximum pressure difference across the tubesheet of 2560 psi between the steady-state secondary side shell metal temperature and the ambient temperature surrounding the steam generator (assumed to be 70°F). The [ ]<sup>a,c,e</sup> °F value is not used in the H\* analysis.

The secondary side temperature during a postulated SLB is used in the H\* analysis for both the Model 44F ([ ]<sup>a,c,e</sup> °F) and Model 51F ([ ]<sup>a,c,e</sup> °F) SGs.

### SLB Primary ΔT

Model 44F: The reduction in no load temperature of [ ]<sup>a,c,e</sup> °F ([ ]<sup>a,c,e</sup> °F) to [ ]<sup>a,c,e</sup> °F that occurs in the reactor coolant system during a postulated SLB during the maximum pressure difference across the tubesheet of 2235 psi. The value in Table 6-6 should be [ ]<sup>a,c,e</sup> °F to be consistent with SSDC 1.3F and Table 5-2. The [ ]<sup>a,c,e</sup> °F value is not used in the H\* analysis.

Model 51F: The reduction in no load temperature of [ ]<sup>a,c,e</sup> °F ([ ]<sup>a,c,e</sup> °F) to [ ]<sup>a,c,e</sup> °F that occurs in the reactor coolant system during a postulated SLB during the maximum pressure difference across the tubesheet of 2560 psi. The value in Table 6-6 is consistent with SSDC 1.3F, Rev 0 and Table 5-2. The [ ]<sup>a,c,e</sup> °F value is not used in the H\* analysis.

The primary side temperature that occurs during a postulated SLB, [ ]<sup>a,c,e</sup> °F, is used in the H\* analysis for the Model 44F. The primary side temperature, [ ]<sup>a,c,e</sup> °F, is used for the Model 51F SGs.

**SLB Secondary  $\Delta T$** 

Model 44F: The reduction in no load temperature of [ ]<sup>a,c,e</sup> °F ([ ]<sup>a,c,e</sup> °F) to [ ]<sup>a,c,e</sup> °F that occurs on the secondary side of the steam generator during a postulated SLB during the maximum pressure difference across the tubesheet of 2235 psi. The value in Table 6-6 should be [ ]<sup>a,c,e</sup> °F to be consistent with Table 5-2.

Model 51F: The reduction in no load temperature of [ ]<sup>a,c,e</sup> °F ([ ]<sup>a,c,e</sup> °F) to [ ]<sup>a,c,e</sup> °F that occurs on the secondary side of the steam generator during a postulated SLB during the maximum pressure difference across the tubesheet of [xxxx]<sup>a,c,e</sup> psi. The value in Table 6-6 should be [ ]<sup>a,c,e</sup> °F to be consistent with SSDC 1.3F, Rev. 0 and Table 5-2.

As noted above, the secondary side temperature during a postulated SLB is used in the H\* analysis for both the Model 44F ([ ]<sup>a,c,e</sup> °F) and Model 51F ([ ]<sup>a,c,e</sup> °F) SGs.

**Secondary Shell  $\Delta T_{Hi}$** 

For the Model 44F SG, [ ]<sup>a,c,e</sup> °F is the average temperature between the secondary side steam temperature and the feedwater temperature during NOP Hi  $T_{avg}$  operation ([ ]<sup>a,c,e</sup> °F + [ ]<sup>a,c,e</sup> °F). This value is the same as the secondary fluid temperature during high  $T_{avg}$  normal operating conditions. The same value calculated for the Model 51F SGs is [ ]<sup>a,c,e</sup> °F.

**Secondary Shell  $\Delta T_{Low}$** 

For the Model 44F SGs, [ ]<sup>a,c,e</sup> °F is the average temperature between the secondary side steam temperature and the feedwater temperature during NOP Low  $T_{avg}$  operation ([ ]<sup>a,c,e</sup> °F + [ ]<sup>a,c,e</sup> °F)/2 = [ ]<sup>a,c,e</sup> °F). This value is the same as the secondary fluid temperature during low  $T_{avg}$  normal operating conditions. The same value calculated for the Model D5 SGs is [ ]<sup>a,c,e</sup> °F.

**Cold Leg  $\Delta T$** 

Model 44F: The temperature difference between the hot and cold leg of the Point Beach Unit 1 SGs during NOP Low  $T_{avg}$  is 70°F. This value is not used in the H\* analysis.

Model 51F: The temperature difference between the hot and cold leg of the Surry Units 1 and 2 SGs during NOP Low  $T_{avg}$  is 67°F. This value is not used in the H\* analysis.

**Hot Standby Temperature**

The zero load temperature, [ ]<sup>a,c,e</sup> °F.

This value is used in the H\* analysis for both the Model 44F and Model 51F SGs.

**Faulted SLB Primary Pressure**

The maximum pressure difference that occurs across the tubesheet during a postulated SLB.

Model 44F: [ ]<sup>a,c,e</sup> psig is consistent with the value reported in Table 5-2.

Model 51F: [ ]<sup>a,c,e</sup> psig is consistent with the value reported in Table 5-2.

**Normal Primary Pressure**

The primary side pressure during normal operation.

Model 44F: 2235 psig is consistent with the absolute primary pressure reported in Table 5-1 of 2250 psia.

Model 51F: 2235 psig is consistent with the absolute primary pressure reported in Table 5-1 of 2250 psia.

**Cold Leg  $\Delta P$** 

The overall pressure drop that occurs in a steam generator tube as fluid flows through the tube from hot leg to cold leg.

Model 44F: [ ]<sup>a,c,e</sup> psig (Point Beach 1). This value is not used in the H\* analysis.

Model 51F: [ ]<sup>a,c,e</sup> psig (Surry 2 and 3). This value is not used in the H\* analysis.

**NOP Secondary Pressure Low**

The steam pressure on the secondary side of the steam generators for NOP Low  $T_{avg}$ .

Model 44F: [ ]<sup>a,c,e</sup> psig is consistent with the value reported in Table 5-1 as [ ]<sup>a,c,e</sup> psia.

Model 51F: [ ]<sup>a,c,e</sup> psig is consistent with the value reported in Table 5-1 as [ ]<sup>a,c,e</sup> psia.

**NOP Secondary Pressure Hi**

The steam pressure on the secondary side of the steam generators for NOP Hi  $T_{avg}$ .

Model 44F: [ ]<sup>a,c,e</sup> psig is consistent with the value reported in Table 5-1 as [ ]<sup>a,c,e</sup> psia.

Model 51F: [ ]<sup>a,c,e</sup> psig is consistent with the value reported in Table 5-1 as [ ]<sup>a,c,e</sup> psia.

Turkey Point	2. Reference 1, Section 6.2.2.2. Why was the FEA analysis not run directly with the modified temperature distribution rather than running with the linear distribution and scaling the results?
Surry	2. Reference 1, Section 6.2.2.2. Why was the FEA analysis not run directly with the modified temperature distribution rather than running with the linear distribution and scaling the results?

Response:

As noted in Section 6.2.2.2 of Reference 5 and 6, the NOP thermal distribution was directly input to the FEA analysis. This differs from the analyses performed for the Model F and Model D5 SGs, which utilized the scaling approach noted in the question. Therefore, the predicted H\* does not include a correction factor resulting from scaling the results based on a linear temperature distribution.

Table RAI2-1 summarized the NOP Thermal Offset Factors for all of the Models of SG that are candidates for application of H\*. No correction is required for the Model 44F and Model 51F SGs.

**Table RAI2-1  
Updated NOP Thermal Offset Factors**

SG Model	Report	Thermal Offset (Scaled Result)
(1)	(2)	(3)
Model F	WCAP 17071-P	[ ] <sup>a,c,e</sup> in.
Model D5	WCAP 17072-P	[ ] <sup>a,c,e</sup> in.
Model 44F	WCAP 17091-P	0.00 in.
Model 51F	WCAP 17092-P	0.00 in.

Turkey Point	3. Reference 1, Section 6.2.3. Why is radial displacement the "figure of merit" for determining the bounding segment? Does circumferential displacement not enter into this? Why is the change in tube hole diameter not the "figure of merit?"
Surry	3. Reference 1, Section 6.2.3. Why is radial displacement the "figure of merit" for determining the bounding segment? Does circumferential displacement not enter into this? Why is the change in tube hole diameter not the "figure of merit?"

## Response:

Radial displacement is calculated in two different ways in the H\* analysis: the global scale and the local scale.

On the scale of the steam generator itself, otherwise referred to as the global scale, the radial displacement of the entire tubesheet is calculated. At this level, the tubes are not included in the structural model and there is no direct way to calculate the change in the tube hole diameter. It is not possible to calculate the change in the tube hole diameter at the global scale because the tube holes physically do not exist but are represented by the effective anisotropic material properties of the tubesheet. Therefore, from the global perspective, it is not possible to use the change in hole diameter as a "figure of merit."

On the local scale, the displacements of the tube and tubesheet collar are calculated in the radial and circumferential directions. As described in Section 6.3 of WCAP-17071-P (Model F) and WCAP -17072-P (Model D5), the expansion of a hole of diameter D in the tubesheet at a radius R is given by:

$$\text{Radial:} \quad \Delta D = D \{dU_R(R)/dR\}$$

$$\text{Circumferential:} \quad \Delta D = D \{U_R(R)/R\}$$

$U_R$  is available directly from the finite element results as the global radial displacement for a given point in the tubesheet. The value for  $dU_R(R)/dR$  is obtained by numerical differentiation of the combined displacement field. The maximum expansion of a hole in the tubesheet is in either the radial or circumferential direction. Typically, these two values are within [ ]<sup>a,c,e</sup>% of each other. However, it is clear from the relationship described in Section 6.3 that maximizing the radial displacement at the global scale (i.e., increasing  $U_R$ ) results in maximizing the circumferential and radial displacement of the tubesheet material at the local scale.

The connection between the local and global scales is the global radial displacement of the tubesheet. This is because the applied boundary conditions and the structures

attached to the tubesheet have the greatest effect on the displacement in the radial direction. The tubesheet displacement in the circumferential direction due to the applied pressure loading is typically constant at a small negative value on the order of [ ]<sup>a,c,e</sup> inch or less. Therefore, the radial displacement is the best indicator, or "figure of merit," of the effect of different operating conditions on tubesheet displacement due to pressure loading. Radial displacement is also a good "figure of merit" for the change in tube hole diameter because maximizing the global radial displacement leads to the maximum calculated circumferential and radial tubesheet displacements at the local level. Therefore, the global radial displacement of the tubesheet as described in Section 6.2.3 is the appropriate choice for determining the bounding segment of the tubesheet with respect to the contact pressure analysis.

RAI	Turkey Point	<p>4. Reference 1, Page 6-66. In Section 6.2.5.3, it is concluded that the tube outside diameter and the tubesheet tube bore inside diameter always maintain contact in the predicted range of tubesheet displacements. However, for tubes with through wall cracks at the <math>H^*</math> distance, there may be little or no net pressure acting on the tube for some distance above <math>H^*</math>. In Tables 6-18 and 6-19, the fourth increment in the step that occurs two steps prior to the last step suggests that there may be no contact between the tube and tubesheet, over a portion of the circumference, for a distance above <math>H^*</math>. Is the conclusion in 6.2.5.3 valid for the entire <math>H^*</math> distance, given the possibility that the tubes may contain through wall cracks at that location? Additionally, please address the following issues:</p> <ol style="list-style-type: none"> <li>a. Clarify the nature of the finite element model ("slice" model versus axisymmetric SG assembly model) used to generate the specific information in Tables 6-1, 2, and 3 (and accompanying graph entitled "Elliptical Hole Factors") of Reference 6-15. What loads were applied? How was the eccentricity produced in the model? (By modeling the eccentricity as part of the geometry? By applying an axisymmetric pressure the inside of the bore?) Explain why this model is not scalable to lower temperatures.</li> <li>b. Provide a table showing the maximum eccentricities (maximum diameter minus minimum diameter) from the 3 dimensional (3-D) finite element analysis for normal operating and steam line break (SLB), for model F and D5.</li> <li>c. In Figure 2 of the White Paper, add plot for original relationship between reductions in contact pressure and eccentricity as given in Reference 6-15 in the graph accompanying Table 6-3. Explain why this original relationship remains conservative in light of the new relationship. Explain the reasons for the differences between the curves.</li> <li>d. When establishing whether contact pressure increases when going from normal operating to steam line break conditions, how can a valid and conservative comparison be made if the normal operating case is based on the original delta contact pressure versus eccentricity curve and the SLB case is based on the new curve?</li> </ol>
-----	--------------	-------------------------------------------------------------------------------------------------------------------------------------------------------------------------------------------------------------------------------------------------------------------------------------------------------------------------------------------------------------------------------------------------------------------------------------------------------------------------------------------------------------------------------------------------------------------------------------------------------------------------------------------------------------------------------------------------------------------------------------------------------------------------------------------------------------------------------------------------------------------------------------------------------------------------------------------------------------------------------------------------------------------------------------------------------------------------------------------------------------------------------------------------------------------------------------------------------------------------------------------------------------------------------------------------------------------------------------------------------------------------------------------------------------------------------------------------------------------------------------------------------------------------------------------------------------------------------------------------------------------------------------------------------------------------------------------------------------------------------------------------------------------------------------------------------------------------------------------------------------------------------------------------------------------------------------------------------------------------------------------------------------------------------------------------------------------------------------------------------------------------------------------------------------------------------------------------------------------------------------------------------------------------------------------------------------------------------------------------------------------------------------------------------------------

Surry	<p>4. Reference 1, Page 6-66. In Section 6.2.5.3, it is concluded that the tube outside diameter and the tubesheet tube bore inside diameter always maintain contact in the predicted range of tubesheet displacements. However, for tubes with through wall cracks at the <math>H^*</math> distance, there may be little or no net pressure acting on the tube for some distance above <math>H^*</math>. In Tables 6-18 and 6-19, the fourth increment in the step that occurs two steps prior to the last step suggests that there may be no contact between the tube and tubesheet, over a portion of the circumference, for a distance above <math>H^*</math>. Is the conclusion in 6.2.5.3 valid for the entire <math>H^*</math> distance, given the possibility that the tubes may contain through wall cracks at that location? Additionally, please address the following issues:</p> <p>a. Clarify the nature of the finite element model ("slice" model versus axisymmetric SG assembly model) used to generate the specific information in Tables 6-1, 2, and 3 (and accompanying graph entitled "Elliptical Hole Factors") of Reference 6-15. What loads were applied? How was the eccentricity produced in the model? (By modeling the eccentricity as part of the geometry? By applying an axisymmetric pressure the inside of the bore?) Explain why this model is not scalable to lower temperatures.</p> <p>b. Provide a table showing the maximum eccentricities (maximum diameter minus minimum diameter) from the 3 dimensional (3-D) finite element analysis for normal operating and steam line break (SLB), for model 51F.</p> <p>c. In Figure 2 of the White Paper, add plot for original relationship between reductions in contact pressure and eccentricity as given in Reference 6-15 in the graph accompanying Table 6-3. Explain why this original relationship remains conservative in light of the new relationship. Explain the reasons for the differences between the curves.</p> <p>d. When establishing whether contact pressure increases when going from normal operating to steam line break conditions, how can a valid and conservative comparison be made if the normal operating case is based on the original delta contact pressure versus eccentricity curve and the SLB case is based on the new curve?</p>
-------	-------------------------------------------------------------------------------------------------------------------------------------------------------------------------------------------------------------------------------------------------------------------------------------------------------------------------------------------------------------------------------------------------------------------------------------------------------------------------------------------------------------------------------------------------------------------------------------------------------------------------------------------------------------------------------------------------------------------------------------------------------------------------------------------------------------------------------------------------------------------------------------------------------------------------------------------------------------------------------------------------------------------------------------------------------------------------------------------------------------------------------------------------------------------------------------------------------------------------------------------------------------------------------------------------------------------------------------------------------------------------------------------------------------------------------------------------------------------------------------------------------------------------------------------------------------------------------------------------------------------------------------------------------------------------------------------------------------------------------------------------------------------------------------------------------------------------------------------------------------------------------------------------------------------------------------------------------------------------------------------------------------------------------------------------------------------------------------------------------------------------------------------------------------------------------------------------------------------------------------------------------------------------------------------------------------------------------------------------------------

Response:

*Note: For Turkey Point, part b of question 4 refers to the Model F and Model D5 steam generators. The SGs in Turkey Point are Model 44F SGs; therefore, it is assumed that the requested information is for the Model 44F SGs.*

A response to RAI#4 was provided by Reference 8 for the Model F and Model D5 steam generators. The questions addressed in Reference 8 are the same questions as above, except that they were provided as various RAIs summarized in Reference 8 for the Model F and Model D5 applicants for a license amendment request for the permanent H\*. The analysis methods utilized in the technical justification reports for H\* are the same for all models of SG. References 5 and 6 are the technical justification reports for the Model 44F and Model 51F SGs, respectively. The technical justifications of H\* for the Model F and Model D5 steam generators are WCAP-17071-P and WCAP-17072-P, respectively.

Because the questions under RAI#4 are the same for all models of SG and the technical justification methods are the same for all models of SG, the response to RAI#4 provided by Reference 8 is applicable for all models of SG.

The response to RAI#4 provided in Reference 8 is lengthy and is attached to this document as Appendix B.

<b>RAI</b>	Turkey Point	5. Reference 1, Section 6.3. Are the previously calculated scale factors and delta D factors in Section 6.3 conservative for steam line break (SLB) and feed line break (FLB)? Are they conservative for an intact divider plate assumption? Are they conservative for all values of primary pressure minus crevice pressure that may exist along the H* distance for intact tubes and tubes with through-wall cracks at the H* distance?
	Surry	5. Reference 1, Section 6.3. Are the previously calculated scale factors and delta D factors in Section 6.3 conservative for steam line break (SLB) and feed line break (FLB)? Are they conservative for an intact divider plate assumption? Are they conservative for all values of primary pressure minus crevice pressure that may exist along the H* distance for intact tubes and tubes with through-wall cracks at the H* distance?

Response:

**Note: RAI#5 for both Turkey Point and Surry requests information related Feed Line Break (FLB). Feed Line Break is not included in the design basis for either the Model 44F or the Model 51F as noted in the applicable H\* reports (references 5 and 6). The response to RAI#5 is limited to Steam Line Break (SLB).**

- 1) The previously calculated scale factors and delta D factors in Section 6.3 are conservative for all of the analyzed Model 44F and Model 51F conditions, including normal operating and steam line break, as appropriate. Use of the contact pressure data described in Reference RA15-1 would increase the tube-to-tubesheet contact pressure in the H\* analysis.
- 2) The previously calculated scale factors and delta D factors in Section 6.3 are conservative for an intact divider plate assumption. The results on page 6-87 assume that a greater level of weld and divider plate degradation exists in the SG (DPF = [ ]<sup>a,c,e</sup>) than in the rest of the H\* structural analysis (DPF = [ ]<sup>a,c,e</sup>). (DPF = Divider Plate Factor).
- 3) The previously calculated scale factors and delta D factors in Section 6.3 are conservative for all values of primary pressure minus crevice pressure regardless of their location within the tubesheet. This is because the calculated scale factors and delta D factors applied unit pressure loads to either side of the tube and weld structure in the model such that either the primary side of the tube and tubesheet were pressurized or the secondary side of the tube and tubesheet (including the crevice) were pressurized. In the reference elliptical hole study, the gap elements that were selected for use in the two dimensional study also penalized the tube-tubesheet contact pressure by preventing line on line contact between the tube

outside diameter (OD) and the tubesheet/sleeve inside diameter (ID) which results in a lower estimate of the tube-to-tubesheet contact pressure.

RAI5 References:

RAI5-1. LTR-NRC-09-26, "LTR-SGMP-09-66 P-Attachment, "White Paper: Low Temperature Steam Line Break Contact Pressure and Local Tube Bore Deformation Analysis for H\*" (Proprietary)," May 13, 2009

RAI	Turkey Point	6. Reference 1, Page 6-90. How is tube temperature ( $T_T$ ) on page 6-90 determined? For normal operating conditions (NOP), how is the $T_T$ assumed to vary as function of elevation?
	Surry	6. Reference 1, Page 6-84. How is tube temperature ( $T_T$ ) on page 6-84 determined? For normal operating conditions (NOP), how is the $T_T$ assumed to vary as function of elevation?

Response:

The tube temperature ( $T_T$ ) is assumed to be equal to the primary fluid temperature for the operating condition of interest. The tube temperature is assumed to not vary as a function of elevation within the tubesheet.

<b>RAI</b>	<i>Turkey Point</i>	<i>7. Reference 1, Page 6-107, Figure 6-75. Contact pressures for nuclear plants with Model F steam generators are plotted in Figure 6-75, but it is not clear what operating conditions are represented in the plotted data, please clarify.</i>
	<i>Surry</i>	<i>7. Reference 1, Page 6-102, Figure 6-75. Contact pressures for nuclear plants with Model F steam generators are plotted in Figure 6-75, but it is not clear what operating conditions are represented in the plotted data, please clarify.</i>

Response:

The question relates to the original Figure 6-75 in WCAP-17071-P. The corresponding figure in WCAP-17091-P (Model 44F) is Figure 6-72 and in WCAP-17092-P (Model 51F) is Figure 6-70. The question requests information about the operating conditions for the curves shown in these figures. In both the reports (WCAP-17091-P and WCAP-17092-P), the figures include the requested information in the legend.

<b>RAI</b>	<i>Turkey Point</i>	<i>8. Reference 1, Page 6-115, Reference 6-5. This reference seems to be incomplete; please provide a complete reference.</i>
	<i>Surry</i>	<i>8. Reference 1, Page 6-108, Reference 6-5. This reference seems to be incomplete; please provide a complete reference.</i>

Response:

The complete reference is:

Slot, Thomas, "Stress Analysis of Thick Perforated Plates," TECHNOMIC Publishing Company, Inc., Westport, Connecticut, 1972.

<b>RAI</b>	Turkey Point	9. Reference 1, Page 6-116, Reference 6-15. Table 6-3 in Reference 6-15 (SM-94-58, Rev 1) appears inconsistent with Table 6-2 in the same reference. Explain how the analysis progresses from Table 6-2 to Table 6-3.
	Surry	9. Reference 1, Page 6-109, Reference 6-15. Table 6-3 in Reference 6-15 (SM-94-58, Rev 1) appears inconsistent with Table 6-2 in the same reference. Explain how the analysis progresses from Table 6-2 to Table 6-3.

Response:

The values for initial and final eccentricity for the contact pressure ratio of 0.91 listed in Table 6-3 of Reference 6-15 (SM-94-58, Rev. 1) are calculated as follows using the values from Table 6-2:

$$\text{Initial Eccentricity} = (D_{\text{max}} - D_{\text{min}}) / [ \quad ]^{a,c,e} \text{ inch Tube Hole ID} = [ \quad ]^{a,c,e}$$

$$\text{Final Eccentricity} = ((\text{Hole Delta D } (90^\circ) - \text{Hole Delta D } (0^\circ)) / [ \quad ]^{a,c,e} \text{ inch Tube Hole ID}) = [ \quad ]^{a,c,e}$$

The values for eccentricity in Table 6-2 of the reference should have been divided by the nominal diameter of the tubesheet hole [  $\quad ]^{a,c,e}$  inch) to be consistent with Table 6-3.

<b>RAI</b>	Turkey Point	10. Reference 1, Page 8-9, Figure 8-1. There is an apparent discontinuity in the plotted data of the adjustment to H* for distributed crevice pressure, please provide any insight you may have as to why this apparent discontinuity exists.
	Surry	10. Reference 1, Page 8-9, Figure 8-1. There is an apparent discontinuity in the plotted data of the adjustment to H* for distributed crevice pressure, please provide any insight you may have as to why this apparent discontinuity exists.

Response:

Figure 8-1 (WCAP-17071-P, WCAP-17072-P, WCAP-17091-P and WCAP-17092-P) summarizes the variability cases run to determine the H\* value response to variation of the input parameters ( $\alpha_T$ ,  $\alpha_{TS}$ ,  $E_T$ ,  $E_{TS}$ ) individually or in combination. The values of the variables were chosen to provide sufficient data to define the potential surface of interactions between the variables. No attempt was made to bias the variables in a

manner that would yield specific  $H^*$  values; therefore apparent discontinuities in the figure are coincidental.

Figure RAI10-1 shows a composite of the  $P_{crev}$  corrections for all of the models of SGs considered, Models F, D5, 44F and 51F SGs under  $H^*$  (Ref: WCAP-17071-P, WCAP-17072-P, WCAP-17091-P and WCAP-17092-P). Figure RAI10-1 shows the same characteristic shape of the  $P_{crev}$  correction but also shows that the  $H^*$  responses are different for the different structures. The “apparent discontinuity” in the curve for the Model F is much less pronounced for the Model D5 and other models of SG and, in the case of the Model 44F, is populated by calculated data points. Because the same analysis methods are employed for all of the Model-specific structures, it is concluded that the apparent discontinuity in Figure 8-1 of WCAP-17071-P and WCAP-17072-P is related principally to the structural response of the specific SG model being addressed, and does not imply a potential calculation error.

Figure RAI10-1 also shows that in each of the structures considered, there are steps in the  $P_{crev}$  correction curves (e.g., between 3.8 and 4.2 inches in the Model F, at about 6.6 inches in the Model D5, at about 3.5 inches and 4.5 inches for the Model 44F and 51F). To investigate the step in the curve between initial predictions of  $H^*$  and the  $P_{crev}$  correction, several cases were considered for the Model F SGs for  $H^*$  values between 3.8 inches and 4.2 inches as a typical case to evaluate the issue generically. These cases were synthesized by adjusting the values of the four influencing parameters ( $\alpha_T$ ,  $\alpha_{TS}$ ,  $E_T$  and  $E_{TS}$ ), based on interpolation among existing variabilities, in an attempt to yield  $H^*$  values in this range. Each of the four parameters was adjusted in at least one case to meet this objective.

The following are the additional cases that were examined:

Input Parameters				$H^*(raw)$	$P_{crev}$	Comment
$a_{TS}$	$E_{TS}$	$a_T$	$E_T$			
1	-1	-2	-2			Original Case
5	4	0	0			
-1	0	-3.25	0			
-1	0	-3	-5			
4.5	0	0	0			
5	4	0	-1			
4.5	0	0	-1			
5	0	0	0			Original Case

Figure RAI10-2 shows the results of this study. The  $P_{crev}$  correction values are essentially constant within the narrow range of initial  $H^*$  predictions that define the step in the overall curve, Figure RAI10-1, except for a single point at approximately [ ]<sup>a,c,e</sup> inches. As discussed below, the interpolation between the limited number of points representing the crevice pressure distribution and the fixed number of points representing the thickness of the tubesheet leads to isolated conditions at which the integration scheme cannot converge to a single value. A minor departure (less than

about 0.005 inch) in either direction results in convergence of the integration. The point at [ ]<sup>a,c,e</sup> inches is at such a condition. It does not suggest that the crevice pressure correction is undefined at that location.

As described in each of the H\* WCAP reports, the correction for P<sub>crev</sub> is an iterative process. Following the initial prediction of H\*, which assumes that a tube separation is located at the primary face of the tubesheet and, therefore, assumes the crevice pressure is distributed over the entire thickness of the tubesheet, the calculation process depicted in Figure 1-1 of the report is repeated but with the crevice pressure distributed over the length of the initial prediction of H\*. The resulting prediction of H\* will exceed the initial prediction. This process is iterated until the input values and output values of H\* converge to the same number. The convergence criteria are set to 2 decimals because the H\* distance cannot practically be measured to the second decimal. In some instances, depending on the specific combination of input parameters that lead to the initial prediction of H\*, the variation of H\* is less than the convergence criteria. In that case, the default is at the larger value of the P<sub>crev</sub>.

The H\* integrator model utilizes discrete, dimensionally fixed points through the thickness of the tubesheet to represent the tube to tubesheet contact pressure. The representation of the distributed crevice pressure as discussed in Section 6 of the report utilizes a discrete number of points whose axial dimensions vary according to the assumed position of the flaw. Thus, the same number of points describes the crevice pressure profile regardless if the flaw is assumed at the bottom of the tubesheet or at some other location within the tubesheet. Only the slope of the distribution between the points changes. Because of a mismatch between the crevice pressure axial definition and the tubesheet contact pressure axial definition, the integration model cannot converge to a single value at certain discrete points, depending on the model of SG under consideration. For the Model F SG, this point occurs at approximately 4 inches from the top of the tubesheet. The axial range within which this occurs is extremely narrow, less than [ ]<sup>a,c,e</sup> inch (see Figure RA10-2), and the non-convergence results in a very limited range of the axial crevice pressure correction factor, less than [ ]<sup>a,c,e</sup> inch. For the Model F SG, a variation of initial H\* prediction of approximately 0.005 inch from the critical axial length results in the model converging again at the lower value of P<sub>crev</sub> correction as also shown on Figure RA10-2. This result applies generically to the Model D5, 44F and 51F SGs as well.

For practical application in determining the final value of H\*, it is noted that when the adjustments for BET and NOP thermal distribution are included, the predicted values of H\* are far removed from the points in the P<sub>crev</sub> correction curves where the model does not converge for all models of SGs. The recommended values of H\*, prior to the correction for P<sub>crev</sub>, for the different models of SG are:

Model F:	9.81 inches (Ref: WCAP-17071-P)
Model D5	12.11 inches (Ref: WCAP-17072-P)
Model 44F	11.06 inches (Ref: WCAP-17091-P)
Model 51F	11.14 inches (Ref: WCAP-17092-P)

In all cases, the point of non-convergence of the model does not affect the final recommended value of  $H^*$ .

**Figure RAI10-1**  
 **$P_{crev}$  Correction Profiles for Models F, D5, 44F and 51F SGs**



**Figure RAI10-2**



a,c,e

RAI	Turkey Point	11. Reference 1, Page 8-5, Section 8.1.4. Clarify whether the "biased" H* distributions for each of the four input variables are sampled from both sides of the mean H* value during the Monte Carlo process, or only on the side of the mean H* value yielding an increased value of H*.
	Surry	11. Reference 1, Page 8-5, Section 8.1.4. Clarify whether the "biased" H* distributions for each of the four input variables are sampled from both sides of the mean H* value during the Monte Carlo process, or only on the side of the mean H* value yielding an increased value of H*.

Response:

As shown in Figure 8-11 of the report (WCAP-17071-P, WCAP-17072-P, WCAP-17091-P and WCAP-17092-P), the variation of the parameters that resulted in the greatest increase in the value of H\* were chosen as the "biased" influence factors from which to sample in the Monte Carlo (MC) process. These distributions were normal distributions determined from the mean H\* and greatest H\* variation resulting from equal valued positive and negative variations of the respective parameters. Note that for the case of coefficient of thermal expansion of the tube, a decrease in the coefficient results in an increase in the H\* value and also reflects the broadest distribution. For the coefficient of thermal expansion of the tubesheet, an increase in the coefficient results in increasing H\* and also results in the broadest distribution.

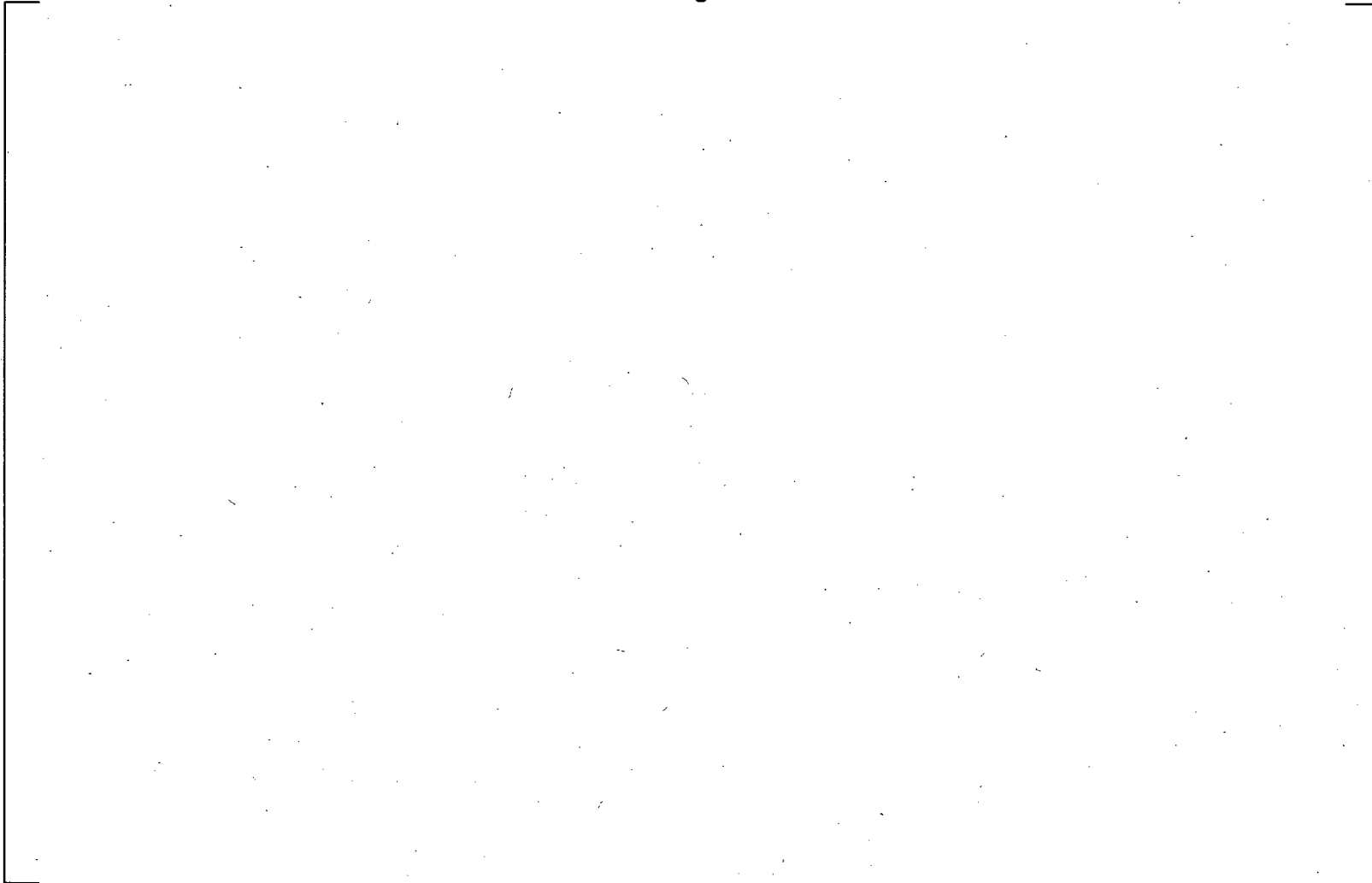
Both sides of the biased influence factors were sampled during the Monte Carlo analysis. Sampling from the broadest distributions results in the broadest H\* distribution and the largest values of H\* corresponding to the desired probabilistic goal, in this case, 95/50.

Figure RAI10-1 shows the results of the Monte Carlo sampling from the interaction surface (see RAI#18 [Turkey Point, Model 44F] and RAI#16 [Surry, Model 51F]) for the resulting values of H\* between the upper 93% and 98% of the simulations. (The 98% upper limit was chosen for convenience). The highest values of H\* are concentrated in a well defined region bounded approximately by the tube coefficient of thermal expansion ( $\alpha_T$ ) between [ ]<sup>a,c,e</sup> and tubesheet coefficient of thermal expansion ( $\alpha_{TS}$ ) between [ ]<sup>a,c,e</sup>. The conclusion that the maximum values of H\* are produced from samples in approximately the center of the interaction surface defined by Figure 8-5 in the report applies to both the Model 44F and Model 51F SGs. Consequently, the use of the broadest distributions that increase the value of H\* will tend to focus on the region in question because the broadest H\* distributions are defined by negative variations of  $\alpha_T$  and by positive variations of  $\alpha_{TS}$ . Selections from the negative sides of the broadest distributions will not result in maximum values of H\*. If picks are made from both distributions on the negative side of the biased influence distributions, the result will be an over-prediction of the lower tail of the H\* distribution. This is noted

in WCAP-17071-P, WCAP-17072-P, WCAP-17091-P and WCAP-17092-P and is of no consequence because only the maximum value of  $H^*$  is of concern.

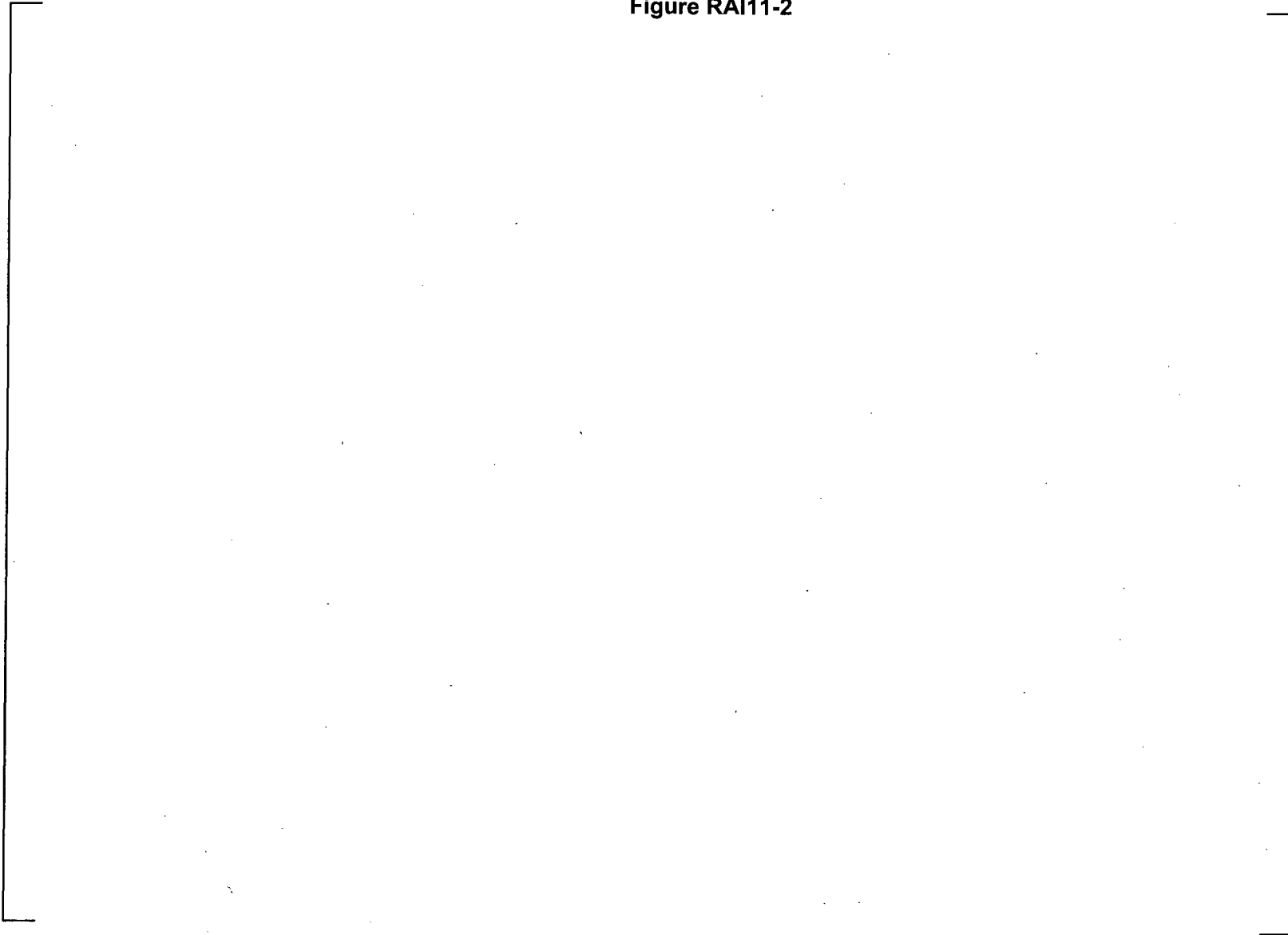
**Figure RAI11-1**

a,c,e



**Figure RAI11-2**

a,c,e



<b>RAI</b>	Turkey Point	12. Reference 1, Page 8-20, Case S-4. Why does the assumption of a 2-sigma value for the coefficient of thermal expansion of the tube ( $\alpha_T$ ) and the tubesheet ( $\alpha_{TS}$ ) to determine a "very conservative biased mean value of $H^*$ " conservatively bound the interaction effects between $\alpha_T$ and $\alpha_{TS}$ ? Describe the specifics of how the "very conservative biased mean value of $H^*$ ," as shown in Table 8-4, was determined.
	Surry	12. Reference 1, Page 8-20, Case S-4. Why does the assumption of a 2-sigma value for the coefficient of thermal expansion of the tube ( $\alpha_T$ ) and the tubesheet ( $\alpha_{TS}$ ) to determine a "very conservative biased mean value of $H^*$ " conservatively bound the interaction effects between $\alpha_T$ and $\alpha_{TS}$ ? Describe the specifics of how the "very conservative biased mean value of $H^*$ ," as shown in Table 8-4, was determined.

Response:

The very conservative mean value of  $H^*$ , [ ]<sup>a,c,e</sup> inches (Model 44F), [ ]<sup>a,c,e</sup> inches, (Model 51F), is determined by arbitrarily assuming that the 2-sigma values of all variables defines the mean value of  $H^*$ . To determine these values, it was assumed that the input variables to the structural evaluation (i.e, the entire  $H^*$  calculation process as shown in Figure 1-1 of the report) were set at their 2-sigma values, and the resulting  $H^*$  was termed the "conservative mean." Table RAI12-1 illustrates the input values that define the mean value of  $H^*$  and the "very conservative mean" value of  $H^*$ . The SRSS approach was then applied using the influence factors from Table 8-2 in the report for the 95/50 whole-bundle value appropriate to the model SG being considered. The result is essentially equivalent to the 5-sigma variation case, Case S4 on Table 8-3 of the report. Note that because the 2-sigma input parameter value of  $H^*$  was determined by the entire calculation process shown in Figure 1-1 of WCAP, the interaction effects of the variables at the 2-sigma level are included in this calculation.

**Table RAI12-1  
Definition of "Conservative Mean"  $H^*$**

Definition	Analysis Input Parameters and their Values			
	$\alpha_T$	$\alpha_{TS}$	$E_T$	$E_{TS}$
Mean $H^*$	mean	mean	mean	mean
Conservative Mean $H^*$	Mean-2 $\sigma^{(1)}$	Mean+2 $\sigma^{(1)}$	Mean-2 $\sigma^{(1)}$	Mean-2 $\sigma^{(1)}$
(1) Values chosen in direction of increasing $H^*$				

<b>RAI</b>	Turkey Point	13. Reference 1, Page 8-22, Case M-5. The description for this case seems to correspond to a single tube H* estimate rather than a whole bundle H* estimate. How is the analysis performed for a whole bundle H* estimate?
	Surry	13. Reference 1, Page 8-22, Case M-5. The description for this case seems to correspond to a single tube H* estimate rather than a whole bundle H* estimate. How is the analysis performed for a whole bundle H* estimate?

## Response:

Case M-5 is the Monte Carlo (MC) sampling analogy to Case S-2. A single tube analysis would sample from the  $1\sigma$  influence distributions to determine the overall distribution of H\*, and from the resulting H\* distribution, choose the 95% probability value of the upper tail. Case M-5 pre-biases the influence factor distributions by choosing the influence factor distributions at the  $4.157\sigma$  (Model 44F) ( $4.166\sigma$  Model 51F) values divided by 4.157 (Model 44F) ( $4.166$ , Model 51F). Thus, the input distributions are pseudo- $1\sigma$  distributions that are already biased by the number of standard deviations required to represent a whole bundle analysis as was done in Case S-2. The use of the greater value influence functions results in a broader final H\* distribution from which the 95/50 value represents the whole bundle. The basis for the  $4.157\sigma$  (Model 44) ( $4.166\sigma$ , Model 51F) value to represent the whole bundle case is discussed in the report.

It was recognized that the assumption of normality of the influence factor distribution could influence the results from the MC approach included in the report. Nevertheless, the MC cases were included in the report to provide a basis for evaluating multiple variability cases that could not be considered using the SRSS approach. The response to RAI#18 (Turkey Point, Model 44F) and RAI#16 (Surry, Model 51F) provides a comprehensive analysis based on the interaction surface of Figure 8-5 and utilization of the Monte Carlo technique.

<b>RAI</b>	Turkey Point	14. Reference 1, Page 8-22, Case M-5 states: "Interaction effects are included because the 4.157 sigma variations were used that already include the effective interactions among the variables." Case M-5 also states that the 4.157 sigma variations come from Table 8-2. However, Table 8-2 does not appear to include interactions among the variables. Explain how the 4.157 sigma variations include the effect of interactions among the variables.
	Surry	14. Reference 1, Page 8-22, Case M-5 states: "Interaction effects are included because the 4.166 sigma variations were used that already include the effective interactions among the variables." Case M-5 also states that the 4.166 sigma variations come from Table 8-2. However, Table 8-2 does not appear to include interactions among the variables. Explain how the 4.166 sigma variations include the effect of interactions among the variables.

## Response:

Because the  $4.157\sigma$  (Model 44F),  $4.166\sigma$  (Model 51F) variations were calculated using the complete calculation process depicted in Figure 1-1 of the report (WCAP-17091-P, WCAP-17092-P), the variations include the structural interaction effects for each variable assuming that all other variables are at their mean value. If multiple variables were perturbed simultaneously, a greater effect on  $H^*$  would be expected. The Monte Carlo sampling scheme used did not support the use of compound parameter variations.

The response to RAI#18 (Turkey Point, Model 44F) and RAI#16 (Surry, Model 51F) provides an in-depth analysis of the interaction effects among the significant variables using the Monte Carlo method and sampling from the interaction surface of Figure 8-5.

<b>RAI</b>	Turkey Point	15. Reference 1, Page 8-23, Case M-7. Was the "2 sigma variation of all variables" divided by a factor of 2?
	Surry	15. Reference 1, Page 8-23, Case M-7. Was the "2 sigma variation of all variables" divided by a factor of 2?

Response:

For case M-7, the 2-sigma variation was treated as if it were 1-sigma variation. This assumption is somewhat arbitrary and intended only as a hypothetical case to show the effect on H\* if it were assumed that the calculated standard deviation are much larger. Therefore, the 2-sigma variation was NOT divided by 2.

This case is an arbitrary sensitivity study that addresses the H\* result if the 1σ influence factors were more than doubled: Starting from the basic mean structural prediction of H\*, [ ]<sup>a,c,e</sup> for the Model 44F, ([ ]<sup>a,c,e</sup> for the Model 51F) inches, it was assumed that the 2σ influence distributions applied instead of the 1σ influence distributions, and the MC sampling was from the 2σ distributions. The principal objective of this case was to show that very conservative assumptions do not lead to a major impact on the value of H\*.

<b>RAI</b>	Turkey Point	16. Reference 1, Page 8-23, Case M-7. Is the number 4.147 supposed to be 4.157?
------------	--------------	---------------------------------------------------------------------------------

Response:

On Page 8-23, in the paragraph headed by "Case M-7", the value 4.147 is a typographical error. The correct value is 4.157.

<b>RAI</b>	Turkey Point	17. Reference 1, Page 8-23, Case M-7. Explain how this case includes the interaction effects between the two principle variables, $\alpha_T$ and $\alpha_{TS}$ .
------------	--------------	------------------------------------------------------------------------------------------------------------------------------------------------------------------

## Response:

Case M-7 assumes that the  $1\sigma$  variability of  $H^*$  in the parameters is based on the  $2\sigma$  influence factors calculated for each parameters. Because the influence factors are calculated using the entire calculation flow depicted in Figure 1-1 of the report, the interactive effect of the key parameters at the  $2\sigma$  is reflected. The calculations were performed by perturbing one parameter at a time; therefore, the combined interaction of perturbing multiple parameters is not reflected. However, the assumption that the  $2\sigma$  variation in the direction of increasing  $H^*$  represent one standard deviation of the  $H^*$  influence factors and the extreme value calculation process provide a very conservative estimate of  $H^*$ .

The response to RAI#18 (Turkey Point, Model 44F) and RAI#16 (Surry, Model 51F) provides an in-depth analysis of the interaction effects among the significant variables.

<b>RAI</b>	Turkey Point	18. Section 8 of Reference 1. The variability of $H^*$ with all relevant parameters is shown in Figure 8-3. The interaction between $\alpha_T$ and $\alpha_{TS}$ are shown in Figure 8-5. Please explain why the direct relationships shown in these two figures were not sampled directly in the Monte Carlo analysis, instead of the sampling method that was chosen. Also, please explain why the sampling method chosen led to a more conservative analysis than directly sampling the relationships in Figures 8-3 and 8-5. As part of response, include discussion of main steam line break and whether it continues to be less limiting, from maximum $H^*$ perspective, than three times normal operating pressure.
	Surry	16. Section 8 of Reference 1. The variability of $H^*$ with all relevant parameters is shown in Figure 8-3. The interaction between $\alpha_T$ and $\alpha_{TS}$ are shown in Figure 8-5. Please explain why the direct relationships shown in these two figures were not sampled directly in the Monte Carlo analysis, instead of the sampling method that was chosen. Also, please explain why the sampling method chosen led to a more conservative analysis than directly sampling the relationships in Figures 8-3 and 8-5. As part of response, include discussion of main steam line break and whether it continues to be less limiting, from maximum $H^*$ perspective, than three times normal operating pressure.

Response:

**Figure numbers, table numbers and references in the response refer to RAI#18 for Turkey Point but are equally applicable to RAI#16 for Surry.**

General

The recommended value of  $H^*$  is based on the square root of the sum of the squares (SRSS) approach to combining the uncertainties for  $H^*$ . The Monte Carlo cases included in the report were included as a vehicle to study different sensitivities to  $H^*$  parameters variations and were provided as support for the SRSS recommendation. The peer review (Expert Panel's) conclusions were that the SRSS approach was a suitably conservative approach given the many conservatisms built into the  $H^*$  analysis. The significant conservatisms included in the  $H^*$  analysis are summarized in Section 1 of the report(s) and again identified in Section 10 of the report(s).

Figures 8-3 and 8-5 were developed during, and immediately after, the peer review of the  $H^*$  project, which was followed in close order by publishing the report. The staff's observation that Figures 8-3 and 8-5 reasonably define an interaction surface, which could be utilized directly for a Monte Carlo sampling assessment, is correct. Therefore, a Monte Carlo analysis based on the interaction surface defined by Figure 8-4 in the respective WCAP reports for the different models of SGs was completed. This analysis provided the opportunity to quantify some of the conservatisms that are included in the

technical justification of H\*. The approach to this issue was to consider the most significant conservatisms in the overall H\* analysis and quantify their effects on the recommended value of H\* to show that the recommended value of H\* is conservative. The sequence of the analysis was as follows:

1. Application of the Monte Carlo methodology discussed in the H\* reports, except for case M-6, assumes that each simulation of H\* includes a different value of the properties of the tubesheet. Thus, if 100,000 simulations are performed, each simulation includes a different random pick of tubesheet properties. Among the population of H\* candidate plants, there are 60 steam generators; therefore, the actual population of tubesheets is limited to 60. To better address the limited population of tubesheets, the reference MC sampling is a staged process corresponding to the simulation of one steam generator tubesheet/tube bundle combination. A set of tubesheet properties is selected, and for that set, the corresponding tube properties are sampled 3214 times for the Model 44F SG tube population (3342 times for the model 51F SG tube population), and as appropriate for the other models of SGs.. The above process is repeated 10,000 times. This provides a more accurate simulation reflecting the limited number of tubesheets in the population.
2. The probabilistic analysis in Section 8 of the report(s) assumes that the entire tube bundle consists of tubes located at the worst case location in the tube bundle (e.g., the most limiting radius in the most limiting sector of the tube bundle as shown in Section 6.2.3). As shown in Figure 6-1 of the report, the worst tube is defined by a very narrow segment of tubes, while all other tubes are shown to have a lower value of H\*. Therefore, the bundle was divided into a number of sectors as discussed below, and the 0.95 probability at 50% confidence value of H\* was defined on the combined probability of the sector probability for all tubes. This analysis is still quite conservative because all tubes are still assumed to be in the limiting azimuthal sector of the tube bundle (the sector perpendicular to the divider plate including about 5° from the centerline of the tubesheet. See Section 6.2.3 of the report). Tubes more than about 5 pitches removed from the centerline perpendicular to the divider plate have been shown to have lower values of H\*.
3. The analyses for the Model 44F and Model 51F SGs do include a correction factor for the NOP thermal distribution through the tubesheet similar to the analyses for the Model F and Model D5 SGs. The NOP tubesheet thermal distribution is applied directly in the structural model for the Model 44F and Model 51F SGs as discussed in section 6.2.2.2.5 of the respective reports, WCAP-17091-P and WCAP - 17092- P.
4. The H\* analysis assumes no contribution from residual contact pressure (RCP). All test data to date, including data from tests performed prior to 2008, has shown that a

positive value of RCP exists after hydraulic expansion of the tubes. Tests were performed during the current H\* program that confirmed a significant level of RCP, and also showed that within a short distance of motion, the forces required to continue to move the tube by far exceeded the maximum pull out forces that could be generated under very conservative assumptions. The analysis quantifies the effect of RCP on the calculated value of H\* and benchmarks the RCP to the tests that were performed during the H\* development.

A. Sector Analysis

Based on the profile of the predicted mean H\*, the tube bundle is divided into 9 annular sectors as shown in Figures RAI18-1, -2, -3 and -4 for the models of SG included in the H\* population (Reference RAI18-1). (In Figure RAI18-4, for the Model 51F SGs, the appropriate sector division results in only 7 sectors; however, additional sectors with 1 tube, each, were added at both ends for convenience of the calculations.) The normalized H\* is determined from the raw H\* calculation results, prior to adjustment of the H\* value by the addition of correction factors for the BET and NOP tubesheet thermal profile. This is done to obtain a true normalization, unaffected by any constants. However, the final value of H\*, after the MC sampling for ΔH, is based on the adjusted maximum mean value of H\* as shown in the appropriate sector in Tables 1, 2, 3 and 4. The adjustment for crevice pressure referenced to the predicted H\* is made after the all other factors have been accounted for. Thus, for each sector:

$$\left[ \quad \quad \quad \right]^{a,c,e}$$

Where,

F is the sector normalization factor from Figures RAI18-1, -2, -3 and -4,

H\*<sub>(BET+ T<sub>nop</sub>)</sub> is the raw H\* value adjusted for BET and NOP thermal distribution

ΔH\*<sub>uncert</sub> is the adjustment for interaction effects from the MC analysis

ΔH\*<sub>pcrev</sub> is the adjustment for crevice pressure

The normalized value of H\* in each sector is based on the maximum value of H\* in that sector; thus, the sector evaluation is inherently conservative.

The number of tubes in each sector is determined from the row and column numbers and the model-specific pitch of the tubes. Tables RAI18-1, -2, -3, and -4 summarize the sector populations for each of the models of SGs.

## B. Interaction Surface and Monte Carlo Sampling

A simulation model was developed to evaluate limiting values of  $H^*$  for specific classes of steam generators. The Monte-Carlo based model evaluates extreme values of  $H^*$  on a single steam generator basis, repeating the process to construct a distribution of maximum  $H^*$  values. The final output of the model is the 95/50 estimate of extreme  $H^*$  within any one steam generator.

The components of variance included in the model are the coefficients of thermal expansion (CTE's) for the tubesheet and the individual tubes. These have been shown in the  $H^*$  reports to be, by far, the most significant contributors to variations in  $H^*$  for the tubesheet/tube bundle combinations. The essential function describing  $H^*$  variation for specific value pairs of the thermal expansion coefficients has been developed and is shown in Figure 8.5 of the  $H^*$  reports. It should be noted that full interaction effects are included.

The basic structure of the simulation is shown in Figure RAI18-5 and represents one Monte Carlo trial. The process shown produces one realization of the extreme  $H^*$  for a given steam generator. Repetition, involving 10,000 trials produces a distribution from which a 95/50 estimate of  $H^*$  can be obtained by robust nonparametric means. As shown in Figure RAI18-5, the core process involves a random selection of one value of tubesheet CTE and  $N$  values of tube CTE, where  $N$  is the number of tubes in the steam generator or specific region of interest. The resulting  $N$  pairs are propagated through the fitted surface to produce  $N$  values of  $H^*$  which are then sorted to identify the maximum (extreme) value of  $H^*$  which is stored for further use.

The above process can be easily applied on a regional (SG sector) basis by running the simulation for each region separately based on region-specific values on tube population size and average  $H^*$ . The composite  $H^*$  for the entire steam generator can be obtained by the following equation:

$$H^*_c = [ \quad ]^{a,c,e} \text{ for M Region model}$$

It is most important that the  $H^*$  values for the individual regions are not sorted prior to application of the above post-processing because of the need to maintain tubesheet identity between regions.

## C. Sector Application of Interaction Effects

The interaction data shown in Figure 8-5 of the  $H^*$  WCAPs were developed for the limiting tube radius (i.e., the tubesheet radius in Figures 1, 2, 3 and 4) where the normalized value of  $H^*$  is 1. Because of the complex nature of the  $H^*$  analysis, it was necessary to determine if the interaction effects at the limiting  $H^*$  radius adequately represented the interactions at other tubesheet radii. Two radii were selected to represent the most probable locations where significant effects, if they exist, might

materialize: 1) A tubesheet sector near the limiting radius, and 2) A tubesheet sector far removed from the limiting radius.

It was shown in the reports that the influence of Young's modulus on the final values of  $H^*$  is negligible and that there was no significant interaction between the Young's moduli of the materials and the coefficient of thermal expansion of the materials. The existing interactions are limited to the coefficients of thermal expansion of the tube and tubesheet materials. Therefore, the same matrix of sensitivity cases that defined Figure 8-5 in the reports was run for each of the two tubesheet sector chosen as noted above.

In all cases it was determined that the interaction effects defined in Figure 8-5 of the report(s) for the location of the maximum mean  $H^*$  value bounded the interaction effects of the other sectors considered. Therefore, for conservatism and simplicity, the range of interaction effects (i.e.,  $\Delta H^* = f(\alpha_T, \alpha_{TS})$ ) for the maximum mean value of  $H^*$  shown on Figure 8-5 was applied for all sectors of the tubesheet.

Figures RAI18-6 and RAI18-7 show the results of this evaluation for the tubesheet sectors selected for the Model F and Model D5 SGs. The interaction profile for the mean,  $3\sigma$  and  $5\sigma$  variation of tubesheet coefficient of thermal expansion are shown to cover the significant range of variability. In all cases, the variability of the location of the maximum value of  $H^*$  is greater than, or equal to, the variability at other radial locations on the tubesheet. Therefore, the application of the variability for the radial location of the maximum value of  $H^*$  for all other radial locations is justified and conservative.

#### D. Results from Sector Based Sampling from the Interaction Surfaces

Table RAI18-5 (a) summarizes the recommended values of  $H^*$  from the  $H^*$  reports for all of the affected Model SGs together with the results of the Monte Carlo (MC) sampling from the interaction surface defined in Figure 8-5 of each report. The MC sampling was based on the sector approach described above and also the approach shown in Figure RAI18-5 to limit the number of tubesheet simulation. The result from this sampling must be adjusted for the crevice pressure distribution referenced to the location of the initially predicted value of  $H^*$ . The correction for crevice pressure is taken from Figure 8-1 of the respective reports. After the adjustments are made for the crevice pressure reference location, the values of  $H^*$  are slightly greater than the recommended values of  $H^*$  from the respective reports.

Table RAI18-5(b) extends the evaluation of the conservatism of the recommended SRSS-based values of  $H^*$  by adjusting the Monte Carlo sampling results for the updated values of the adder for the NOP thermal distribution in the tubesheet for the Model F and Model D5 SGs. The updated NOP thermal distribution factor for the Model 44F and Model 51F SGs are already included in the respective reports (WCAP-17091-P and WCAP-17092-P); consequently there is no adjustment made for these models of SG.

The original NOP thermal distribution adjustment factor was developed on a very conservative basis, using the scaling method described in Section 6.2.2.2.5 of WCAP-17071-P and WCAP-17072-P. As the analysis for H\* evolved, a direct method of applying the tubesheet NOP thermal distribution in the structural analysis was developed; this method is describe in Section 6.2.2.2.5 of WCAP-17072-P (Model D5 report). For the Model D5 SG, the necessary correction based on the updated method was [ ]<sup>a,c,e</sup> inch compared to [ ]<sup>a,c,e</sup> inch based on the scaling technique. A similar analysis was subsequently performed for the Model F SG and it was determined that the appropriate correction for the NOP thermal distribution is [ ]<sup>a,c,e</sup> inch instead of the [ ]<sup>a,c,e</sup> inches included in the recommended value of H\* in WCAP-17071-P.

When the updated correction for the NOP thermal distributions are applied, and the necessary correction for crevice pressure reference location is applied, the final value of H\* for the Model F SG is [ ]<sup>a,c,e</sup> inches and, for the Model D5, is [ ]<sup>a,c,e</sup> inches (see Table RA118-5(b)). Both of these values are less than the recommended values of H\*, respectively, for the Model F and Model D5 SGs. Thus, it is concluded that the recommended values of H\*, based on the SRSS approach as shown in the respective reports for the Model F and Model D5 SGs, are conservative.

It should be noted that the adjustment of the NOP thermal distribution correction factor does not impact which operating condition, NOP or SLB, is the limiting condition. The limiting value of H\* is determined by three times normal operating pressure before and after the adjustment for the NOP thermal distribution. Section 6.4.5 of the Model F report, WCAP-17071-P, and the Model D5 report, WCAP-17072-P, discusses the determination of the H\* values. When the NOP thermal distribution is directly included in the structural analysis to determine tubesheet displacements, the NOP condition remains the limiting condition for H\*.

#### E. Determination of Residual Contact Loads from Pull Out Tests

In prior analyses for H\*, pull out test data has been used to calculate a residual contact pressure, which is distributed over the length of the tubesheet and included in the integration of pull out force over length to determine the length at which the pull out and resisting forces are equal. However, the pull out resistance can also be used to offset the pull out forces. Both methods were studied and it was determined that the same result was achieved, regardless of which method was applied. Because offsetting the applied loads requires fewer assumption (i.e., coefficient of friction) and results in more conservative values of H\*, this approach was selected to determine the effect of the hydraulic expansion only on the calculated value of H\*.

Reference RA118-2, provided as Appendix A to this document, summarizes the pull out test program performed in support of the H\* development. The data from the pull out tests and Monte Carlo simulation were used to determine a conservative value of end cap load reduction. As in prior pull out tests, there was considerable scatter in the pull test data. The highest pull force recorded at 0.25 inch cross head displacement was

[ ]<sup>a,c,e</sup> lbf, and the lowest pull force recorded at 0.25 inch cross head displacement was [ ]<sup>a,c,e</sup> lbf. Monte Carlo simulation was then used to determine a 5/50 value (i.e., the lower 95% bound) of the pull test data.

The Monte Carlo simulations used the pull test data to establish means and standard deviations for the pull forces that were observed. Two sets of data for each of three tube diameters (0.688 inch, 0.750 inch, and 0.875 inch) were provided: One considered the 13 in. expansion lengths only and the other considered all expansion lengths (13, 15 and 17 inches) combined. Seven distributions were used: 1) A truncated (at 0) normal distribution, 2) a lognormal distribution, 3) an Erlang distribution, 4) a Gamma distribution, 5) an inverse Gaussian distribution, 6) a Pearson Type V distribution, and 7) a Weibull distribution. All except the truncated normal were chosen because their domains range from 0 to + infinity, their domains are continuous, and their fitting parameters for the means and standard deviations used were within their allowable values. One hundred thousand iterations were run for each simulation, and the 5/50 values of pull force recorded for each distribution. The most conservative result, [ ]<sup>a,c,e</sup>, came from the simulation that used the Weibull distribution, and this number is very consistent with the lowest observed pull test datum. Note that the Weibull distribution is widely recommended to model distributions in lieu of a truncated normal distribution. The figure below illustrates the results of the Monte Carlo sampling based on the Weibull distribution of the test data. Complete details of the above analysis can be found in Reference RAI18-2.

The recommended end cap load reduction is [ ]<sup>a,c,e</sup> lbf.



(Figure corresponding to the Monte Carlo simulation using a Weibull distribution for the Model F SG data, using the 13 inch expansion length only. The 5/50 value of pull force is [ ]<sup>a,c,e</sup> lbf.)

#### F. Application of Residual Contact Load

The  $H^*$  results in Figure 8-5 of WCAP-17071-P, WCAP-17072-P, WCAP-17091-P and WCAP-17092-P show that  $H^*$  is sensitive to the variations in the coefficient of thermal expansion (CTE) of the tube ( $\alpha_T$ ) and the tubesheet ( $\alpha_{TS}$ ). The reports also show that  $H^*$  is not significantly sensitive to variations in the Young's modulus (E) of the tube or the tubesheet. The results in Figure 8-5 in WCAP-17071-P, WCAP-17072-P, WCAP-17091-P and WCAP-17092-P also demonstrate that the worst case trend in the variation of the thermal expansion coefficients is when the  $\alpha_T$  is decreasing and  $\alpha_{TS}$  is increasing. In other words,  $H^*$  increases the most when the coefficients of thermal expansion are varied to reduce the contact pressure between the tube and the tubesheet due to thermal growth.

It is possible to reduce the order of the problem (i.e., reduce the number of dimensions involved in the sensitivity study) given the knowledge of which values and directions of variation in CTE are most important to the problem. Figures RA10-1 and RA10-2 show the combinations of  $\alpha_T$  and  $\alpha_{TS}$  that are most likely to produce a worst case  $H^*$  value. The values of CTE standard deviations for both the tube and tubesheet are combined into an effective variable using the following relationship:

$$\alpha_{srss} = \sqrt{(-\sigma_{\alpha_T})^2 + (\sigma_{\alpha_{TS}})^2}$$

The possible variation in sign of either CTE standard deviations is not included in this equation because the only values of interest occur when the tube CTE variation is negative relative to the mean and the tubesheet CTE variation is positive relative to the mean. This reduced form of variation in CTE is then used to compare the change in  $H^*$  due to the application of residual pre-load between the tube and the tubesheet due to the installation and hydraulic expansion of the tube.

There are multiple ways to achieve the same value of  $\alpha_{srss}$ . For example, a TS CTE variation of  $+5\sigma$  about the mean and a tube CTE variation of  $-5\sigma$  about the mean are each equal to a combined  $\alpha$  of 5 (assuming only one is non-zero). Likewise, a combination of tube and TS CTE variations of  $-3/+4$  and  $-4/+3$  will also yield an  $\alpha$  of 5. However, the net change in  $H^*$  with respect to the material properties are very similar for a single value of  $\alpha_{srss}$  regardless of values of its component parts. In cases where there are multiple possibilities for a unique value of  $\alpha_{srss}$ , the combination of TS and tube CTE that produced the smallest reduction in  $H^*$  was used. Figure RA18-8 shows the multiple curves that were used to create the surface seen in RA18-9.

Hydraulic expansion of the tube into contact with the tubesheet tube bore introduces a pre-load that must be overcome before the tube can translate within the tubesheet tube bore. This means that in addition to the pull out resistance that a tube develops due to internal pressure, thermal growth, etc., the pull out resistance of the tube due to the hydraulic expansion must also be overcome in order for the tube to freely translate within the tube bore. However, the hydraulic expansion process has only a small effect on the development of contact pressure between the tube and the tubesheet compared to that developed due to operating pressure and temperature. Therefore, the installation effect, termed residual contact load (RCL), is included as a reduction of the applied end cap load. Recall that the end cap loads are based on the mean  $+2\sigma$  tubesheet bore diameter and are thus very conservative.

The reduction in end cap load, for the  $i^{\text{th}}$  value of pull out resistance due to installation effects is:

$$P_i = \text{End Cap Load} = n\Delta p\pi r_o^2 - DL - RCL_i$$

Where,

$n$  is the applicable safety factor for the SG operating condition based on the SIPC,

$\Delta p$  is the primary to secondary pressure differential,

$r_o$  is the outside tube radius,

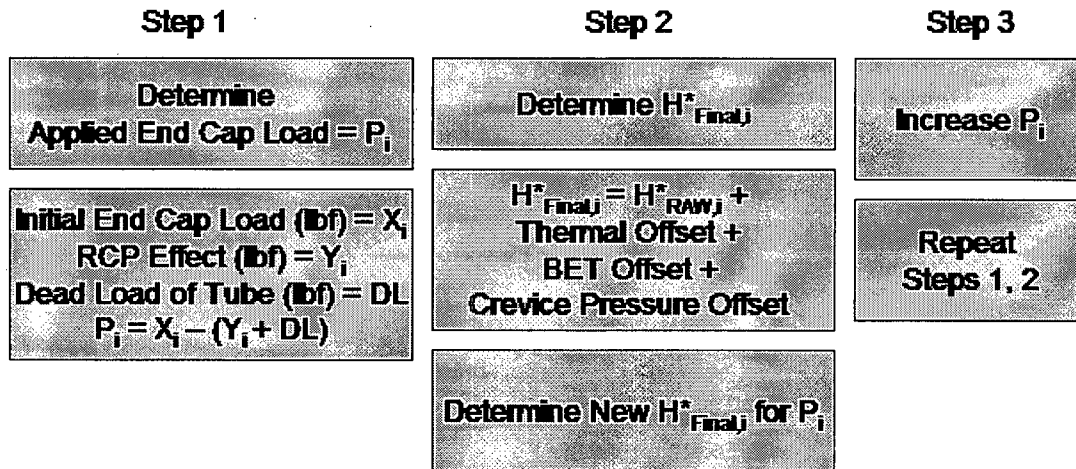
$DL$  is the dead load of the tube straight leg above the top of the tubesheet and  $RCL$  is the value of installation pre-load determined from test results.

The minimum pull out force from section F above, [ ]<sup>a,c,e</sup> lbf, was used. The dead weight of the straight leg portion of the tube above the tubesheet was also included because it also provides a resistance to tube pull out. The dead weight of the straight legs of the tubes varies between [ ]<sup>a,c,e</sup> and [ ]<sup>a,c,e</sup> lbs depending on the length of the tube straight leg; an average value of [ ]<sup>a,c,e</sup> lbs was used.

As an example, for the NOP Low  $T_{avg}$  condition at Millstone Unit 3, the end cap load due to the pressure acting on the tube is [ ]<sup>a,c,e</sup> lbf. Assuming the minimum value of pull out force from the test data and an average dead weight of the tube straight leg, the applied end cap load that must be balanced by the distribution of contact pressure between the tube and the tubesheet is equal to [ ]<sup>a,c,e</sup> lbf - [ ]<sup>a,c,e</sup> lbf - [ ]<sup>a,c,e</sup> lbf, or [ ]<sup>a,c,e</sup> lbf.

Using the RCL to reduce the end cap load on the tube has been shown to be conservative in a direct comparison with the alternative method, that is, converting the pull out force to a residual contact pressure and including it in the integration for  $H^*$ . Further, reduction of the applied load does not affect the contact pressure distribution between the tube and the tubesheet. For instance, if there was a combination of material properties and operating conditions that resulted in a very small or zero value of contact pressure for some portion of the tube below the top of the tubesheet, the application of RCL as a reduction of applied load does not change the predicted contact pressure. The first point of positive contact between the tube and the tubesheet is still determined based on the structural analysis of the tubesheet. An additional benefit from applying the RCL as a reduction to the applied end cap load is that there is no need to develop a distribution of the residual effect of the tube installation as a function of elevation in the tubesheet. The test results can be directly used to determine the pre-load on the tube.

A value of  $H^*$  is determined for any value of RCL for the limiting SG operating condition at the limiting TS radius and sector in the bundle. The process for determining the  $H^*$  value is shown in the following flow chart.



The result of this process is a surface of the response in  $H^*$  to changes in RCL and  $\alpha_{srss}$  (the square root of the sum of squares of the specific variations in CTE from one MC simulation). If the values for RCL are normalized to an assumed value, say [ ]<sup>a,c,e</sup> lbf, and the values of  $H^*$  are taken as the change in  $H^*$  relative to the value of  $H^*$  with an RCL of zero, the result is a non-dimensional surface that can be used in conjunction with a Monte Carlo analysis to determine the reduction in  $H^*$  due to the inclusion of RCL. Figure RAI18-9 is a surface plot of the change in the Model F  $H^*$  values as a function of RCL and  $\alpha_{srss}$ . Figure RAI18-10 is a surface plot of the change in the Model D5  $H^*$  values as a function of RCL and  $\alpha_{srss}$ .

Figure RAI18-9 and RAI18-10 illustrate that the effect of including the RCL as a reduction in the applied tube end cap load is dependent on both the  $H^*$  value and the material parameters. This is a logical result because if  $H^*$  is small (correlated to a small value of  $\alpha_{srss}$ ) then the effect of RCL should also be small because there is enough contact pressure to maintain equilibrium with the load on the tube regardless of the value of RCL. However, if  $H^*$  is large, because of some combination of material parameters or operating conditions that produce less contact pressure between the tube and the tubesheet, then the presence of any value of RCL has a much larger effect on  $H^*$ . For example, in Figure RAI18-8, assuming an RCL ratio of 1 (RCL ~ [ ]<sup>a,c,e</sup> lbf) with an  $\alpha_{srss}$  of 0 results in a very small correction to the final  $H^*$  distance on the order of [ ]<sup>a,c,e</sup> inch. However, if the RCL ratio is equal to 1 and  $\alpha_{srss}$  is equal to 5, the change in  $H^*$  is 2 or more inches, or a factor of 4 greater.

The effects of residual contact pressure (RCP) are implemented in the extreme-value simulation model using a functional representation of the developed steam generator-specific data described above. The function describes the correction term (  $\Delta H^*$  ) in terms of two variables:

$$\Delta H^* = G(\text{RCL}, \text{Alpha})$$

Where:

RCL = Residual contact load

Alpha = Effective thermal expansion coefficient

A typical description of this surface is shown in Figure RAI18-8. As can be seen from the figure, the behavior of the function is somewhat complex. The value of the function generally increases with both independent variables which makes some simplification possible based on a conservatively low estimate of one of the variables.

A lower limit constant value of RCL was chosen, in part to assure a more robust computational behavior in the implementation of the RCL effects modeling. The value cited in the response to part F of this RAI corresponds to a RCL ratio of approximately 1.0. Figure RAI18-11 shows the resulting  $\Delta H^*$  as a function only of Alpha. This and corresponding functions for each steam generator class, were implemented in the full simulation model.

The actual implementation into the simulation model was straightforward. Since the RCL correction is subtractive, the computation of Alpha and  $\Delta H^*$  is performed directly after the computation of  $H^*$  within the simulation. The computation is performed for all tube/tubesheet combinations in the entire simulation process. The reduction in the computed extreme values of  $H^*$  is typically on the order of 1-2 inches, and is steam generator-specific.

It is important to note that the change in  $H^*$  due to the crevice pressure adjustment, thermal offset and BET is already included in the analysis. The distribution of the crevice pressure adjustment shown in Figure 8-1 of the  $H^*$  reports is not required in this instance. That is because the reduction of the end cap load changes how the  $H^*$  value will react to a change in contact pressure distribution. So it is necessary to incorporate the change in  $H^*$  due to the RCL reduction of the end cap load with the crevice pressure adjustment to produce a net change in  $H^*$  using consistent methods. Therefore, the result of using the RCL surface to determine the change in  $H^*$  is the net effect of all adjustments to  $H^*$  and no further corrections are required.

Table RAI18-05(c) summarizes the effects of the application of residual pull out load (RCL) on the value of  $H^*$ . When the 5/50 pull out force from the test data is applied using the Monte Carlo approach that samples from Figure 8-5 in the reports and also from the RCL correction surface discussed above, the values of  $H^*$  are reduced approximately 1 to 2 inches for all affected models of SGs. The resulting values of  $H^*$  for the Model F and Model D5 SGs are further reduced by application of the updated NOP temperature distribution correction factor. As can be seen from Table RAI18-5, the recommended values of  $H^*$  for the respective SGs in the applicable reports exceeds the values determined when the conservative factors inherent in the recommended values are considered in the analysis.

### G. Limiting Condition for H\*

This issue is also addressed by the response to RAI#4.

H\* is defined as that location within the span of the tubesheet expansion region at which the forces between the tube and the tubesheet resulting from all loading conditions (pressure and thermal) are equal to the applied loads (end-cap loads) under the most limiting conditions (normal operating or design basis accident) with required factors of safety. The forces resisting tube pull-out result from the contact pressures between the tubes and the tubesheet. Tables 6-25 and 6-26 in WCAP-17091-P (44F) and WCAP-17092-P (51F) summarize the contact pressures and cumulative pull-out resisting forces calculated for the normal operating and steam line break conditions for various radial positions on the tubesheet. In all cases, the pull-out resisting forces under normal operating conditions are less than those under steam line break conditions. Therefore, as the end cap load with required factor of safety for normal operating conditions exceeds the end cap load for a postulated SLB event with the required factor of safety, the limiting value of H\* is always determined by the normal operating conditions.

The probabilistic analysis of H\* does not change this conclusion. The probabilistic analysis considers the principal variables that affect the structural interaction between the tube and the tubesheet. There is no functional relationship between the loads applied to the structure and the variables that affect the structural response. For any given combination of the principal variables that affect the structural interaction, the relative response of the structure to the specific applied loading condition (NOP or SLB) will be the same. Therefore, it is concluded that the 95/50 value determined for H\* for a postulated steam line break event would be bounded by the 95/50 value determined for H\* for normal operating conditions.

### H. Summary and Conclusions

The recommended values of H\* for the different models of SGs as provided in the respective reports (WCAP-17071-P [Model F], WCAP-17072-P [Model D5], WCAP-17091-P [Model 44F] and WCAP-17092-P [Model 51F]) were based on very conservative assumptions. Additional analysis, using Monte Carlo techniques and the variables interaction surfaces defined in Figure 8.5 of the reports, was performed to quantify the conservatism of these assumption with regard to the recommended values of H\* for the different models of SGs. Four principal conservatisms were evaluated:

1. The number of tubesheets was limited to a number less than the number of tubes in the bundles of the respective SG models. The total population of SGs among the H\* candidate plants is 60 including 4 different models of SGs. The number of tubesheets simulated for each SG was limited to 10,000.
2. Instead of assuming that all tubes in the bundle are located at the single worst case position that defines the recommended value of H\*, the bundles were divided into sectors. This approach retains significant conservatism because the maximum value

of  $H^*$  in each sector was used for the analysis and the limiting interaction variances were applied to all sectors. It is noted that all sectors considered are located in the limiting azimuthal sector of the tubesheet as discussed in Section 6.2.3 of the reports.

3. The conservative adder for NOP tubesheet thermal distribution was re-evaluated by including the thermal distribution directly in the structural analysis. The resulting adders to  $H^*$  are realistic values that reflect the actual response of the tubesheet structure to the applied thermal distribution. This applies only for the Model F and Model D5 SGs because the updated thermal correction factor is already included in the recommended  $H^*$  values for the Model 44F and 51F SG. Modification of the thermal distribution factors does not change that the NOP conditions are the limiting conditions that determine the value of  $H^*$ .
4. Based on pull out tests performed during the  $H^*$  development, the effect of the minimum measured pull out forces at 0.25 inch of tube travel on the values of  $H^*$  were evaluated. The pull out force data was applied directly as a reduction of the applied loading instead of utilizing an intermediate conversion of pull out force to contact pressure. This approach is more direct, and its specific application is conservative because the 5/50 value of pull out force was used. In reality, much greater values of pull out force were demonstrated in the tests at 0.25 inch travel. Still greater pull out forces were observed during the tests for greater values of tube travel, even exceeding the limiting applied design loads for  $H^*$ . Therefore, the application of the 5/50 value of pull out force from the tests is conservative.

After addressing the above factors, the final values of  $H^*$  are significantly less than the values recommended for all affected models of SGs. Therefore, the recommended values of  $H^*$  for each of the models of SG are shown to be conservative.

RAI#20 References:

- RAI18-1 LTR-SGMP-09-92; "Tubesheet Sector Definition for  $H^*$  Revised Probabilistic Analysis," July 10, 2009.
- RAI18-2 LTR-SGMP-09-98, " $H^*$  Pull Test Program Summary," July 27, 2009.

**Figure RAI18-1  
Model F**



a,c,e

**Figure RAI18-2  
Model D5**



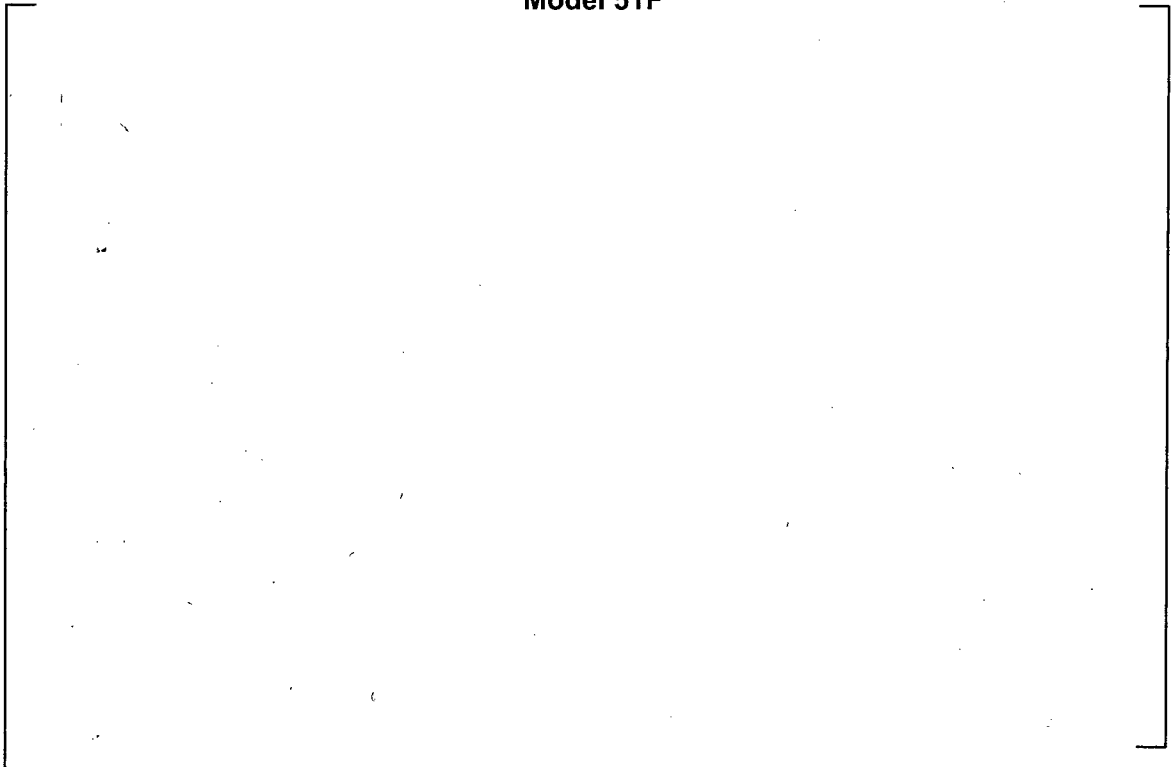
a,c,e

**Figure RAI18-3  
Model 44F**



a,c,e

**Figure RAI18-4  
Model 51F**



a,c,e

**Figure RAI18-5**  
**Monte Carlo Simulation Process**

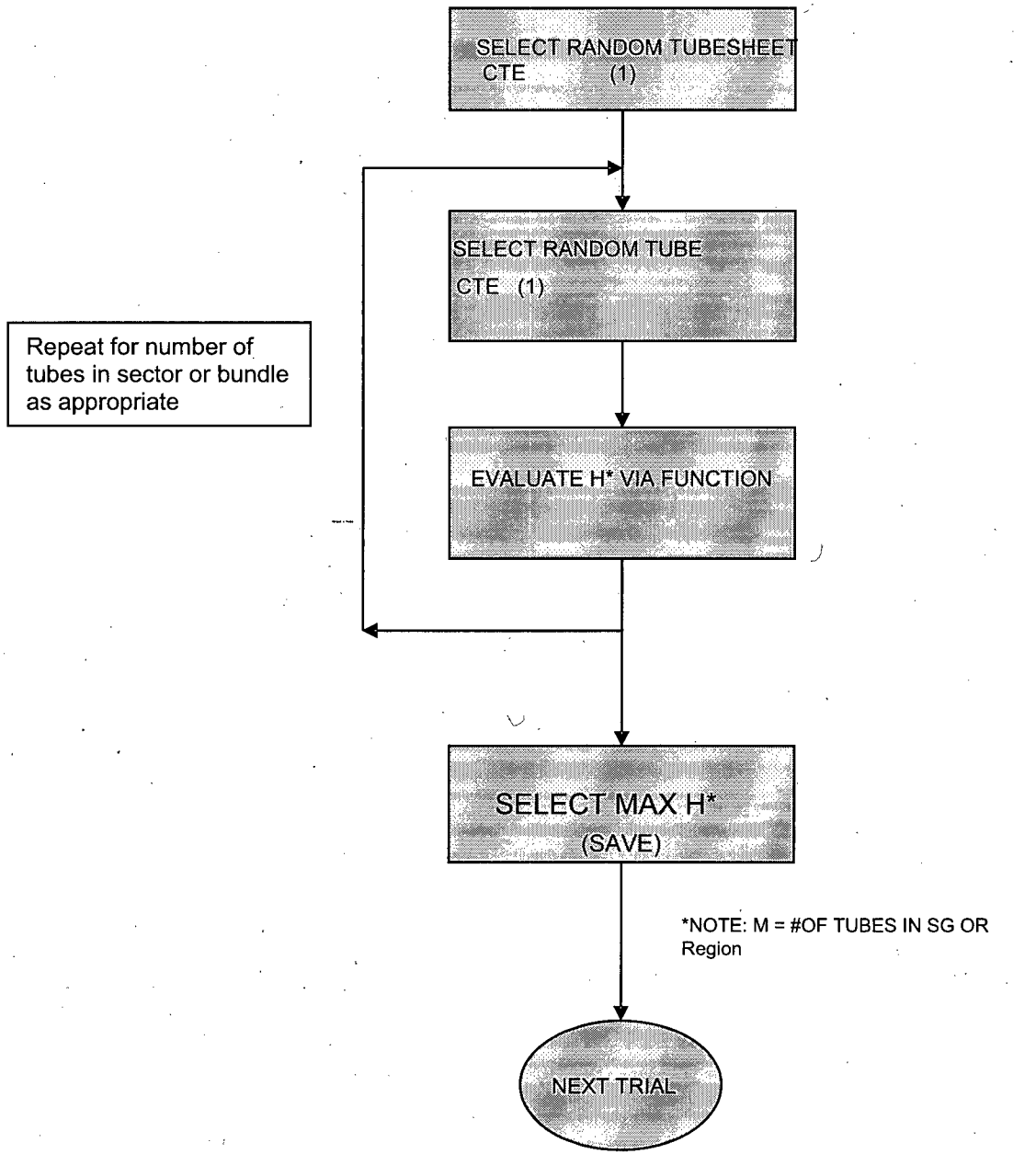


**Figure RAI18-6**  
**Model F: Interaction Profiles for Sector-Base Sampling**

a,c,e



**Figure RAI18-7**  
**Model D5: Interaction Profiles for Sector-Base Sampling**

a,c,e



**Figure RAI18-8**  
 **$\Delta H^*$  for Various Values of  $\alpha_{srss}$  and RCL Ratio**  
( $a = \alpha_{srss}$ ,  $RCL_{ref} = 800\text{lb}$ )

a,c,e



**Figure RAI18-9**  
**Model F Response Surface for the Change in  $H^*$  as a Function of RCL and  $\alpha_{srss}$**



**Figure RAI18-10**  
**Model D5 Response Surface for the Change in  $H^*$  as a Function of RCL and  $\alpha_{srss}$**



**Figure RAI18-11**  
**Change in  $H^*$  as a Function of  $\alpha_{srss}$**



**Table RAI18-1  
Model F SG Sector Populations**

Model F									
TS Radius	0-11	11-17	17-23	23-29	29-35	35-41	41-47	47-53	53-60
Max Mean H*			[ ] <sup>a,c,e</sup>						
Max Mean H*Factor	[								]
Number of Tubes	[								]

a,c,e

**Table RAI18-2  
Model D5 SG Sector Populations**

Model D5									
TS Radius	0-6	6-12	12-18	18-24	24-30	30-36	36-42	42-48	>48
Max Mean H*					[ ] <sup>a,c,e</sup>				
Max Mean H*Factor	[								]
Number of Tubes	[								]

a,c,e

**Table RAI18-3  
Model 44F SG Sector Populations**

Model 44F									
TS Radius	<9	9-15	15-21	21-27	27-33	33-39	39-45	45-51	>51
Max Mean H*			[ ] <sup>a,c,e</sup>						
Max Mean H*Factor	[								]
Number of Tubes	[								]

a,c,e

**Table RAI18-4  
Model 51F SG Sector Populations**

Model 51F								
TS Radius		<9	9-17	17-24	24-32	32-41.85	41.85-52.52	>52.52
Max Mean H*				[ ] <sup>a,c,e</sup>				
Max Mean H*Factor		[						]
Number of Tubes		[						]

a,c,e

**Table RAI18-5  
Results of Monte Carlo Sampling and Valuation of Conservatism**

SG Model	Report Case S-2			Surface Sampling from Figure 8-5 of the Report(s) with Limited Number of Tubesheets and Sector Based Approach		
	95/50 (inch)	P <sub>crev</sub> (inch)	Final H* (inch)	95/50 (inch)	P <sub>crev</sub>	Final H*
F			11.2			
D5			13.8			
44F			13.31			
51F			13.14			

(a) Sampling from Interaction Surface Figure 8-5

SG Model	H* After Surface Sampling	Correction for NOP Thermal Distribution			Surface Sampling, Limited Tubesheets Corrected for NOP Thermal Offset		
	95/50 H* (inch)	Original (inch)	Revised (inch)		95/50 H* (inch)	P <sub>crev</sub> (inch)	Final H* (inch)
F				=			
D5				=			
44F				=			
51F				=			

SG Model	Surface Sampling from Figure 8-5 of the Report(s) with Limited Number of Tubesheets	□ H* for Minimum Pull Out Force (inch)	Final H* After Including Minimum Pull Out Force	Correction for NOP Thermal Distribution	Final H* (inch)
	95/50 (inch)	NA	(95/50) (inch)	(inch)	(95/50) (inch)
F					
D5					
44F					
51F					

(c) Adjustment for Residual Contact Pressure

Notes:

1. The value of H\* before correction for P<sub>crev</sub> is used because the interaction surface is based on the H\* value without the P<sub>crev</sub> adjustment.

**APPENDIX A**  
**SUMMARY OF 2008-2009 PULL OUT TEST PROGRAM IN SUPPORT OF H\***

## Abstract

Steam generator tubes made of Alloy 600 (A600) were hydraulically expanded in AISI 1018 cold rolled, carbon steel, cylindrical collars, which simulate the steam generator tubesheet, and then pulled by an MTS machine out of the collars in order that tube-to-tubesheet joint (hereafter referred to as "joint" or "the joint") strength might be measured. Nine tubes from each of Model F, Model D5, and Model 44F tubes were tested for pull out resistance, three at each expansion length (13 inches, 15 inches, and 17 inches). The pull out test parameters were established so that the results can be considered to be prototypic of the as-built condition of the steam generators within the H\* fleet (i.e., the test specimens were designed and manufactured to be within the manufacturing tolerances for dimensional variations, material properties, and process control parameters for the H\* fleet steam generator tube joints).

The pull force capacity associated with 0.25 inch tube displacement relative to the tubesheet ranged from approximately [ ]<sup>a,b,c</sup> lbf to approximately [ ]<sup>a,b,c</sup> lbf. The values for the maximum pull force ranged from approximately [ ]<sup>a,b,c</sup> lbf to approximately [ ]<sup>a,b,c</sup> lbf within a maximum relative displacement of 2.02 inches, regardless of the tube outside diameter or hydraulic expansion length[10].

Monte Carlo simulations were performed in order to better define a 5/50 value of pull force, which is based on the presence of residual contact pressure, for use in the H\* analysis. The minimum 5/50 value of the pull force has been observed to be [ ]<sup>a,b,c</sup> lbf, and this corresponds very well to the lowest recorded pull force from the testing.

## Introduction

H\* (pronounced "H star") is the length of hydraulically expanded steam generator tube that must remain intact within the tubesheet in order for the joint to resist pull out and leakage due to normal operating or accident conditions. The basis of the H\* program is such that residual contact pressure between the tube and the tubesheet is not considered in the structural or leakage calculations. Hence, any indication of joint strength from test program data is a measure of conservatism contained in the H\* analysis.

Westinghouse commenced a test program in which steam generator tubes were hydraulically expanded in cylindrical collars representing the tubesheet and pulled to measure joint strength. There were no tack expansions, hard rolled expansions, or welds to consider. Initially, the H\* program applied to Model F steam generators, but it has been expanded to include Model D5, Model 44F, and Model 51F steam generators. The following sections of this document summarize the results of this test program.

## Experimental

### *Materials*

Alloy 600 tubes representing those from Model F, Model D5, and Model 44F steam generators were cut to seventeen, nineteen, and twenty-one inch lengths. The Model F steam generator tube was taken from Heat NX7368 and is believed to be mill annealed. The Model D5 and Model 44F steam generator tubes were taken from Heats 2645 and 752570, respectively, and both are in the thermally treated condition. The chemical analyses for these materials are contained in Table 1 and the mechanical properties are contained in Table 2. Note that the mechanical properties listed in Table 2 are from the providers' certifications and from testing done at Industrial Testing Laboratory Services (ITLS). The latter tests were done according to ASTM E8-08 [1].

The cylindrical collars representing the tubesheet were cut to fifteen, seventeen, and nineteen inch lengths from AISI 1018 cold-rolled, carbon steel. The chemical analysis and mechanical properties of Heat 777553 are contained in Tables 3 and 4, respectively. It should be noted that the outer diameters of the collars were chosen to be [ ]<sup>a,c,e</sup> times the outer diameter of the tubes so that the stiffness of the actual tubesheet plate is correctly represented. This ratio is based on the work of Middlebrooks et al. [2].

The list of tube and collar pairings is presented in Table 5. The indices are to be read as follows: the first two indices refer to the overall length of the tube or collar, the second three indices refer to the nominal OD of the tube or the nominal ID of the collar, and the last two indices refer to the sample number. The "A" suffix refers to a second manufacture of the same sample. It should be noted that two of the tests done were originally planned to be diagnostic in nature. The collars were rebores so that they would contain an inner diameter surface finish of 250 micro-inch rms max. vice an engineered finish of 250 micro-inch rms. These collars were from Heat 730492, and its properties are also contained in Tables 3 and 4.

### *Pre-Expansion Measurements*

The inner diameters of the collars were measured by the vendor (Tooling Specialists, Inc., Latrobe, PA) at distances corresponding to 25%, 50%, and 75% of the length of the collar, relative to the serialized end. Two measurements, ninety degrees apart, were made with an intramic at each location, and the two values at each location were then averaged. Surface roughness measurements were also made by the vendor at the 25% and 75% distances using a profilometer. Lack of an extension device for the profilometer did not permit roughness measurements at the 50% distance.

After being cut, the inner and outer diameters of the A600 tubes were measured by an intramic and the surface roughness of the outer diameters were measured with a profilometer at Westinghouse RRAS (R. Fetter). The diameter measurements were made, relative to the non serialized end, at distances that overlap those made in the collars. Thus, the 25%, 50%, and 75% distances correspond to those percents of the collar's length, not the tube's length. The

inner and outer diameters were also measured at two points for each distance, ninety degrees apart, and the two values were averaged.

### *Hydraulic Expansion*

The tubes were inserted in the collars such that the non serialized end of the tube was flush with the serialized end of the collar. Thus, the serialized end of the tubes protruded from the collars by two inches. The tube/collar assemblies were then inserted on an O-ring mandrel, which was connected to a screw drive pressurizing system. The tube/collar assemblies were pressurized to a nominal pressure of [ ]<sup>a,c,e</sup> psi per Process Specification 81013RM, Revs. 4 through 10 applicable [ ]. The nominal expansion pressure was typically exceeded, but the excess was less than [ ]<sup>a,c,e</sup> psi, which is within the tolerance of the equipment ([ ]<sup>a,c,e</sup> psi). This work was performed at Westinghouse's Waltz Mill facility by M. Gallik and A. Stett. The details of the tube expansion test plan are contained in [4].

### *Post-Expansion Measurements*

After the hydraulic expansions were completed, measurements of the tubes' inner diameters were again made with an intramic by Westinghouse RRAS (R. Fetter), and eddy current measurements of individual tube/collar assemblies were performed by Westinghouse with the 3-coil +point and standard bobbin coil probes (R. Pocratsky). Once the measurements were complete, the end caps were welded to the tubes at their serialized ends. The tube/collar assemblies with the end caps welded on are shown in Figures 1 through 9.

### *Heat Treatment*

Real tubesheet Z-channels are given a post-weld heat treatment (PWHT) with an electric "belt" wrapped around the channel. In order to simulate that PWHT, the tube/collar assemblies were heat treated in air at nominally [ ]<sup>a,c,e</sup> °F for nominally 3 hours in a Blue M furnace, Model B-2730-Q. This was accomplished at Westinghouse's Churchill site (A. Neville). The actual PWHT temperature applied to the Z-channel is 1150°F. However, it was determined [5] that [ ]<sup>a,c,e</sup> °F is higher than the vast majority of the tubes will experience by the PWHT.

### *Instrumentation*

Prior to testing, the exposed ends of the tubes were fitted with two 350 ohm, quarter bridge strain gauges. Additionally, two linear variable differential transformers (LVDTs) were used in order to model the displacement of each end of the tube relative to the collar. All electronic readouts (load cell, cross-head displacement, displacements of the LVDTs, and strains) were recorded on a Strainbook data acquisition system.

### *Pull Tests*

The pull tests were performed according to the test program described in [6] in air and at room temperature. The mechanical operation of the MTS system was performed by M. Gallik and

A. Stett, while the electronic recording of the data was done by A. Roslund, all of whom work at Westinghouse's Waltz Mill facility. The sequence of the testing was activation of the Strainbook and confirmation of its recording, initiation of the pull test, continuation of the pull test until approximately two inches of cross-head displacement were achieved, and finally, the cessation of pull testing and electronic recording of data.

#### *Post-Test Evaluations*

After the pull testing was complete, another set of eddy current measurements were made at Westinghouse's Waltz Mill facility by R. Pocratsky. Again, both the 3-coil +point and standard bobbin coil probes were used.

#### *Monte Carlo Analysis*

In support of the test program, Monte Carlo simulations were run, based on means and standard deviations from the test data, in order to determine a 5/50 bound on pull force. The simulations were performed in two ways and on a tube OD basis: one simulation considered the thirteen inch expansions only, and the other simulation considered all nine tests together, ignoring expansion length difference. Seven distributions were chosen and the fitting parameters set so that the resulting distribution has the mean and standard deviation of the test data. The first was a truncated normal distribution. The other six were chosen so that their domains span zero to positive infinity, their domains are continuous, and fitting parameters are within their allowable ranges. They were lognormal, Erlang, Gamma, inverse Gaussian, Pearson Type V, and Weibull. In each simulation, 100,000 iterations were run.

#### **Discussion of Key Parameters**

Tube pull out force capacity (based on residual contact pressure) can be derived from the measured pull out forces from the test that simulate the as-manufactured condition of the steam generators. All of the tests performed to date have demonstrated that a positive value of residual contact pressure exists after the hydraulic expansion process. However, the results from these tests depend on a number of factors including dimensional variations of the tubes and tube collars, surface finish variations, potential manufacturing artifacts on the tubesheet (collar) bore, tube joint process variables, and material properties of the test specimens. The key items identified are addressed below.

The NRC staff has raised the concern that sufficient information must be provided to adequately characterize the potential range in values of residual contact pressure between the tube and the tubesheet (due to the hydraulic expansion process) which may be encountered within the whole plant [7]. At that time, only limited pull out data existed upon which the residual contact pressure was estimated. The staff pointed out [7] that the residual contact pressure, and thus the residual load capacity, is highly sensitive to several parameters including hydraulic expansion pressure, tube yield strength, tube material strain hardening properties, and initial (pre-expansion) gap between the tube and the tubesheet. The NRC staff further pointed out in [7] that additional information was necessary to establish whether the pull out test specimens

adequately envelop the range of values of those parameters that may be encountered in the as-built steam generators.

Consequently, two actions have been taken to address the NRC staff concerns. First, an analysis was performed to identify the key parameters that affect the residual contact pressure and to quantify the effects of uncertainties. Secondly, a new pull out test program was initiated to provide test results that can be directly compared to the key parameters as identified by analysis in support of the development of the  $H^*$  criterion.

The analysis model used to evaluate the residual contact pressure was a two-dimensional, plane strain, finite element model using the ANSYS computer code as described in Section 7 of [8]. Based on a review of Table 7-3 of [8], the key parameters impacting pull out force capacity are:

- Initial tube gap
- Tube yield strength
- Tube joint expansion pressure
- Strain hardening.

Other parameters important to pull out force capacity not considered in the analytical model are surface roughness and variations in the diameter of the tubesheet bore (waviness).

Table 6 provides a comparison of the as-built to as-tested parameters in the new test program. Based on a review of Table 6, several points can be made regarding the key parameters of the pull out testing.

- It is expected that standard gun drilling practices used in the manufacture of steam generators would typically result in nominal gaps between the tube and tubesheet. No special controls were placed on the initial gap size as the test program was meant to be as prototypic as possible.
- The yield strength of the tubes used for the test specimens simulating the as-built configuration of the Model F and Model D5 steam generators was conservatively high compared to the as-built mean values ( $[ ]^{a,b,c}$  ksi vs.  $[ ]^{a,b,c}$  ksi), because higher yield strengths result in less tube deformation for a given expansion pressure. The yield strength for the tubes used for the Model 44F steam generators was slightly less than the as-built mean yield strength ( $[ ]^{a,b,c}$  ksi vs.  $[ ]^{a,b,c}$  ksi).
- The expansion pressure used in the manufacture of the test specimen was consistent with what is specified in [3] and is directly applicable to the as-built conditions of the steam generators in the  $H^*$  fleet.
- The surface roughness of the tubes outer diameters and the collars inner diameters was well within the tolerances of the as-built conditions of the steam generators in the  $H^*$  fleet.
- The mechanical properties of the materials used for the test specimens are within ASME Code specifications for the respective materials. Thus, use of the ASME Code values for the key parameters of the  $H^*$  study is valid.

Other differences between the materials used for the test specimens for the pull out tests are addressed below.

The use of mill annealed tube vice thermally treated tubing for the Model F specimens has been evaluated and found to be acceptable. For room temperature testing, the key material property affecting the residual contact pressure is yield strength. The difference between yield strength of mill annealed material and thermally treated material is presented in Table 7 and further discussed below. Based on the similarity of mechanical properties between the two materials, it is concluded that there is no adverse effect on the test results. The yield strength value used for the Model F test specimens was [ ]<sup>a,b,c</sup> ksi, which would result in a reduction of residual contact pressure [9].

The test specimen collar is manufactured from AISI 1018 cold rolled, carbon steel. The material used in the H\* fleet is actually A508 Class 2a carbon steel. The use of the different material does not adversely affect the pull test results since the primary property of the material in this case is elastic flexural rigidity of the tubesheet (i.e., elastic modulus), and since the tube expansion operation does not produce significant yielding of the tubesheet (the yield strength of the AISI 1018 cold rolled, carbon steel at room temperature is ~83 ksi), the use of higher strength material for the collar is acceptable (see pp. 8-9 of [8]). Thus, it is concluded that the pull out testing is representative of the as-built condition of the steam generators in the H\* fleet.

## Results

Table 8 shows the results of the pull tests, while Table 9 through Table 15 shows the results of the Monte Carlo simulations. The latter results are calculated for the pull out force at 0.25 inch displacement.

## Discussion

Discussion between Westinghouse and the NRC staff has led to the decision that the pull out force of record should be the pull out force at 0.25 inch cross head displacement. The following discussion and analysis will, therefore, be based on that quantity.

Figure 10 plots the pull out force as a function of the collar ID surface roughness. The graph also provides information on the tube expansion lengths and the tube diameters that were tested. Intuitively, it would be expected that tube pull out force would increase with increasing tube diameter (which provides greater surface area in contact), increasing tube expansion length (which does the same thing), and increasing surface roughness. However, the results in Figure 10 do not necessarily support these assumptions. The highest pull out force for 0.25 inch cross head displacement (approximately [ ]<sup>a,b,c</sup> kips) occurred for both a test specimen with the largest tube OD, the largest collar ID surface roughness, and the smallest expansion length, as well as for a test specimen having the largest tube OD, one of the lowest collar ID surface roughness values, and the smallest expansion length. The next highest pull out force ([ ]<sup>a,b,c</sup> kips) occurred for tubes with varying degrees of collar ID surface roughness, for all tube ODs, and for all expansion lengths. The lowest pull out force ([ ]<sup>a,b,c</sup> lbf) occurred for a test

specimen with a 0.75 inch tube OD, a collar ID surface roughness of ~ 50 micro-inch (rms), and an expansion length of 15 inches. The lowest pull out force for a Model F test specimen was less than [ ]<sup>a,b,c</sup> kips. This specimen had a collar ID surface roughness less than 40 micro-inch (rms) and an expansion length of 13 inches. The lowest pull out force for a Model 44F specimen was less than [ ]<sup>a,b,c</sup> kips. This specimen had a collar ID surface roughness of less than 40 micro-inch (rms) and a tube expansion length of 15 inches.

Similarly, the pull test results are shown as a function of tube expansion length in Figure 11. These results also show the lack of correlation between pull out force and tube OD and expansion length.

The pull force necessary to move a tube in the collar is a consequence of three main factors: the residual contact pressure due to the hydraulic expansion, the surface roughness of the tube and the collar, and any geometric irregularities due to machining of the tube and collar, which are then subject to hydraulic expansion. As shown by analysis, the initial gap between the outer diameter of the unexpanded tube and the tubesheet bore hole can adversely affect the resulting residual contact pressure. Small variations along the length of the collar ID (waviness) due to the gun drilling process are significant contributors to the pull out resistance. Geometric irregularities are present as initial gaps between the tube and the collar and as bulges in the tubes. One possible explanation for the significant variation in the test results may be that the waviness was not well profiled due to the difficulty of quantifying this variable. Nonetheless, the pull out test results do appear to be consistent with the expected as-built condition.

Recall that nine pull out tests were performed for each tube OD. Analysis of variance (ANOVA in statistics) is a collection of statistical models and their associated procedures in which the observed variance is partitioned into components due to different explanatory variables. In its simplest form, ANOVA provides a statistical test of whether the means of several groups of data are all equal. One such method is called the F-test. Therefore, the F-test was conducted on the pull out test capabilities comparing the variance of each set of 9 samples for each tube diameter using Microsoft EXCEL. The F-test was used to determine whether or not there was any statistical difference between tube OD and pull test results. The answer was that it cannot be concluded that there is any difference in the variance between each sample set and that the means for tube pull out force for each of the outer diameters may be equal. Therefore, it is judged that all of the data can be considered to be one data set.

However, the NRC staff stated in [7] that there is a need to adjust the pull out data so as to produce an estimate of the residual contact pressure that is conservative for the range of H\* values that are being proposed. In order to address this concern for the new pull out test data (i.e., the expansion length of some of the pull out test data exceed the calculated H\* values), the sample sets for the different tube ODs were not combined. They were separated by expansion length, even though the F-test results suggest that the mean values of the tube pull out capacity are the same for different tube ODs and considering variations in expansion length and surface roughness.

To investigate this further, the Monte Carlo simulations were performed. Each tube OD was broken up into two sets (13 inch expansion length only and all expansion lengths) and distributions were chosen based on the criteria previously defined. Using the calculated means and standard deviations from each data set, the fitting parameters for the seven distributions chosen were calculated. Note that the fitting parameters for the normal and lognormal distributions are simply the mean and standard deviation. In each case the 5/50 value was recorded, and the lowest of these corresponded to a pull force of [ ]<sup>a,c,e</sup> lbf. This was calculated for the Model F tube, 13 inch expansion length only, and using the Weibull distribution (see Table 15). This value is very consistent with the lowest actual pull force from the test data ([ ]<sup>a,b,c</sup> lbf).

## Conclusion

Based on the results of the pull tests and Monte Carlo analyses, it is concluded that the end cap load used in the H\* analysis can be conservatively reduced by [ ]<sup>a,c,e</sup> lbf. H\* can then be recalculated accordingly.

## References

- (1) ASTM E8/E8M-08, "Standard Test Method for Tension Testing of Metallic Materials," West Conshohocken: ASTM International, 2008.
- (2) W. B. Middlebrooks, D. L. Harrod, and R. E. Gold, *Nuclear Engineering and Design* 143, 1993, pp. 159-169.
- (3) Process Specification 81013RM, "Hydraulic Tube Expansion," Rev.4 through Rev. 10, February 1, 1979 through July 24, 1981.
- (4) J. T. Kandra, TP-CDME-08-3, "Test Procedure for Tube Expansion for H\*," August 25, 2008.
- (5) D. L. Harrod, WNEP-9725, "The Westinghouse Tube-to-Tubesheet Joint Hydraulic Expansion Process," July 1997.
- (6) J. T. Kandra, TP-CDME-08-1, "Pull-Out Test Program for H\*," August 25, 2008.
- (7) NRC Letter, "Wolf Creek Generating Station – Withdrawal of License Amendment on Steam Generator Tube Inspections (TAC No. MD0197)," United States Nuclear Regulatory Commission, Washington, D.C., February 28, 2008.
- (8) WCAP-17071-P, "H\*: Alternate Repair Criteria for the Tubesheet Expansion Region in Steam Generators with Hydraulically Expanded Tubes (Model F)," April 2009.
- (9) DP-SGDA-05-2, "Data Package for H-Star Pull Test of 7/8 Inch Tubing form Simulated Tubesheet, PA-MS-0199 WOG Program for Steam Generator Models 44F and 51F," November 2005.
- (10) LTR-SGMP-09-98, "H\* Pull Test Program Summary," Westinghouse Electric Company LLC, July 27, 2009.

**Table 1**  
**Chemical Analyses of the A600 Materials Used in This Test Program**

Steam Generator Model	F	D5	44F
Chemical Analysis Source	Plymouth Tube Co. Salisbury, MD	Huntington Alloys, Inc. Huntington, WV	AB Sandvik Steel
Heat	NX7368	2645	752570
Element (w/o)			
C	0.04	0.033	0.025
Mn	0.41	0.34	0.79
P	N/A	0.007	0.009
S	0.001	0.001	0.002
Si	0.30	0.09	0.33
Cr	14.87	15.44	16.60
Ni	76.21	75.45	72.45
Cu	0.15	0.23	0.010
Co	0.04	0.04	0.011
Fe	7.98	8.42	9.29
B	N/A	0.003	N/A

**Table 2**  
**Mechanical Properties of the A600 Materials Used in This Test Program**

Steam Generator Model	Heat	Mechanical Property Source	$\sigma_y$ (psi)	$\sigma_{UT}$ (psi)	Elongation (%)
F	NX7368	Vendor	59,700	106,600	39
		ITLS	58,000	108,000	32
D5	2645	Vendor	43,000	97,000	41.5
		ITLS	54,000	110,000	35
44F	752570	Vendor	47,500	101,700	45.5
		ITLS	46,000	101,000	40

**Table 3**  
**Chemical Analyses of the 1018 Cold-Rolled, Carbon Steel Used in This Test Program**

Steel	Chemical Analysis Source	Heat	Element (w/o)				
			C	Mn	Si	S	P
AISI 1018	Steel Bar Corp. Greensboro, NC	777553	0.17	0.84	0.27	0.030	0.005
AISI 1018	Steel Bar Corp. Greensboro, NC	730492	0.18	0.79	0.22	0.030	0.010

**Table 4**  
**Mechanical Properties of the 1018 Cold-Rolled, Carbon Steel Used in This Test Program**

Steel	Heat	Mechanical Property Source	$\sigma_y$ (ksi)	$\sigma_{UT}$ (ksi)	Elongation (%)
AISI 1018	777553	DuBose National Energy Services, Inc. Clinton, NC	83.0	90.0	18
AISI 1018	730492	DuBose National Energy Services, Inc. Clinton, NC	67.5	79.3	25

**Table 5**  
**Steam Generator Tube and Collar Pairings Used in This Test Program**

Tube	Heat	Collar	Heat
17-688-01A	NX7368	15-699-01A	777553
17-688-02A	NX7368	15-699-02A	777553
17-688-03	NX7368	15-699-03A	777553
19-688-01	NX7368	17-699-01A	777553
19-688-02	NX7368	17-699-02A	777553
19-688-03	NX7368	17-699-03A	777553
21-688-01	NX7368	19-699-01A	777553
21-688-02	NX7368	19-699-02A	777553
21-688-03	NX7368	19-699-03A	777553
17-750-01A	2645	15-762-01A	777553
17-750-02A	2645	15-762-02A	777553
17-750-03	2645	15-699-03	730492
19-750-01	2645	17-762-01A	777553
19-750-02	2645	17-762-02A	777553
19-750-03	2645	17-762-03A	777553
21-750-01	2645	19-762-01A	777553
21-750-02	2645	19-762-02A	777553
21-750-03	2645	19-762-03A	777553
17-875-01A	752570	15-888-01A	777553
17-875-02A	752570	15-888-02A	777553
17-875-03	752570	15-762-03	730492
19-875-01	752570	17-888-01A	777553
19-875-02	752570	17-888-02A	777553
19-875-03	752570	17-888-03A	777553
21-875-01	752570	19-888-01A	777553
21-875-02	752570	19-888-02A	777553
21-875-03	752570	19-888-03A	777553

**Table 6**  
**Residual Contact Pressure Critical Parameter Comparison**

Key Parameters	Model F		Model D5		Models 44F -51F		
	As-Built	As-Tested	As-Built	As-Tested	As-Built	As-Tested	
Average Initial Gap (inches)							a,c,e
Tube Yield Strength (ksi)							
Expansion Pressure (ksi)							
Tube Outer Diameter Surface Roughness $\mu$ in. rms							
Collar Inner Diameter Surface Roughness $\mu$ in. rms							
Tube OD (in)							
Collar ID (in)							

**Table 7**  
**Comparison of Yield Strength Between Mill Annealed and Thermally Treated Alloy 600**

	Alloy 600 Mill Annealed As-Tested	Alloy 600 Thermally Treated As-Built	
Minimum			a,c,e
Mean			
Maximum			
Standard Deviation			
Number of Tests	361	307	
Tube Size (OD)	7/8 inch	7/8 inch	
Data	Reference [1]	Reference [1]	
Yield Strength values are in units of ksi.			

**Table 8  
Results of the Pull Testing**

Tube ID	Heat	Collar ID	Heat	Load at 0.25" Displacement (kip)	Max. Load (kip)	Displacement at Max. Load (in)
17-688-01A	NX7368	15-699-01A	777553			
17-688-02A	NX7368	15-699-02A	777553			
17-688-03	NX7368	15-699-03A	777553			
19-688-01	NX7368	17-699-01A	777553			
19-688-02	NX7368	17-699-02A	777553			
19-688-03	NX7368	17-699-03A	777553			
21-688-01	NX7368	19-699-01A	777553			
21-688-02	NX7368	19-699-02A	777553			
21-688-03	NX7368	19-699-03A	777553			
17-750-01A	2645	15-762-01A	777553			
17-750-02A	2645	15-762-02A	777553			
17-750-03	2645	15-699-03	730492			
19-750-01	2645	17-762-01A	777553			
19-750-02	2645	17-762-02A	777553			
19-750-03	2645	17-762-03A	777553			
21-750-01	2645	19-762-01A	777553			
21-750-02	2645	19-762-02A	777553			
21-750-03	2645	19-762-03A	777553			
17-875-01A	752570	15-888-01A	777553			
17-875-02A	752570	15-888-02A	777553			
17-875-03	752570	15-762-03	730492			
19-875-01	752570	17-888-01A	777553			
19-875-02	752570	17-888-02A	777553			
19-875-03	752570	17-888-03A	777553			
21-875-01	752570	19-888-01A	777553			
21-875-02	752570	19-888-02A	777553			
21-875-03	752570	19-888-03A	777553			

a,b,c

**Table 9**  
**Monte Carlo Results for the Truncated Normal Distribution**

Distribution	Normal Distribution (truncated at 0)			
Case 1	Parameters to Define the Distribution			5/50 Pull Out Force (kip)
Model F 13" Expansion	Name	Mean	Stand. Dev.	[ ] <sup>a,c,e</sup>
	Symbol	$\mu$	$\sigma$	
	Value	[ ] <sup>a,c,e</sup>	[ ] <sup>a,c,e</sup>	
Case 2	Parameters to Define the Distribution			5/50 Pull Out Force (kip)
Model F All Expansions	Name	Mean	Stand. Dev.	[ ] <sup>a,c,e</sup>
	Symbol	$\mu$	$\sigma$	
	Value	[ ] <sup>a,c,e</sup>	[ ] <sup>a,c,e</sup>	
Case 3	Parameters to Define the Distribution			5/50 Pull Out Force (kip)
Model D5 13" Expansion	Name	Mean	Stand. Dev.	[ ] <sup>a,c,e</sup>
	Symbol	$\mu$	$\sigma$	
	Value	[ ] <sup>a,c,e</sup>	[ ] <sup>a,c,e</sup>	
Case 4	Parameters to Define the Distribution			5/50 Pull Out Force (kip)
Model D5 All Expansions	Name	Mean	Stand. Dev.	[ ] <sup>a,c,e</sup>
	Symbol	$\mu$	$\sigma$	
	Value	[ ] <sup>a,c,e</sup>	[ ] <sup>a,c,e</sup>	
Case 5	Parameters to Define the Distribution			5/50 Pull Out Force (kip)
Model 44F 13" Expansion	Name	Mean	Stand. Dev.	[ ] <sup>a,c,e</sup>
	Symbol	$\mu$	$\sigma$	
	Value	[ ] <sup>a,c,e</sup>	[ ] <sup>a,c,e</sup>	
Case 6	Parameters to Define the Distribution			5/50 Pull Out Force (kip)
Model 44F All Expansions	Name	Mean	Stand. Dev.	[ ] <sup>a,c,e</sup>
	Symbol	$\mu$	$\sigma$	
	Value	[ ] <sup>a,c,e</sup>	[ ] <sup>a,c,e</sup>	

**Table 10**  
**Monte Carlo Results for the LogNormal Distribution**

Distribution	Lognormal Distribution			
Case 1	Parameters to Define the Distribution			5/50 Pull Out Force (kip)
Model F 13" Expansion	Name	Mean	Stand. Dev.	[ ] <sup>a,c,e</sup>
	Symbol	$\mu$	$\sigma$	
	Value	[ ] <sup>a,c,e</sup>	[ ] <sup>a,c,e</sup>	
Case 2	Parameters to Define the Distribution			5/50 Pull Out Force (kip)
Model F All Expansions	Name	Mean	Stand. Dev.	[ ] <sup>a,c,e</sup>
	Symbol	$\mu$	$\sigma$	
	Value	[ ] <sup>a,c,e</sup>	[ ] <sup>a,c,e</sup>	
Case 3	Parameters to Define the Distribution			5/50 Pull Out Force (kip)
Model D5 13" Expansion	Name	Mean	Stand. Dev.	[ ] <sup>a,c,e</sup>
	Symbol	$\mu$	$\sigma$	
	Value	[ ] <sup>a,c,e</sup>	[ ] <sup>a,c,e</sup>	
Case 4	Parameters to Define the Distribution			5/50 Pull Out Force (kip)
Model D5 All Expansions	Name	Mean	Stand. Dev.	[ ] <sup>a,c,e</sup>
	Symbol	$\mu$	$\sigma$	
	Value	[ ] <sup>a,c,e</sup>	[ ] <sup>a,c,e</sup>	
Case 5	Parameters to Define the Distribution			5/50 Pull Out Force (kip)
Model 44F 13" Expansion	Name	Mean	Stand. Dev.	[ ] <sup>a,c,e</sup>
	Symbol	$\mu$	$\sigma$	
	Value	[ ] <sup>a,c,e</sup>	[ ] <sup>a,c,e</sup>	
Case 6	Parameters to Define the Distribution			5/50 Pull Out Force (kip)
Model 44F All Expansions	Name	Mean	Stand. Dev.	[ ] <sup>a,c,e</sup>
	Symbol	$\mu$	$\sigma$	
	Value	[ ] <sup>a,c,e</sup>	[ ] <sup>a,c,e</sup>	

**Table 11**  
**Monte Carlo Results for the Erlang Distribution**

Distribution	Erlang Distribution			
Case 1	Parameters to Define the Distribution			5/50 Pull Out Force (kip)
Model F 13" Expansion	Name	Cont. Shape Par.	Cont. Scale Par.	[ ] <sup>a,c,e</sup>
	Symbol	m	β	
	Value	[ ] <sup>a,c,e</sup>	[ ] <sup>a,c,e</sup>	
Case 2	Parameters to Define the Distribution			5/50 Pull Out Force (kip)
Model F All Expansions	Name	Cont. Shape Par.	Cont. Scale Par.	[ ] <sup>a,c,e</sup>
	Symbol	m	β	
	Value	[ ] <sup>a,c,e</sup>	[ ] <sup>a,c,e</sup>	
Case 3	Parameters to Define the Distribution			5/50 Pull Out Force (kip)
Model D5 13" Expansion	Name	Cont. Shape Par.	Cont. Scale Par.	[ ] <sup>a,c,e</sup>
	Symbol	m	β	
	Value	[ ] <sup>a,c,e</sup>	[ ] <sup>a,c,e</sup>	
Case 4	Parameters to Define the Distribution			5/50 Pull Out Force (kip)
Model D5 All Expansions	Name	Cont. Shape Par.	Cont. Scale Par.	[ ] <sup>a,c,e</sup>
	Symbol	m	β	
	Value	[ ] <sup>a,c,e</sup>	[ ] <sup>a,c,e</sup>	
Case 5	Parameters to Define the Distribution			5/50 Pull Out Force (kip)
Model 44F 13" Expansion	Name	Cont. Shape Par.	Cont. Scale Par.	[ ] <sup>a,c,e</sup>
	Symbol	m	β	
	Value	[ ] <sup>a,c,e</sup>	[ ] <sup>a,c,e</sup>	
Case 6	Parameters to Define the Distribution			5/50 Pull Out Force (kip)
Model 44F All Expansions	Name	Cont. Shape Par.	Cont. Scale Par.	[ ] <sup>a,c,e</sup>
	Symbol	m	β	
	Value	[ ] <sup>a,c,e</sup>	[ ] <sup>a,c,e</sup>	

**Table 12**  
**Monte Carlo Results for the Gamma Distribution**

Distribution	Gamma Distribution			
Case 1	Parameters to Define the Distribution			5/50 Pull Out Force (kip)
Model F 13" Expansion	Name	Cont. Shape Par.	Cont. Scale Par.	[ ] <sup>a,c,e</sup>
	Symbol	$\alpha$	$\beta$	
	Value	[ ] <sup>a,c,e</sup>	[ ] <sup>a,c,e</sup>	
Case 2	Parameters to Define the Distribution			5/50 Pull Out Force (kip)
Model F All Expansions	Name	Cont. Shape Par.	Cont. Scale Par.	[ ] <sup>a,c,e</sup>
	Symbol	$\alpha$	$\beta$	
	Value	[ ] <sup>a,c,e</sup>	[ ] <sup>a,c,e</sup>	
Case 3	Parameters to Define the Distribution			5/50 Pull Out Force (kip)
Model D5 13" Expansion	Name	Cont. Shape Par.	Cont. Scale Par.	[ ] <sup>a,c,e</sup>
	Symbol	$\alpha$	$\beta$	
	Value	[ ] <sup>a,c,e</sup>	[ ] <sup>a,c,e</sup>	
Case 4	Parameters to Define the Distribution			5/50 Pull Out Force (kip)
Model D5 All Expansions	Name	Cont. Shape Par.	Cont. Scale Par.	[ ] <sup>a,c,e</sup>
	Symbol	$\alpha$	$\beta$	
	Value	[ ] <sup>a,c,e</sup>	[ ] <sup>a,c,e</sup>	
Case 5	Parameters to Define the Distribution			5/50 Pull Out Force (kip)
Model 44F 13" Expansion	Name	Cont. Shape Par.	Cont. Scale Par.	[ ] <sup>a,c,e</sup>
	Symbol	$\alpha$	$\beta$	
	Value	[ ] <sup>a,c,e</sup>	[ ] <sup>a,c,e</sup>	
Case 6	Parameters to Define the Distribution			5/50 Pull Out Force (kip)
Model 44F All Expansions	Name	Cont. Shape Par.	Cont. Scale Par.	[ ] <sup>a,c,e</sup>
	Symbol	$\alpha$	$\beta$	
	Value	[ ] <sup>a,c,e</sup>	[ ] <sup>a,c,e</sup>	

**Table 13  
Monte Carlo Results for the Inverse Gaussian Distribution**

Distribution	Inverse Gaussian Distribution			
Case 1	Parameters to Define the Distribution			5/50 Pull Out Force (kip)
Model F 13" Expansion	Name	Cont. Par.	Cont. Par.	[ ] <sup>a,c,e</sup>
	Symbol	$\mu$	$\lambda$	
	Value	[ ] <sup>a,c,e</sup>	[ ] <sup>a,c,e</sup>	
Case 2	Parameters to Define the Distribution			5/50 Pull Out Force (kip)
Model F All Expansions	Name	Cont. Par.	Cont. Par.	[ ] <sup>a,c,e</sup>
	Symbol	$\mu$	$\lambda$	
	Value	[ ] <sup>a,c,e</sup>	[ ] <sup>a,c,e</sup>	
Case 3	Parameters to Define the Distribution			5/50 Pull Out Force (kip)
Model D5 13" Expansion	Name	Cont. Par.	Cont. Par.	[ ] <sup>a,c,e</sup>
	Symbol	$\mu$	$\lambda$	
	Value	[ ] <sup>a,c,e</sup>	[ ] <sup>a,c,e</sup>	
Case 4	Parameters to Define the Distribution			5/50 Pull Out Force (kip)
Model D5 All Expansions	Name	Cont. Par.	Cont. Par.	[ ] <sup>a,c,e</sup>
	Symbol	$\mu$	$\lambda$	
	Value	[ ] <sup>a,c,e</sup>	[ ] <sup>a,c,e</sup>	
Case 5	Parameters to Define the Distribution			5/50 Pull Out Force (kip)
Model 44F 13" Expansion	Name	Cont. Par.	Cont. Par.	[ ] <sup>a,c,e</sup>
	Symbol	$\mu$	$\lambda$	
	Value	[ ] <sup>a,c,e</sup>	[ ] <sup>a,c,e</sup>	
Case 6	Parameters to Define the Distribution			5/50 Pull Out Force (kip)
Model 44F All Expansions	Name	Cont. Par.	Cont. Par.	[ ] <sup>a,c,e</sup>
	Symbol	$\mu$	$\lambda$	
	Value	[ ] <sup>a,c,e</sup>	[ ] <sup>a,c,e</sup>	

**Table 14  
Monte Carlo Results for the Pearson Type V Distribution**

Distribution	Pearson Type V Distribution			
Case 1	Parameters to Define the Distribution			5/50 Pull Out Force (kip)
Model F 13" Expansion	Name	Cont. Shape Par.	Cont. Scale Par.	[ ] <sup>a,c,e</sup>
	Symbol	$\alpha$	$\beta$	
	Value	[ ] <sup>a,c,e</sup>	[ ] <sup>a,c,e</sup>	
Case 2	Parameters to Define the Distribution			5/50 Pull Out Force (kip)
Model F All Expansions	Name	Cont. Shape Par.	Cont. Scale Par.	[ ] <sup>a,c,e</sup>
	Symbol	$\alpha$	$\beta$	
	Value	[ ] <sup>a,c,e</sup>	[ ] <sup>a,c,e</sup>	
Case 3	Parameters to Define the Distribution			5/50 Pull Out Force (kip)
Model D5 13" Expansion	Name	Cont. Shape Par.	Cont. Scale Par.	[ ] <sup>a,c,e</sup>
	Symbol	$\alpha$	$\beta$	
	Value	[ ] <sup>a,c,e</sup>	[ ] <sup>a,c,e</sup>	
Case 4	Parameters to Define the Distribution			5/50 Pull Out Force (kip)
Model D5 All Expansions	Name	Cont. Shape Par.	Cont. Scale Par.	[ ] <sup>a,c,e</sup>
	Symbol	$\alpha$	$\beta$	
	Value	[ ] <sup>a,c,e</sup>	[ ] <sup>a,c,e</sup>	
Case 5	Parameters to Define the Distribution			5/50 Pull Out Force (kip)
Model 44F 13" Expansion	Name	Cont. Shape Par.	Cont. Scale Par.	[ ] <sup>a,c,e</sup>
	Symbol	$\alpha$	$\beta$	
	Value	[ ] <sup>a,c,e</sup>	[ ] <sup>a,c,e</sup>	
Case 6	Parameters to Define the Distribution			5/50 Pull Out Force (kip)
Model 44F All Expansions	Name	Cont. Shape Par.	Cont. Scale Par.	[ ] <sup>a,c,e</sup>
	Symbol	$\alpha$	$\beta$	
	Value	[ ] <sup>a,c,e</sup>	[ ] <sup>a,c,e</sup>	

**Table 15**  
**Monte Carlo Results for the Weibull Distribution**

Distribution	Weibull Distribution			
Case 1	Parameters to Define the Distribution			5/50 Pull Out Force (kip)
Model F 13" Expansion	Name	Cont. Shape Par.	Cont. Scale Par.	[ ] <sup>a,c,e</sup>
	Symbol	$\alpha$	$\beta$	
	Value	[ ] <sup>a,c,e</sup>	[ ] <sup>a,c,e</sup>	
Case 2	Parameters to Define the Distribution			5/50 Pull Out Force (kip)
Model F All Expansions	Name	Cont. Shape Par.	Cont. Scale Par.	[ ] <sup>a,c,e</sup>
	Symbol	$\alpha$	$\beta$	
	Value	[ ] <sup>a,c,e</sup>	[ ] <sup>a,c,e</sup>	
Case 3	Parameters to Define the Distribution			5/50 Pull Out Force (kip)
Model D5 13" Expansion	Name	Cont. Shape Par.	Cont. Scale Par.	[ ] <sup>a,c,e</sup>
	Symbol	$\alpha$	$\beta$	
	Value	[ ] <sup>a,c,e</sup>	[ ] <sup>a,c,e</sup>	
Case 4	Parameters to Define the Distribution			5/50 Pull Out Force (kip)
Model D5 All Expansions	Name	Cont. Shape Par.	Cont. Scale Par.	[ ] <sup>a,c,e</sup>
	Symbol	$\alpha$	$\beta$	
	Value	[ ] <sup>a,c,e</sup>	[ ] <sup>a,c,e</sup>	
Case 5	Parameters to Define the Distribution			5/50 Pull Out Force (kip)
Model 44F 13" Expansion	Name	Cont. Shape Par.	Cont. Scale Par.	[ ] <sup>a,c,e</sup>
	Symbol	$\alpha$	$\beta$	
	Value	[ ] <sup>a,c,e</sup>	[ ] <sup>a,c,e</sup>	
Case 6	Parameters to Define the Distribution			5/50 Pull Out Force (kip)
Model 44F All Expansions	Name	Cont. Shape Par.	Cont. Scale Par.	[ ] <sup>a,c,e</sup>
	Symbol	$\alpha$	$\beta$	
	Value	[ ] <sup>a,c,e</sup>	[ ] <sup>a,c,e</sup>	

**Figure 1**  
**The Model F 13 Inch Expansion Tube/Collar Assembly**

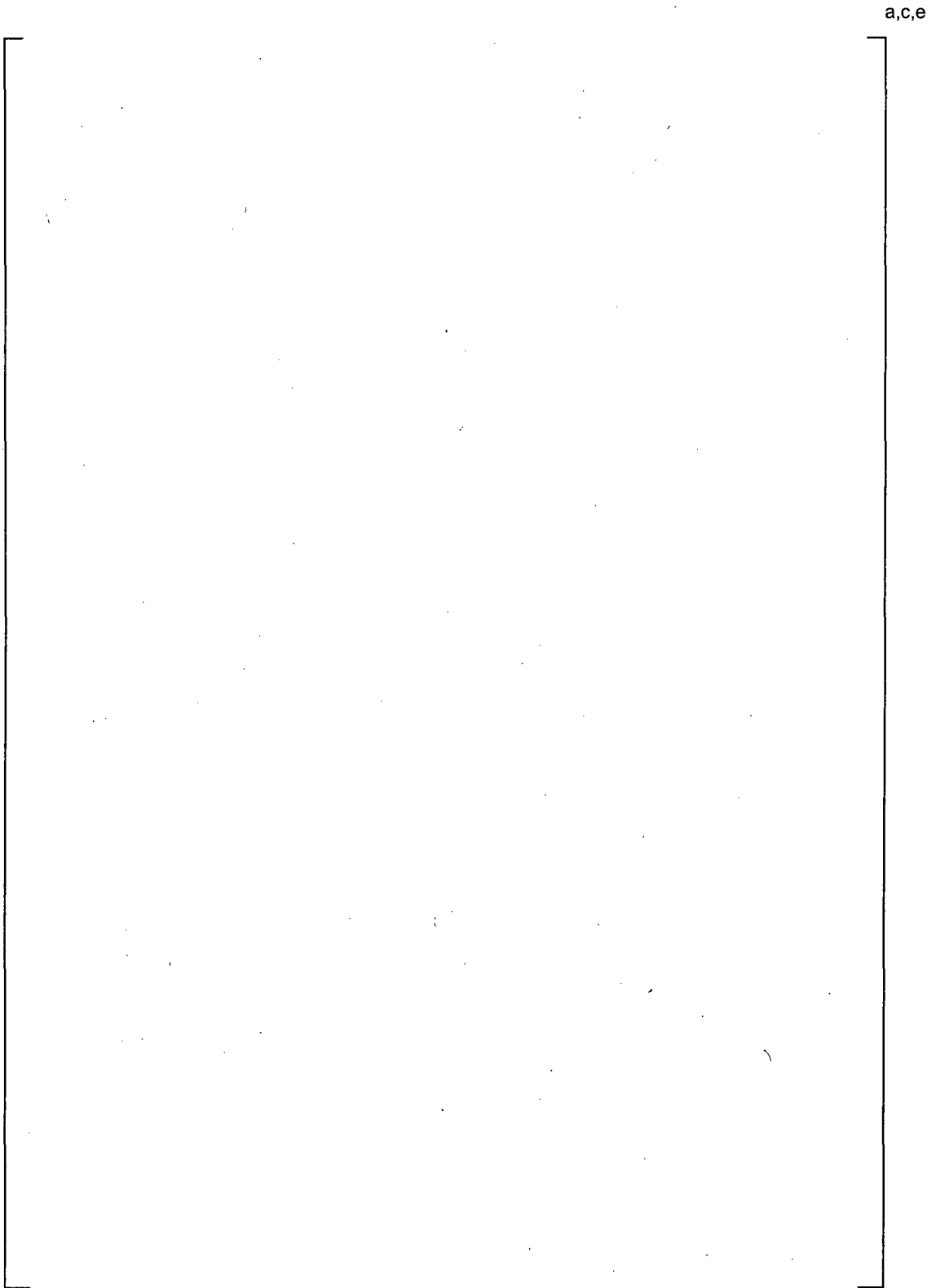


**Figure 2**  
**The Model F 15 Inch Expansion Tube/Collar Assembly**

a,c,e

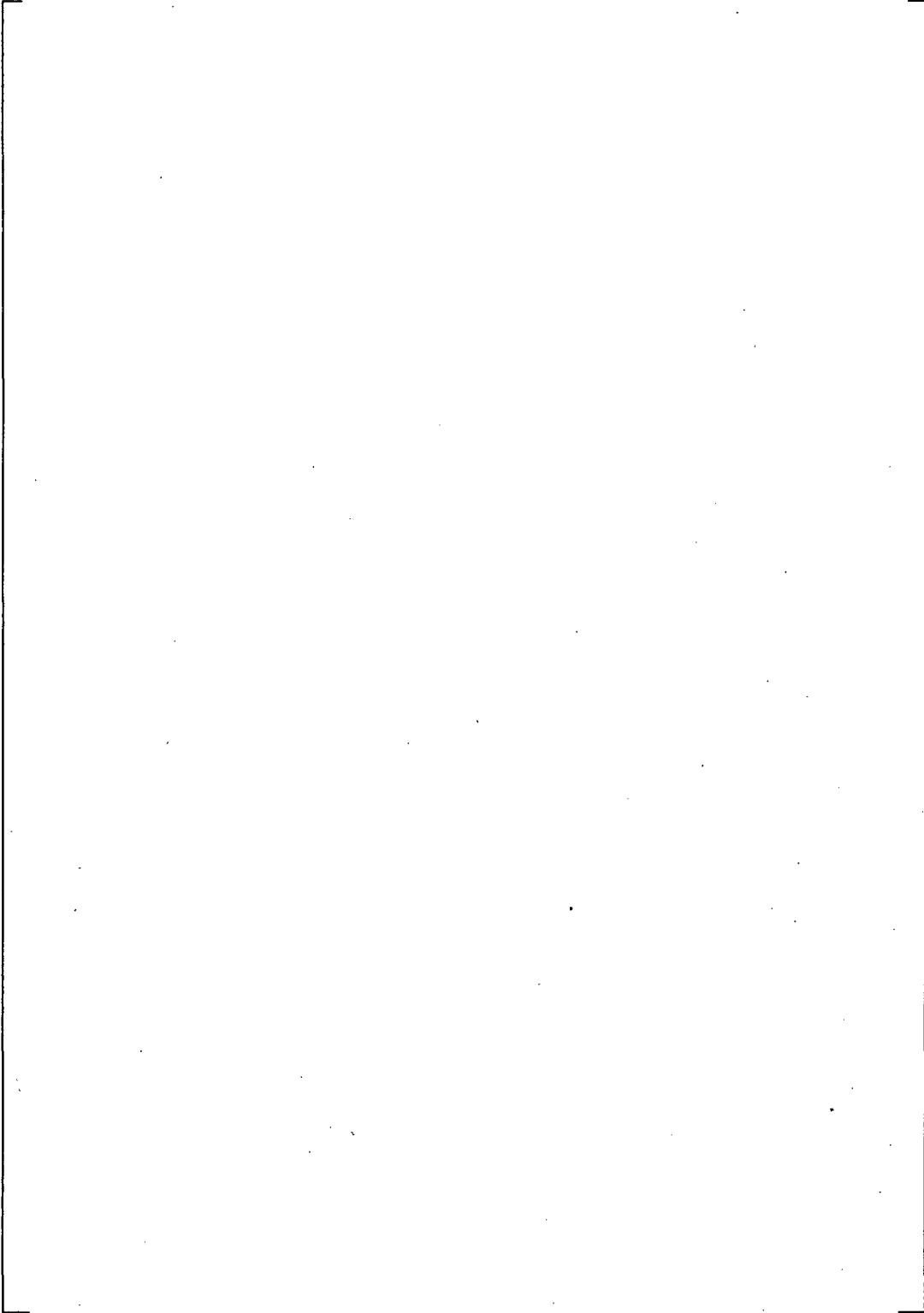
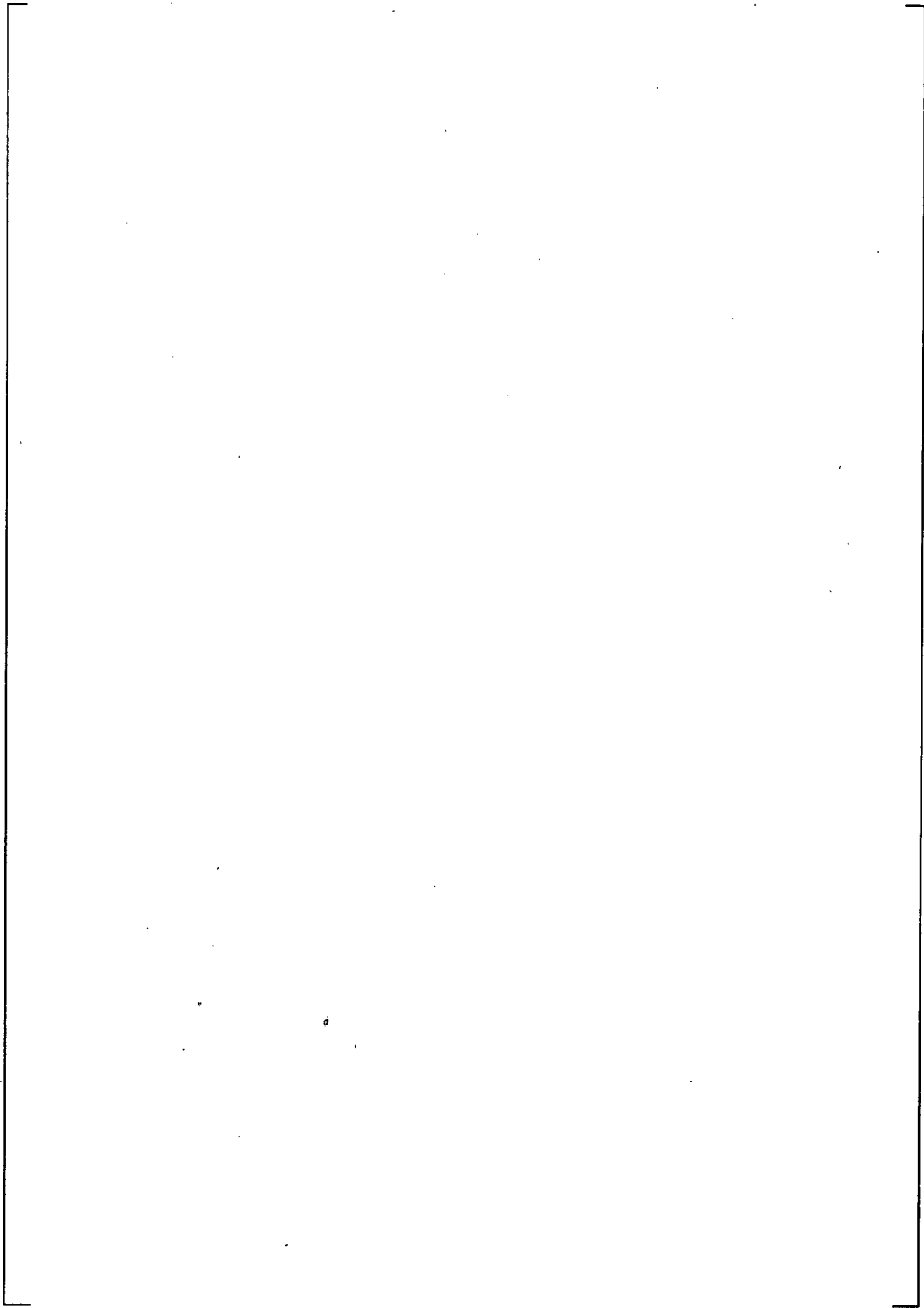


**Figure 3**  
**The Model F 17 Inch Expansion Tube/Collar Assembly**



a,c,e

**Figure 4**  
**The Model D5 13 Inch Expansion Tube/Collar Assembly**

a,c,e

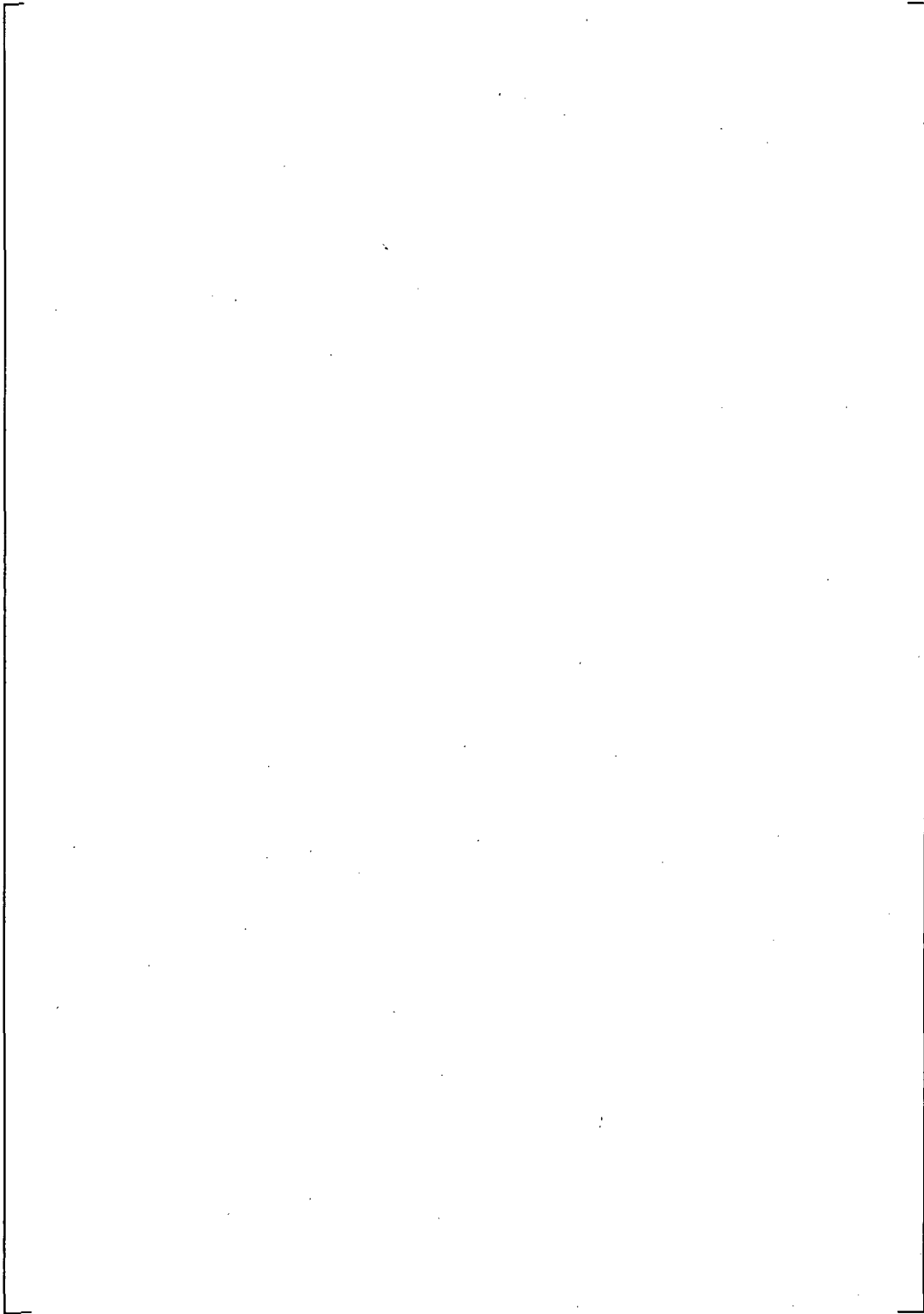


**Figure 5**  
**The Model D5 15 Inch Expansion Tube/Collar Assembly**

a,c,e

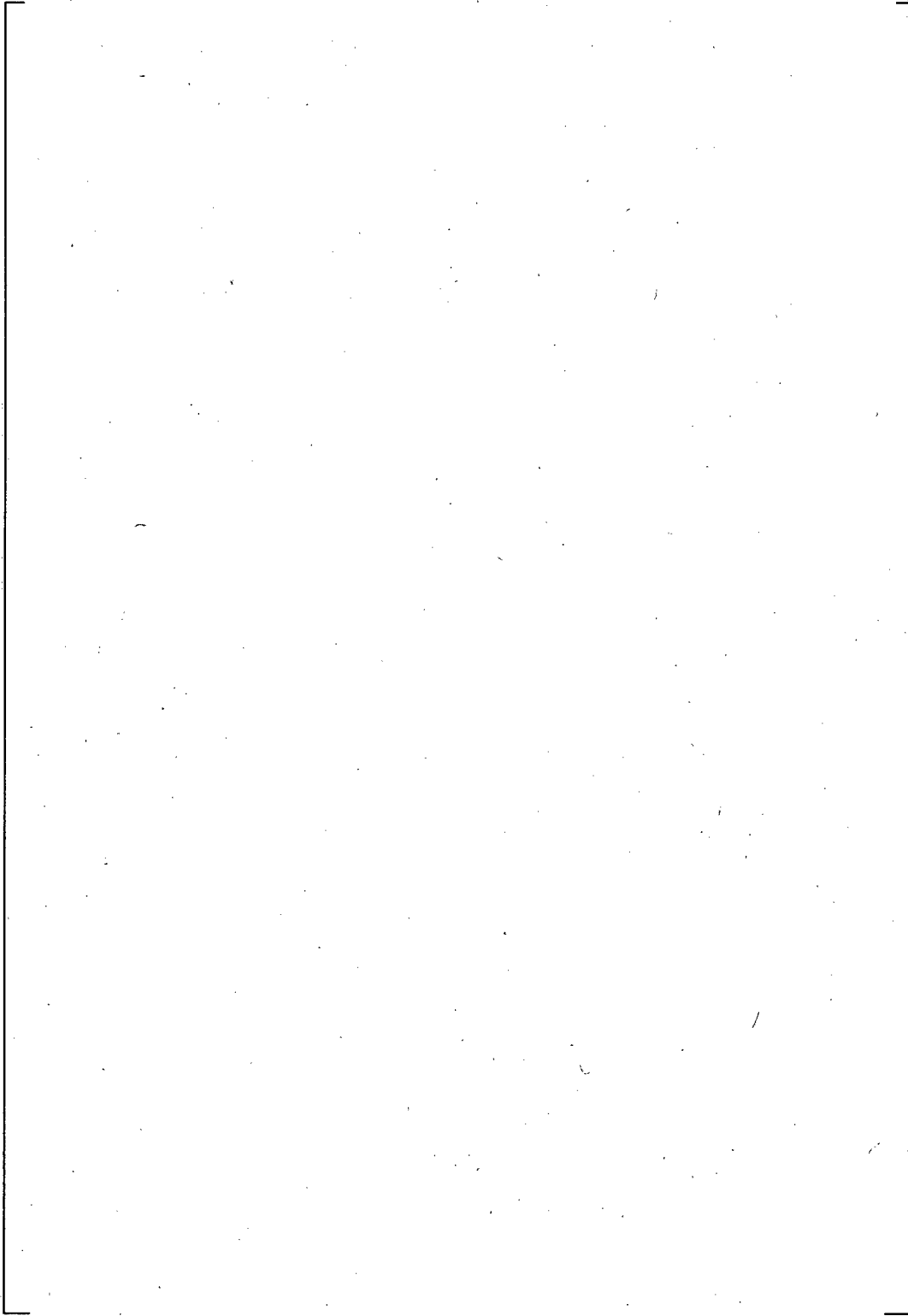


**Figure 6**  
**The Model D5 17 Inch Expansion Tube/Collar Assembly**

a,c,e

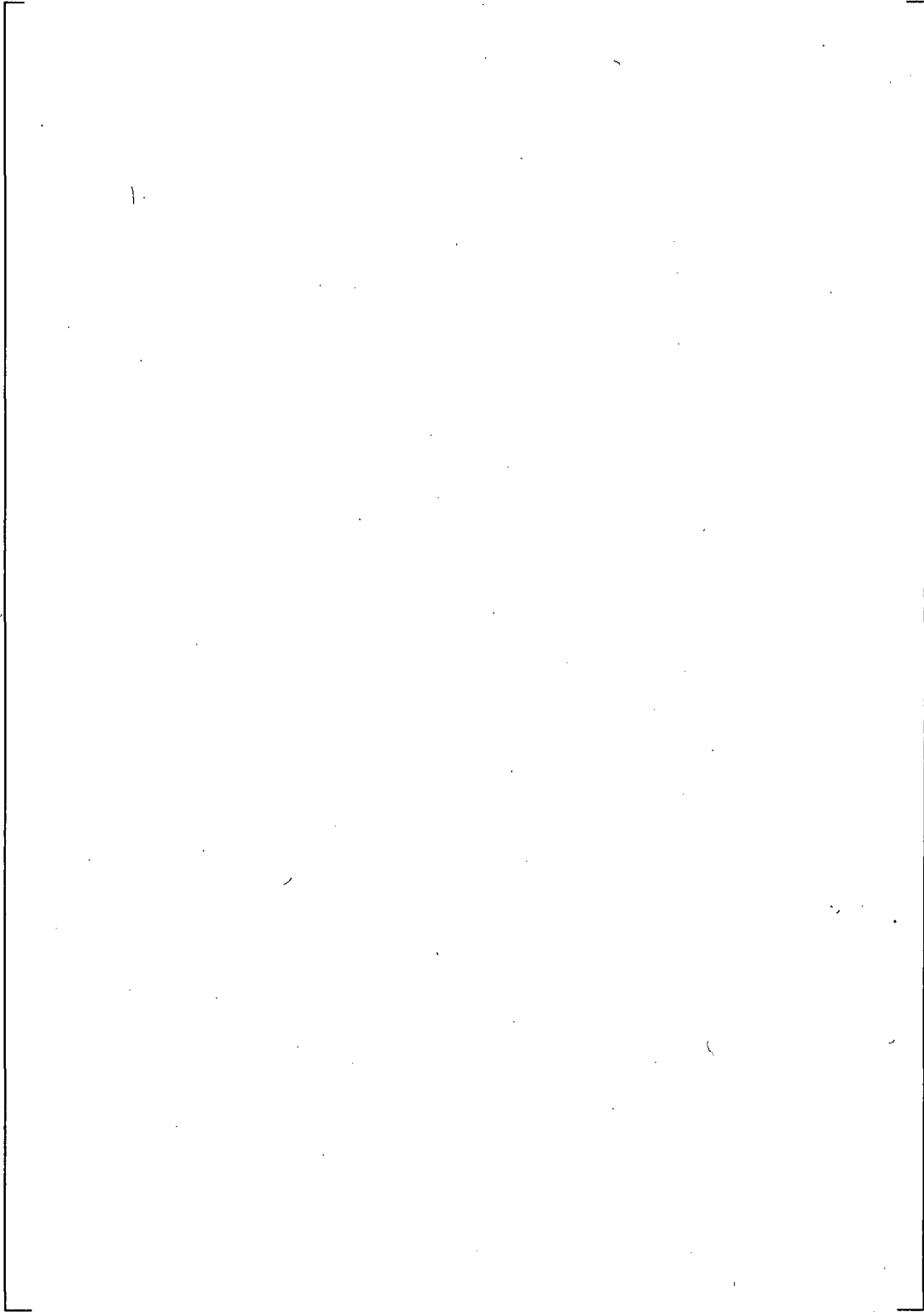
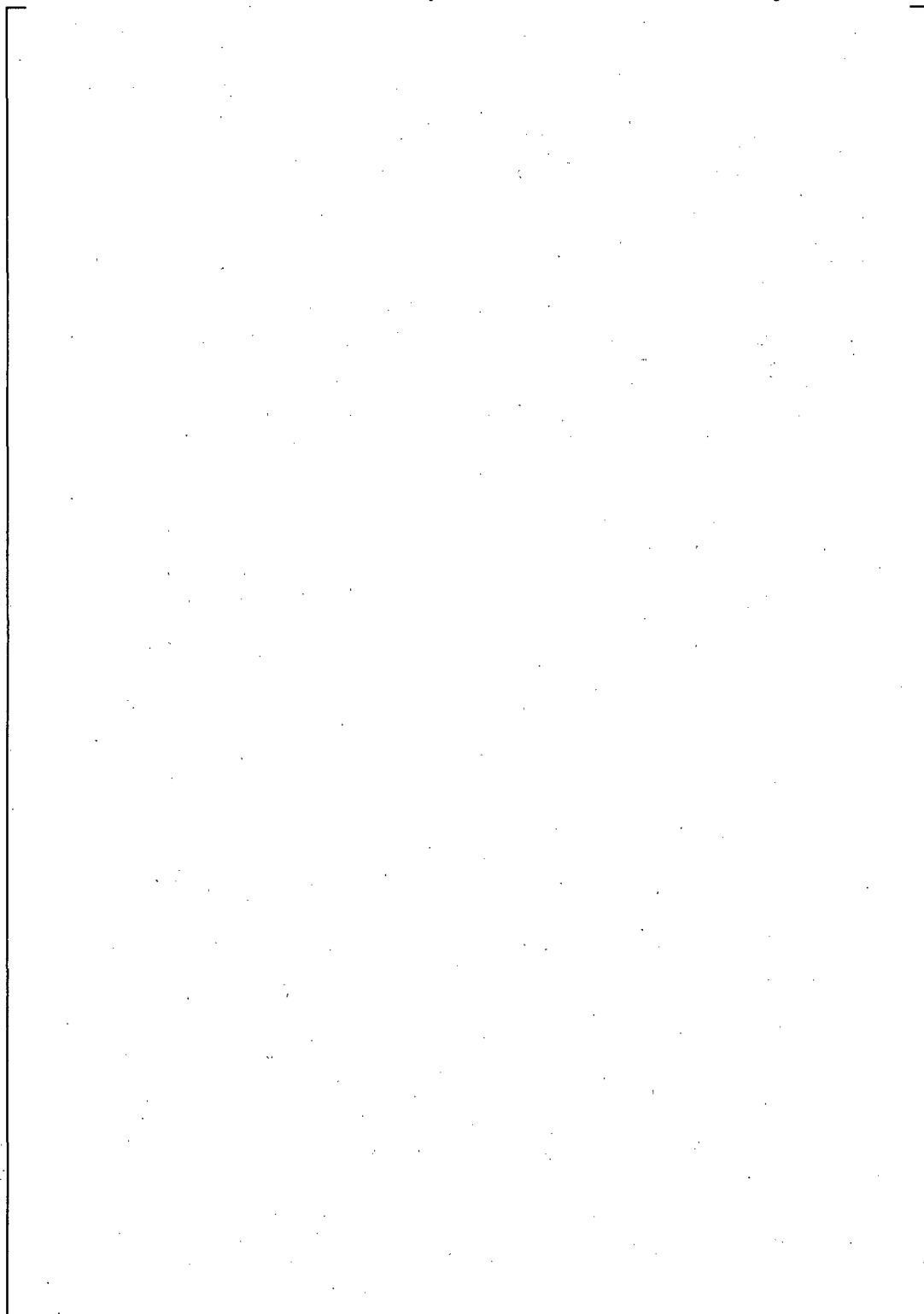


**Figure 7**  
**The Model 44F 13 Inch Expansion Tube/Collar Assembly**



a,c,e

**Figure 8**  
**The Model 44F 15 Inch Expansion Tube/Collar Assembly**

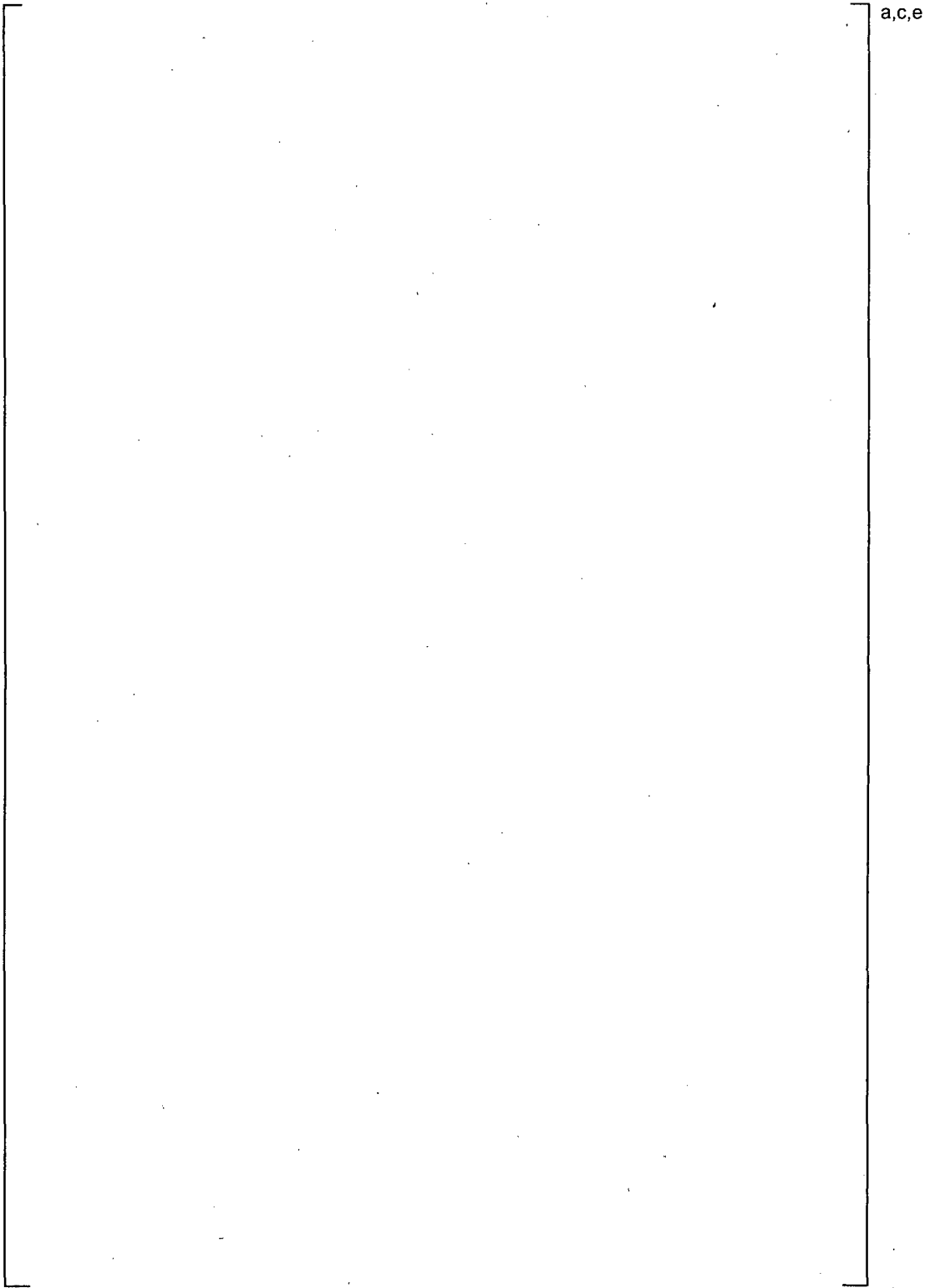


**Figure 9**  
**The Model 44F 17 Inch Expansion Tube/Collar Assembly**

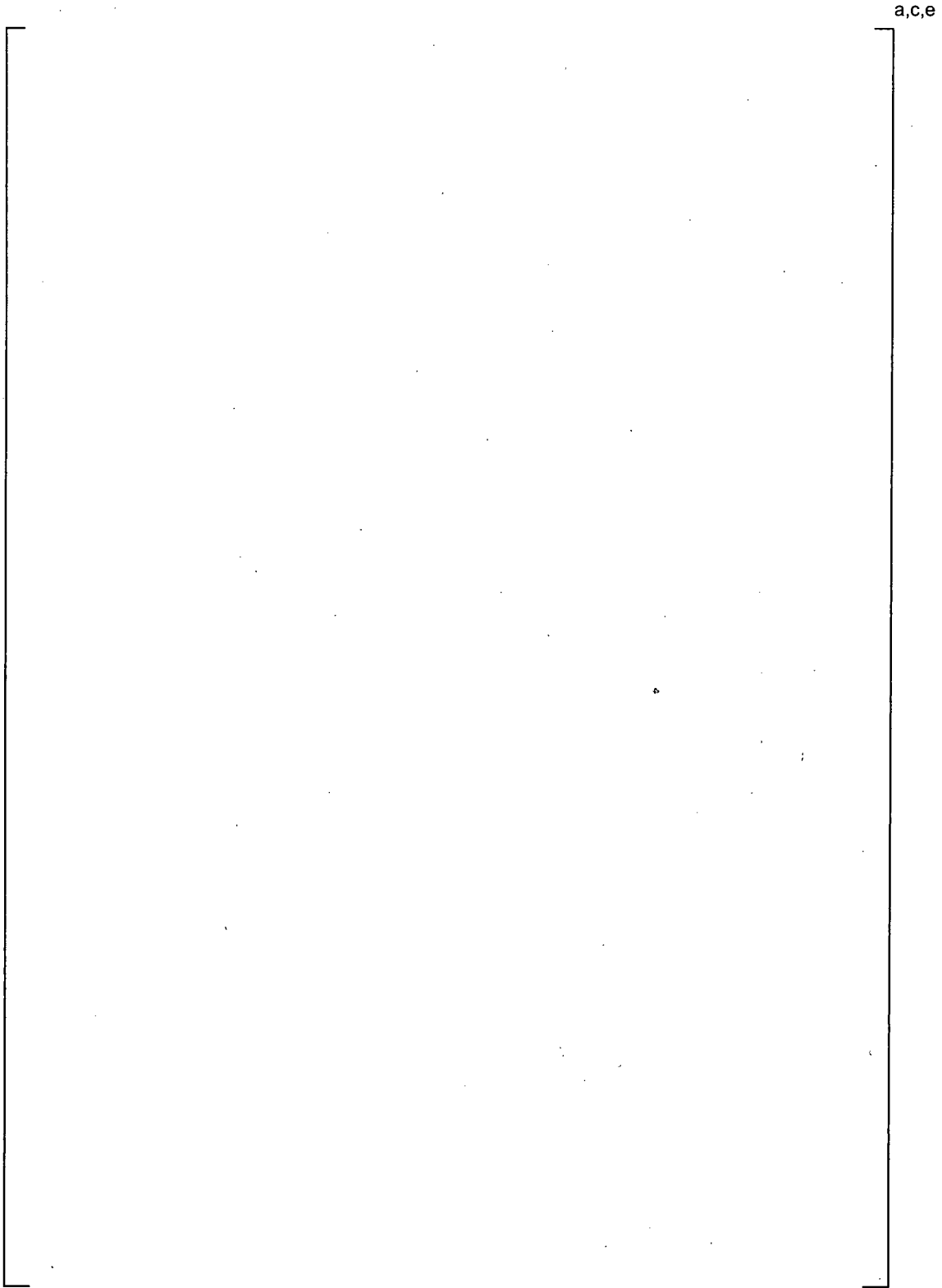


**Figure 10**  
**A Plot of Pull Out Force vs. Surface Roughness**



**Figure 11**  
**The Pull Out Force vs. Expansion Length for a Given Tube OD**



a,c,e

**Appendix B**

**Response to  
NRC Request for Additional Information on H\*; RAI#4**

**Response to  
NRC Request for Additional Information on H\*; RAI #4;  
Model 44F and Model 51F Steam Generators**

**Introduction**

In response to formal requests for technical specification amendments, References 1, and 2, the USNRC informally requested additional information in References 3 and 4. The Turkey Point and Surry requests for a permanent license amendment to implement H\* represent the Model 44F and Model 51F steam generators for which the H\* technical justification is provided in References 5 and 6.

Subsequent to the initial issue of the RAIs for Vogtle (Reference 7), the NRC issued follow-up questions (Reference 8) to questions numbers 4, 20 and 24 and an additional request regarding a technical specification (TS) commitment for applying the leakage factors. Except for RAI#4, responses to all of the RAIs, including the follow-up questions in Reference 8, were provided in Reference 9. The follow-up questions in Reference 8 are included in RAI#4 for Turkey Point and Surry as reproduced below. The affected licensees provided separate responses in regard to the commitment for applying leakage factors.

The response to RAI#4 required additional explanation as discussed with the NRC staff on August 11, 2009 and was, therefore, not included in Reference 9. The additional questions related to RAI#4 that were identified during the August 11, 2009 telephone conference were summarized by Westinghouse and were the basis of the discussion at a meeting among the NRC, several licensees and Westinghouse on August 17 and 18, 2009. These additional questions are reproduced in the response to RAI#4, below. Specific discussion is included in the response to address the additional questions.

To summarize, this appendix provides the response to RAI#4 as included in References 3 and 4 and responses to the additional questions raised during the conference call on August 11, 2009.

Utilities, other than referenced in this document, have requested amendments to their licenses in parallel with the response to these RAI's. The technical RAIs are generic in nature because the analysis methods are the same for all affected plants. This response to RAI#4 is generic for all Models of SGs that are candidates for application of H\*. However, this letter specifically provides the response to RAI#4 as provided in References 3 and 4 regarding WCAP-17091-P (Model 44F H\*) and WCAP-17092-P (Model 51F H\*) and the additional questions identified during the August 11, 2009 telephone conference as discussed at the August 17, 2009 meeting.

<p><b>RAI</b></p>	<p>Turkey Point</p>	<p>4. Reference 1, Page 6-66. In Section 6.2.5.3, it is concluded that the tube outside diameter and the tubesheet tube bore inside diameter always maintain contact in the predicted range of tubesheet displacements. However, for tubes with through wall cracks at the <math>H^*</math> distance, there may be little or no net pressure acting on the tube for some distance above <math>H^*</math>. In Tables 6-18 and 6-19, the fourth increment in the step that occurs two steps prior to the last step suggests that there may be no contact between the tube and tubesheet, over a portion of the circumference, for a distance above <math>H^*</math>. Is the conclusion in 6.2.5.3 valid for the entire <math>H^*</math> distance, given the possibility that the tubes may contain through wall cracks at that location? Additionally, please address the following issues:</p> <ul style="list-style-type: none"> <li>a. Clarify the nature of the finite element model ("slice" model versus axisymmetric SG assembly model) used to generate the specific information in Tables 6-1, 2, and 3 (and accompanying graph entitled "Elliptical Hole Factors") of Reference 6-15. What loads were applied? How was the eccentricity produced in the model? (By modeling the eccentricity as part of the geometry? By applying an axisymmetric pressure the inside of the bore?) Explain why this model is not scalable to lower temperatures.</li> <li>b. Provide a table showing the maximum eccentricities (maximum diameter minus minimum diameter) from the 3 dimensional (3-D) finite element analysis for normal operating and steam line break (SLB), for model F and D5.</li> <li>c. In Figure 2 of the White Paper, add plot for original relationship between reductions in contact pressure and eccentricity as given in Reference 6-15 in the graph accompanying Table 6-3. Explain why this original relationship remains conservative in light of the new relationship. Explain the reasons for the differences between the curves.</li> <li>d. When establishing whether contact pressure increases when going from normal operating to steam line break conditions, how can a valid and conservative comparison be made if the normal operating case is based on the original delta contact pressure versus eccentricity curve and the SLB case is based on the new curve?</li> </ul>
-------------------	---------------------	-------------------------------------------------------------------------------------------------------------------------------------------------------------------------------------------------------------------------------------------------------------------------------------------------------------------------------------------------------------------------------------------------------------------------------------------------------------------------------------------------------------------------------------------------------------------------------------------------------------------------------------------------------------------------------------------------------------------------------------------------------------------------------------------------------------------------------------------------------------------------------------------------------------------------------------------------------------------------------------------------------------------------------------------------------------------------------------------------------------------------------------------------------------------------------------------------------------------------------------------------------------------------------------------------------------------------------------------------------------------------------------------------------------------------------------------------------------------------------------------------------------------------------------------------------------------------------------------------------------------------------------------------------------------------------------------------------------------------------------------------------------------------------------------------------------------------------------------------------------------------------------------------------------------------------------------------------------------------------------------------------------------------------------------------------------------------------------------------------------------------------------------------------------------------------------------------------------------------------------------------------------------------------------------------------------------------------------------------------------------------------------------------------------------

	Surry	<p>4. Reference 1, Page 6-66. In Section 6.2.5.3, it is concluded that the tube outside diameter and the tubesheet tube bore inside diameter always maintain contact in the predicted range of tubesheet displacements. However, for tubes with through wall cracks at the <math>H^*</math> distance, there may be little or no net pressure acting on the tube for some distance above <math>H^*</math>. In Tables 6-18 and 6-19, the fourth increment in the step that occurs two steps prior to the last step suggests that there may be no contact between the tube and tubesheet, over a portion of the circumference, for a distance above <math>H^*</math>. Is the conclusion in 6.2.5.3 valid for the entire <math>H^*</math> distance, given the possibility that the tubes may contain through wall cracks at that location? Additionally, please address the following issues:</p> <p>a. Clarify the nature of the finite element model ("slice" model versus axisymmetric SG assembly model) used to generate the specific information in Tables 6-1, 2, and 3 (and accompanying graph entitled "Elliptical Hole Factors") of Reference 6-15. What loads were applied? How was the eccentricity produced in the model? (By modeling the eccentricity as part of the geometry? By applying an axisymmetric pressure the inside of the bore?) Explain why this model is not scalable to lower temperatures.</p> <p>b. Provide a table showing the maximum eccentricities (maximum diameter minus minimum diameter) from the 3 dimensional (3-D) finite element analysis for normal operating and steam line break (SLB), for model 51F.</p> <p>c. In Figure 2 of the White Paper, add plot for original relationship between reductions in contact pressure and eccentricity as given in Reference 6-15 in the graph accompanying Table 6-3. Explain why this original relationship remains conservative in light of the new relationship. Explain the reasons for the differences between the curves.</p> <p>d. When establishing whether contact pressure increases when going from normal operating to steam line break conditions, how can a valid and conservative comparison be made if the normal operating case is based on the original delta contact pressure versus eccentricity curve and the SLB case is based on the new curve?</p>
--	-------	-------------------------------------------------------------------------------------------------------------------------------------------------------------------------------------------------------------------------------------------------------------------------------------------------------------------------------------------------------------------------------------------------------------------------------------------------------------------------------------------------------------------------------------------------------------------------------------------------------------------------------------------------------------------------------------------------------------------------------------------------------------------------------------------------------------------------------------------------------------------------------------------------------------------------------------------------------------------------------------------------------------------------------------------------------------------------------------------------------------------------------------------------------------------------------------------------------------------------------------------------------------------------------------------------------------------------------------------------------------------------------------------------------------------------------------------------------------------------------------------------------------------------------------------------------------------------------------------------------------------------------------------------------------------------------------------------------------------------------------------------------------------------------------------------------------------------------------------------------------------------------------------------------------------------------------------------------------------------------------------------------------------------------------------------------------------------------------------------------------------------------------------------------------------------------------------------------------------------------------------------------------------------------------------------------------------------------------------------------------

**Part B: Additional Questions Provided in the August 11, 2009 telephone conference:****a. Overall High Level Question**

1. Discuss if the eccentricity effect on contact pressure is occurring as described. It is the opinion of the NRC staff that the eccentricity effect may not be as significant as being reported by Westinghouse.

**b. Other Key Questions**

1. The eccentricities included in Table RAI 4-4 appear larger than anticipated. Need to confirm that positive contact pressure exists around the entire circumference of the tube and state this clearly in the response.
2. The difference between initial and final eccentricity included in Table RAI4-2 needs to be explained. In particular, the exclusive use of the relationship between initial eccentricity and scale factor in calculating contact pressure needs to be justified.
3. The basis for applying the correlation for scale factor outside an "eccentricity" range of between 1E-3 to 1E-4 inch in the calculation of contact pressure needs to be further explained. Values for displacements included in Table 6-18 (of WCAP-17071) suggest that contact pressure may be lost at displacement ranging between 1E-3 in to 1E-4 inch.
4. Provide the calculation basis for the upper and lower curves provided in Figure RAI 4-2
5. Resolve the apparent inconsistency between Item 4 on page 25 and the statement below Figure RAI4-1 regarding how the model in Figure RAI4-1 is loaded.

**c. Key Remaining Issues**

1. Provide the basis for why the  $\Delta D_{\text{hole}}$  adjustment for contact pressure made using the old model remains conservative.
2. Provide an appropriate basis for demonstrating that joints tighten during a postulated SLB event. Why is it acceptable to compare the contact pressures calculated using the original model for NOP to the contact pressures calculated using the new model for SLB for the Model D5 SGs?
3. If both old and new models are conservative, is there an appropriate basis to show the relative conservatism of the methods?

**General:**

These questions were originally raised as a result of a White Paper (Reference 10) issued to address the conditions of the apparent limiting accident for the Model D5 SGs. The questions evolved to include aspects of the analysis for the Model F SGs, principally because these were the models of SG under consideration by the MRC. As a result, the response is focused principally on the Model D5 and Model F SGs. Since the original RAI was issued, LARs were filed for the Model 44F and Model 51 F SGs. Because the analysis methods for H\* are common to all models of SGs, the response provided is generic in nature and applies equally to the Model 44F and Model 51F SGs.

To facilitate a continuous response to the total RAI#4 questions, the questions received originally (Part A), those received as follow-up questions (Part A, sub parts a, b, c and d) and those identified during the 8/11/09 telephone conference (Part B) are re-arranged as noted below. The location of responses to specific questions is shown in bold type after the question. Also, in the responses, the specific questions addressed by the responses are repeated in bold type in the box at the start of the response.

**Part B: Sub a.**

*Discuss if the eccentricity effect on contact pressure is occurring as described. It is the opinion of the NRC staff that the eccentricity effect may not be as significant as being reported by Westinghouse. (See Section 1.0)*

**Part A: Sub a, b, c and d.**

*a. Clarify the nature of the finite element model ("slice" model versus axisymmetric SG assembly model) used to generate the specific information in Tables 6-1, 2, and 3 (and accompanying graph entitled "Elliptical Hole Factors") of Reference 6-15. What loads were applied? How was the eccentricity produced in the model? (By modeling the eccentricity as part of the geometry? By applying an axisymmetric pressure the inside of the bore?) Explain why this model is not scalable to lower temperatures. (See Section 1.2)*

*b. Provide table showing maximum delta diameters (total diameter distortion) and maximum eccentricities (maximum diameter minus minimum diameter) from the 3 dimensional (3-D) finite element analysis for normal operating and steam line break (SLB), for model F and D5. (The Surry question requests information for the Model 51F) (See Section 1.1)*

*c. In Figure 2 of the White Paper, add plot for original relationship between reductions in contact pressure and eccentricity as given in Reference 6-15 in the graph accompanying Table 6-3. Explain why this original relationship remains conservative in light of the new*

relationship. Explain the reasons for the differences between the curves. (See Section 4.1)

d. When establishing whether contact pressure increases when going from normal operating to steam line break conditions, how can a valid and conservative comparison be made if the normal operating case is based on the original delta contact pressure versus eccentricity curve and the SLB case is based on the new curve? (See Section 4.2)

**Part B: Sub b. Other Key Questions**

1. The eccentricities included in Table RAI 4-4 appear larger than anticipated. Need to confirm that positive contact pressure exists around the entire circumference of the tube and state this clearly in the response. (See Section 3)
2. The difference between initial and final eccentricity included in Table RAI4-2 needs to be explained. In particular, the exclusive use of the relationship between initial eccentricity and scale factor in calculating contact pressure needs to be justified. (See Section 1.2)
3. The basis for applying the correlation for scale factor outside an "eccentricity" range of between 1E-3 to 1E-4 inch in the calculation of contact pressure needs to be further explained. Values for displacements included in Table 6-18 (of WCAP-1707.1) suggest that contact pressure may be lost at displacement ranging between 1E-3 in to 1E-4 inch. (See Section 2.0)
4. Provide the calculation basis for the upper and lower curves provided in Figure RAI 4-2. (See Section 2.1)
5. Resolve the apparent inconsistency between Item 4 on page 25 and the statement below Figure RAI4-1 regarding how the model in Figure RAI4-1 is loaded. (See Section 1.2)

**Part B: Sub c. Key Remaining Issues.**

1. Provide the basis for why the  $\Delta D_{hole}$  adjustment for contact pressure made using the old model remains conservative. (See Section 2.2)
2. Provide an appropriate basis for demonstrating that joints tighten during a postulated SLB event. Why is it acceptable to compare the contact pressures calculated using the original model for NOP to the contact pressures calculated using the new model for SLB for the Model D5 SGs? (See Section 2.3)
3. If both old and new models are conservative, is there an appropriate basis to show the relative conservatism of the methods? (See Section 2.4)

**Part A: (Original RAI#4)**

*Reference 1, Page 6-69: In Section 6.2.5.3, it is concluded that the tube outside diameter and the tubesheet tube bore inside diameter always maintain contact in the predicted range of tubesheet displacements. However, for tubes with through-wall cracks at the  $H^*$  distance, there may be little or no net pressure acting on the tube for some distance above  $H^*$ . In Tables 6-18 and 6-19, the fourth increment in the step that occurs two steps prior to the last step suggests that there may be no contact between the tube and tubesheet, over a portion of the circumference, for a distance above  $H^*$ . Is the conclusion in 6.2.5.3 valid for the entire  $H^*$  distance, given the possibility that the tubes may contain through-wall cracks at that location? (See Section 5.0)*

## 1.0 General Background on Approach and Models

***Discuss if the eccentricity effect on contact pressure is occurring as described. It is the opinion of the NRC staff that the eccentricity effect may not be as significant as being reported by Westinghouse.***

Response:

The reference structural model for the  $H^*$  calculation as described in References 5 and 6 is a 3D FEA model that utilizes the equivalent properties approach for perforated plates in accordance with Reference 6-15 of the  $H^*$  WCAP reports. This model provides the tubesheet displacements that are utilized in the calculation of  $H^*$ . Included in the displacement output from the 3D FEA model are the radius and depth dependent x- and y- axis displacements for the tubesheet. These displacements are the input to the  $H^*$  integrator model that uses the inputs to calculate contact pressures based on thick-shell equations. The tubesheet displacements from the FEA model indicate that the tubesheet bores become eccentric after application of all thermal and pressure loads. The displacement results from the 3D FEA model are the difference between the completely unloaded case and the fully loaded case for the conditions of interest (i.e., NOP, SLB).

The information from the 3D FEA model, that the tubesheet bores become eccentric, led to a question regarding continued tube-to-tubesheet contact in the eccentric tubesheet bore. The impact of tubesheet bore hole out-of-roundness (eccentricity) on the calculation of tube to-tubesheet contact pressures was originally addressed using a scale factor approach as described below and in Reference 6-15 of the  $H^*$  WCAP reports. The fit developed in Reference 6-15, a third order polynomial, was appropriate for the conditions for which it was developed but it provided physically impossible results when extrapolated significantly outside its data basis such as was the case for the SLB conditions for the Model D5 SGs.

To resolve this issue, a separate model, was developed as described in Section 6.2.5 and shown in Figure 6-48 of Reference 5 and 6, to assess tube-to-tubesheet contact under the fully loaded condition (e.g.,  $\Delta P$  and thermal loading) for the small eccentricities that were calculated during the much "colder" temperature postulated SLB conditions for the Model D5 SGs than for the Model F SGs. To properly represent the tube in tubesheet condition, this model considered a tubesheet equivalent cell (the local TS material around a tubesheet bore) and a tube. To address the question if continued contact would exist between the tube and tubesheet after the tubesheet bore becomes eccentric, the tube expansion was analytically simulated to provide a condition of tube to tubesheet contact in a non-eccentric tubesheet bore. This condition was the reference condition for the subsequent loading of the model by pressure loads (thermal loads were not included) and by applying displacement boundary conditions ( $e$ -bar) to simulate the expected range of tubesheet bore eccentricity. The unloaded, post-tube expansion simulation conditions of the model was the reference condition for the displacements provided in Tables 6-18 and 6-19 of the  $H^*$  reports, References 5 and 6.

While eccentricity was the specific focus of this study because of the question raised about continued tube to tubesheet contact in an eccentric condition, the analytical model naturally also provided information on tubesheet bore dilation, the diametral growth of the tubesheet bore represented by the average of the maximum and minimum diameters of the eccentric tubesheet bore. Examination of the results from this model, as is discussed further below, resulted in two significant conclusions:

1. For the tubesheet bore eccentricities and dilation due to the applied loading in the limiting plants in the models of SG considered, the tube remains in contact with the tubesheet bore.
2. While tubesheet bore eccentricity contributes to the reduction in contact pressure between the tube and the tubesheet, tubesheet bore dilation appears to be the principal cause of reduction of contact pressure between the tube and the tubesheet.

### 1.1 Discussion of 3D FEA Model for H\* Analysis

***Provide table showing maximum delta diameters (total diameter distortion) and maximum eccentricities (maximum diameter minus minimum diameter) from the 3 dimensional (3-D) finite element analysis for normal operating and steam line break (SLB), for model F and D5. (The Surry question requests information for the Model 51F)***

Response:

This question is a generic question that is not dependent on a single model of SG. Consequently, the response is provided based on the model F and D5 steam generators as requested in the Turkey Point question and also in the RAIs for the Model F and Model D5 steam generators.

The 3D FEA Model and its application for determining the tubesheet displacements are extensively described in Section 6 of the H\* WCAP reports (References 5 and 6). It is important to note that the 3D FEA model includes the entire tubesheet complex (i.e., tubesheet, stub barrel, channelhead and divider plate) but excludes the tubes. The model utilizes an equivalent material approach from Reference 6-5 in the WCAP reports to represent the deformation of the tubesheet under the applied loading conditions (NOP, SLB/FLB). Displacements in Cartesian coordinates are calculated for these conditions at any location on the tubesheet. The displacements calculated are the changes from an unstressed, room temperature condition after all thermal and pressure loads appropriate to the operating conditions are applied. Application of a uniform temperature increase causes uniform dilation at each tubesheet bore. Application of pressure loads causes distortions in the structure due to bending. The 3D FEA model provides integrated total displacements of each tubesheet bore location.

Table RAI4-1 is a summary of the maximum eccentricities and  $\Delta D$ s for the Model F and Model D5 limiting plants as calculated based on the  $U_R$  (tubesheet radial displacement) results from the 3-D lower SG complex model.

**Table RAI4-1: Summary of Model D5 and Model F NOP and SLB Eccentricity Results**

SG Model	Elev.	Avg. Eccentricity Data		Max. Eccentricity Data		Avg. Δ D		Max. Δ D	
		NOP	SLB	NOP	SLB	NOP	SLB	NOP	SLB
-	Above BTS <sup>(1)</sup>								
-	in	in/in	in/in	in/in	in/in	in	in	in	in
F									
F									
F									
D5									
D5									
D5									
F									
D5									

Notes:  
1. BTS is Bottom of the Tubesheet

The original Table RAI4-4 is provided here for convenience

			Eccentricity, e	Δ D, 0°	Δ D, 90°
Plant	Condition	Value	inch/inch	inch	inch
Byron	SLB	MAX			
Byron	SLB	MIN			
Byron	SLB	AVG			
Millstone	SLB	MAX			
Millstone	SLB	MIN			
Millstone	SLB	AVG			
Byron	NOP	MAX			
Byron	NOP	MIN			
Byron	NOP	AVG			
Millstone	NOP	MAX			
Millstone	NOP	MIN			
Millstone	NOP	AVG			

## 1.2 Discussion of the "Slice" Model

**Clarify the nature of the finite element model ("slice" model versus axisymmetric SG assembly model) used to generate the specific information in Tables 6-1, 2, and 3 (and accompanying graph entitled "Elliptical Hole Factors") of Reference 6-15. What loads were applied? How was the eccentricity produced in the model? (By modeling the eccentricity as part of the geometry? By applying an axisymmetric pressure the inside of the bore?) Explain why this model is not scalable to lower temperatures.**

**The difference between initial and final eccentricity included in Table RAI4-2 needs to be explained. In particular, the exclusive use of the relationship between initial eccentricity and scale factor in calculating contact pressure needs to be justified.**

**Resolve the apparent inconsistency between Item 4 on page 25 and the statement below Figure RAI4-1 regarding how the model in Figure RAI4-1 is loaded.**

Response:

The "slice model" is shown in Figure 6-9 of Reference 6-15 in WCAP-17071-P, WCAP-17072-P, WCAP-17091-P, and WCAP-17092-P.

The data in Tables 6-1, 6-2, and 6-3 of Reference 6-15 of the H\* WCAP reports, are derived from this plane stress model ("slice model") developed in WECAN/PLUS and the contact pressure equation identified on page 6-87 of WCAP-17071-P, page 6-95 of WCAP-17072-P, page 6-91 of WCAP-17091-P and page 6-84 of WCAP-17092-P as described below.

For convenience Tables 6-1, 6-2, and 6-3 of Reference 6-15 are replicated below and re-named as follows: Table 6-1 is renamed as Table RAI4-2, Table 6-2 is renamed as Table RAI 4-3, and Table 6-3 is renamed as Table RAI4-4.

The "initial" eccentricities (defined as  $D_{MAX} - D_{MIN}$ ) applied in the "slice" model in Table RAI4-3 and Table RAI4-4 are directly incorporated into the model geometry. That is, the initial eccentricity is built into the model geometry. The eccentricity values in the model were assumed values for tubesheet tube bore deformation based on engineering judgment and prior experience.

In the "slice" model analysis, the tubesheet is assumed to have a thermal expansion coefficient of zero (0) in/in/°F and the tube material is assumed to have the appropriate ASME Code thermal expansion coefficient values. (The TS coefficient of thermal expansion is set to zero to provide a loading mechanism for the model. When a temperature is applied, the tube "grows" into the tubesheet collar. The temperature difference applied to the tube in the "slice" model was 500°F, for a total tube temperature of 570°F. [Applied 500°F + 70°F assumed room temperature]). The sole purpose of the development of the "slice" model was to provide a sensitivity study to relate the effects of assumed eccentricity ( $D_{MAX} - D_{MIN}$ ) conditions to contact pressures from which the contact pressure ratios were developed. No attempt was made to

reproduce the contact pressures that would be calculated by the 2-D axisymmetric model that was previously used to develop the tubesheet displacements.

The "final" eccentricity ( $D_{MAX} - D_{MIN}$ ) values in Table RAI4-3 and Table RAI4-4 were also determined using the "slice model": The final eccentricity values are the ( $D_{MAX} - D_{MIN}$ ) results of applying the loading conditions on the slice model: The loads applied to the "slice" model were thermal loads only as follows:

- 0 psig - Primary Side Pressure
- 0 psig - Secondary Side Pressure
- 500 °F- Tubesheet  $\Delta T$
- 500 °F- Channel Head  $\Delta T$
- 500 °F- Shell  $\Delta T$

As discussed in Reference 6-15, Table RAI4-3 was constructed using the displacement results from the plane stress model analysis for the elliptical holes along with the contact pressure equations. The effective change in hole diameter was calculated as follows using a series of assumed scale factors:

$$\left[ \begin{array}{c} \Delta D_{MAX} \\ \Delta D_{MIN} \end{array} \right]^{a,c,e} \quad (RAI4-1)$$

The  $\Delta D_{MAX}$  and  $\Delta D_{MIN}$  were taken from the radial and circumferential change in tube bore diameter in the "slice" model.

The corresponding contact pressure for each scale factor was then determined as follows:

$$\left[ \begin{array}{c} P_{MAX} \\ P_{MIN} \end{array} \right]^{a,c,e} \quad (RAI4-2)$$

Equation RAI4-2 is a generic representation of how tube to tubesheet contact pressure is calculated in the H\* integrator spreadsheet analysis. The equation is equivalent to the equation for P2 shown on page 6-87 in WCAP-17071-P, page 6-95 in WCAP-17072-P, page 6-91 in WCAP-10791-P and page 6-84 in WCAP-17092-P.

The scale factors for a given input eccentricity in Table RAI 4-3 result in contact pressure ratios using the thick shell equations that are equal to the contact pressure ratios calculated using the "slice" model for initial eccentricities (defined as  $D_{MAX} - D_{MIN}$ ) equivalent to 0.0002, 0.0004, 0.0006 and 0.0008 inches, respectively, compared to the contact pressures for a circular hole ( $D_{MAX} - D_{MIN} = 0$ ). These scale factors are identified in bold print in Table RAI4-3. The data for the scale factors as a function of "initial" eccentricity was fit by a third order polynomial equation provided on page 6-85 of WCAP-17071-P and page 6-86 of WCAP-17072-P.

Based on a review of Table RAI4-3 and Table RAI4-4, the scale factor [ ]<sup>a,c,e</sup> is the appropriate scale factor for calculating a reduction factor for contact pressure of [ ]<sup>a,c,e</sup> associated with an initial eccentricity of [ ]<sup>a,c,e</sup> ((D<sub>MAX</sub> - D<sub>MIN</sub>)/ [ ]<sup>a,c,e</sup> inch) from the "slice" model. The scale factor of [ ]<sup>a,c,e</sup> relates to a contact pressure reduction factor of [ ]<sup>a,c,e</sup> and corresponds to an initial eccentricity of [ ]<sup>a,c,e</sup> inch, and so forth.

The "final eccentricity" values corresponding to the same scale factors highlighted in bold in Table RAI 4-3 (and Table RAI4-4) are not used in determining the reduction in contact pressure because the resulting third order polynomial relationship between scale factor and eccentricity is bounded by the relationship for "initial eccentricity", i.e., the resultant scale factors, and hence the reduction in contact pressure due to eccentricity, would be less using the third order fit resulting from the "final" eccentricity values from Table RAI 4-3. For example, for an eccentricity of 1E-3 in/in, the scale factor is [ ]<sup>a,c,e</sup> as compared to [ ]<sup>a,c,e</sup> for the trend line associated with the "initial" eccentricity results. Figure RAI 4-1 illustrates this. This figure shows a comparison of the trend line analysis for "initial" eccentricity and "final" eccentricity. Referring to Equation RAI 4-1, larger scale factors result in a greater reduction in contact pressure due to eccentricity.

**Table RAI4-2**  
**Reproduced Table 6-1 of Reference 6-15**

Eccentricity (inch)	Sleeve O.D.			Tube O.D.			a,c,e
	Average <sup>(1)</sup>	Ratio <sup>(3)</sup>	Delta <sup>(1)(2)</sup>	Average <sup>(1)</sup>	Ratio <sup>(3)</sup>	Delta <sup>(1)(2)</sup>	
0.0000							
0.0002							
0.0004							
0.0006							
0.0008							

Notes: This table is developed from the model shown in Figure RAI4-1, below.

1. The units of these columns are stress in psi.
2. The "delta" in this table refers to the maximum deviation from a constant value of the mean linearized radial stress around the tube bore.
3. The ratio is calculated by dividing the contact pressure between the tube and the tubesheet at a given eccentricity by the contact pressure between the tube and the tubesheet in a round tube bore (e=0.0). For example, the ratio of [ ]<sup>a,c,e</sup> calculated in Table 6-1 is a ratio of the average contact pressure at an eccentricity of 0.0002 in of [ ]<sup>a,c,e</sup> psi divided by the average contact pressure at an eccentricity of [ ]<sup>a,c,e</sup> psi.

Table RAI4-3

Reproduction of Table 6-2 of Reference 6-15

Primary Pressure	0	psig
Secondary Pressure	0	psig
Tubesheet Delta T	500	°F
Shell Delta T	500	°F
Channel Head Delta T	500	°F
Sleeve OD Delta D	[ ] <sup>a,c,e</sup>	in
Tube ID Delta D	[ ] <sup>a,c,e</sup>	in
Tube OD Delta D (Thermal)	[ ] <sup>a,c,e</sup>	in
Sleeve/Tube Interaction Coefficients	[ ] <sup>a,c,e</sup>	
Tube/Tubesheet Interaction Coefficients	[ ] <sup>a,c,e</sup>	

Eccentricity		(1)	(2)	(3)	(4)	(5)	(6)
Initial (inch)	Final (inch)	Max/Min Combination <small>a,c,e</small>	Hole Delta D (0 Deg)	Hole Delta D (90 Deg)	S/T Contract Pressure	T/T.S. Contact Pressure	Ratio
0.0000		Minimum <b>Average</b> Maximum					<small>a,c,e</small>
0.0002		Minimum Average <small>a,c,e</small> <div style="border: 1px solid black; height: 40px; width: 60px; margin: 5px auto;"></div> Maximum					
0.0004		Minimum Average <small>a,c,e</small> <div style="border: 1px solid black; height: 40px; width: 60px; margin: 5px auto;"></div> Maximum					

**Table RAI4-3 (Cont'd.)**

Eccentricity <sup>a,c,e</sup>	(1)	(2)	(3)	(4)	(5)	(6)	<sup>a,c,e</sup>
<b>0.0006</b>	Minimum						
	Average <sup>a,c,e</sup>						
	Maximum						
<b>0.0008</b>	Minimum						
	Average <sup>a,c,e</sup>						
	Maximum						

Note: The values in **Bold** identify the source data for Table RAI4-3

**Table RAI4-4**

**Reproduction of Table 6-3 of Reference 6-15**

Initial Delta Dia (in)	Eccentricity <sup>(1)</sup>			Pressure Ratio
	Initial (in/in)	Final (in/in)	Max/Min Factor	
0.0000				
0.0002				
0.0004				
0.0006				
0.0008				

(1) These values are the values for initial and final eccentricity from Table RAI4-2 are divided by the nominal tubesheet hole diameter [ <sup>a,c,e</sup>

[ <sup>a,c,e</sup>

a,c,e



**Figure RAI4-2: Scale Factor Comparison (Initial versus Final Eccentricity)**

The method for calculating the contact pressure for using the "old" method for the Model F SGs (all plant conditions) and the Model D5 SGs (NOP and FLB conditions) and the "new" method for calculating the contact pressure the Model D5 SGs only (SLB conditions) are described below:

**Old Method (Reference 6-15):**

1. The  $U_R$  used in the calculation of the circumferential and radial  $\Delta D$  is based on the linearly scaled 2D axisymmetric FEA model (3-D model for the current  $H^*$  analysis) of the lower SG complex
2. The circumferential and radial  $\Delta D$ 's are used in the scale factor (SF) equation to determine the  $\Delta D_{\text{hole}}$  (see equation RAI4-1) that is used to determine the reduction in contact pressure as a function of eccentricity (e), equation RAI4-2.
3. The relationship between  $\Delta D$  and e is based on the 2-D plane model shown in Figure 6-9 of SM-94-58, Rev.1.

4. The model in Figure 6-9 of SM-94-58, Rev.1 includes the initial applied eccentricities ( $D_{MAX} - D_{MIN}$ ) geometry definition of the model.
5. The "slice" model provides the input for using the SF relationship (Eqn. RAI4-1). The SF is determined by comparing the "slice" model results to the axisymmetric model results for a TS collar and tube model at a given radius in the TS over the full thickness of the TS.
6. The result is then used to calculate the reduction in contact pressure as a function of TS elevation and radius due to TS displacement and tube bore eccentricity. This is appropriate because the conditions for the Model F SG and Model D5 SG (NOP and FLB conditions) are within the range of data for which the scale factor relationship is applicable.

**New Method (WCAP-17091-P, WCAP-17092-P):**

1. The  $U_R$  used in the calculation of the circumferential and radial  $\Delta D$  comes from a 3-D FEA model of the lower SG complex with condition-specific inputs applied.
2. The circumferential and radial  $\Delta D$ 's are compared to determine the maximum  $\Delta D$  that will give the maximum reduction in contact pressure as a function of eccentricity ( $e$ ).
3. The relationship between  $\Delta D$  and  $e$  is based on the 2-D [ ]<sup>a,c,e</sup> model shown in WCAP-17091-P and WCAP-17092-P, section 6.2.5. The model is shown in Figure 6-49 of the WCAP reports. The range of eccentricity used in this study conservatively exceeds the values of tube bore eccentricity calculated from the perforated TS model in Section 6.2.4.
4. The model in Figure 6-49 of the H\* WCAP reports applies boundary conditions to the outer edge of the tube pitch material and does not directly affect the material that is deforming in the tube and tubesheet cell.
5. The TS deformations and tube to tubesheet contact pressure results that produce the maximum reduction in contact pressure at the minimum value of TS tube bore eccentricity are then fit with a linear relationship.
6. The result of the linear relationship is used to determine the reduction in contact pressure between the tube and the tubesheet directly. There are no intermediate equations or results.

A correct prediction of contact pressure loss requires the knowledge of both the proper values of  $D_{MAX}$  and  $D_{MIN}$  associated with the different pressure and temperature conditions at a given tubesheet radius and elevation as well as the value of eccentricity. The values of  $D_{MAX}$  and  $D_{MIN}$  are a function of the radial deflection of the tubesheet,  $U_R$ , as determined by the finite element analysis model (which previously was a 2-D axisymmetric model of the SG lower assembly and at present, is a 3-D model of the SG lower assembly). The results from the "slice" model cannot be linearly scaled to lower temperatures because the method of super-

position has been shown during the development of the current H\* analysis to not apply to the non-linear combination of materials and loading in the lower SG complex. This conclusion led to the development of the 3D FEA model that is the reference model for the H\* analysis. A discussion of this is provided in Section 6.1.2 of WCAP-17091-P and WCAP-17092-P.

### 1.3 Discussion of the Unit Cell Model to Calculate Contact Pressures

The "Unit Cell" model is extensively discussed in Section 6.2.5 of the H\* WCAPs (References 5 and 6). The specific goal of this model was to determine if tube to tube contact would remain when the tubesheet is deformed due to operating loads. An equivalent tubesheet cell is modeled, that is, a tubesheet bore with surrounding tubesheet material, and a tube in the tubesheet bore (see Figure 6-48 of the H\* WCAPs). For the primary purpose of this model – to study if tube-to-tubesheet contact is present during the limiting tubesheet deformations – the model was initialized by simulating the tube expansion process. The expansion process was conservatively simulated by applying a low value of expansion pressure [ ]<sup>a,c,e</sup> inside the tube, resulting in initial tube to tubesheet contact, and then removing the tube expansion internal pressure. The calculated dilation of the tubesheet bore due to the simulation of the tube expansion is [ ]<sup>a,c,e</sup> inch for all models of SG considered.

As discussed in Section 6.2.5 of the H\* WCAP reports, the operating pressure loads, were applied to the initialized model in a sequential manner, and the resulting contact pressures were calculated when a range of displacements (termed "E-bar") were applied as boundary conditions to the model. Figure RAI4-2 shows the updated sequential loading (includes application of thermal loads) of the model and relates it to the steps discussed in Section 6.2.5 and Tables 6-18 and 6-19 of the H\* WCAPs. The "E-bar" values shown as the displacement inputs on Tables 6-18 and 6-19 in the H\* WCAP reports are uni-directional displacements (in inches) that are NOT the same as eccentricity and also not the same as  $\Delta D$ . (Eccentricity is defined as the difference between the maximum and minimum diameters of a bore divided by the nominal diameter of the bore. The units of eccentricity are inch/inch.) The displacement inputs applied to the unit cell model are assumed values that based on prior analyses that envelope the expected tubesheet displacement for all of the applicable operating conditions. It is important to note that the unit cell model as described in Section 6.2.5 of the H\* WCAP reports utilizes boundary conditions chosen to minimize the tube-to-tubesheet contact pressures for the applied relative displacements.

To interpret the results from the unit cell model properly, the following must be observed:

- To address if tube to tubesheet contact continues for all the assumed tubesheet displacements, the appropriate reference condition is the initialized condition (after Step 4) of the model that simulates a tube expanded in the tubesheet bore.

- To compare the results of the unit cell model with the 3D FEA model, the appropriate reference condition of the unit cell model is the initial model (Step 0) without the tube expansion simulated and thermal loads must be included.

Figures RAI4-3 and RAI4-4 show the average tubesheet bore dilation ( $\Delta D$ ) as a function of tubesheet relative displacement (E-bar) for the Model F and Model D5. The average tube bore dilation at zero E-bar input is the result of the temperature and pressure loading of the unit cell model. Initially, application of the displacement input "E-bar" results in more significant hole dilation, but rapidly takes on a shallower slope as the applied displacement increases. The curves are characteristically the same for the Model F and Model D5 steam generators and also for the different operating conditions, NOP and SLB, for the different models of SGs.

Similarly, Figures RAI4-5 and RAI4-6 show the tubesheet bore eccentricity "e" as a function of tubesheet relative displacement (E-bar) for the Model F and Model D5. Eccentricity initially increases with application of the displacement boundary condition (E-bar) simulating the load due to pressure differential across the tubesheet, but the rate of increase decays with increasing E-bar. A significant difference is noted between NOP and SLB conditions at large values of E-bar. This difference reflects the fact that the uniform growth of the tube bore hole due to increased temperature overwhelms the effect of application of the displacement boundary condition (E-bar) on tubesheet bore eccentricity. During the SLB event, the temperature is decreased and the differences in  $D_{MAX}$  and  $D_{MIN}$  remain more significant as the displacement boundary condition is increased, although the rate of increase in the difference between  $D_{MAX}$  and  $D_{MIN}$  is reduced at some point. . Eventually, at NOP conditions, the difference between  $D_{MAX}$  and  $D_{MIN}$  tends to become decrease even though a greater displacement (E-bar) is applied, leading to a reduction of eccentricity "e."

Figures RAI4-7 and RAI4-8 show the contact pressure as a function of tubesheet relative displacement (E-bar) for the Model F and Model D5 for both NOP and SLB conditions based on the unit cell model. As expected, both NOP and SLB contact pressure decrease with increasing displacement inputs, ultimately going to zero at a very large value of applied displacements. It is to be noted that the maximum displacement assumed is significantly greater than would be predicted by the 3D FEA model. Over the entire range of assumed displacement conditions, the SLB contact pressure exceeds that for NOP conditions.

Table RAI4-5 summarizes the eccentricity,  $\Delta D$  and predicted contact pressure using the unit cell model for various values of applied displacement (E-bar) for both the model F and Model D5 SGs. The true eccentricity ( $[D_{max}-D_{min}]/D_{nom}$ ) is shown for the applied displacement, E-bar. Table RAI4-5 also provides a comparison of the  $\Delta D$  predicted by the unit cell model for the two reference conditions noted above, that is, for the total  $\Delta D$  from the model without the simulated tube expansion (reference step 0 in Table 6-18) and for the initialized case with the tube expansion simulated (reference step 4 in Table 6-18).

Further, Table RAI4-5 provides a summary of contact pressures between the tube and the tubesheet for various applied values of E-bar for the Model F and Model D5 SGs. The "Modified Contact Pressure" is the "Raw Contact Pressure" from the unit cell model adjusted for the actual tube expansion process ([ ]<sup>a,c,e</sup> psi compared to the simulation at [ ]<sup>a,c,e</sup> psi) real Model F and Model D5 geometry and more realistic operating conditions of pressures and temperatures. For all cases of applied displacement, positive contact pressure remains between the tube and tubesheet. It should be noted that the largest value of applied displacement (E-bar) is well in excess of the displacement predicted by the 3D FEA model.

Table RAI4-6 provides similar data to that in Table RAI4-5, except that the data is based on the 3D FEA model.

Comparison of Tables RAI4-5 and RAI4-6 leads to the following observations:

1. The  $\Delta D$ s from the 3D FEA model are significantly less than the corresponding  $\Delta D$ s from the unit cell model from the unloaded to the fully loaded condition (i.e., from step 0 to step 9) for both NOP and SLB conditions. This leads to the conclusion that the unit cell model displacement results and contact pressure predictions conservatively represent the reference 3D FEA model results.
2. The eccentricities from the unit cell model are generally comparable to those from the 3D FEA model. A more exact comparison is difficult based on the available data; however, it is clear that the actual range of eccentricities from the 3D FEA model was adequately addressed by the unit cell model.
3. The method of Reference 6-15 of the H\* WCAP report for adjusting contact pressure provides acceptable results for all conditions except the SLB condition for the Model D5 SGs. The method of Reference 6-15 significantly under-predicts contact pressure for the Model D5 SLB conditions. Referring to Figure RAI4-6, the method for calculating the reduction in contact pressure defined by the White Paper, when adjusted for temperature effects, shows that SLB contact pressure is increased relative to normal operating conditions.

**Table RAI4-5  
Eccentricity, Contact Pressure and ΔD Results from Unit Cell Model**

SG Model	"E bar"	Square Cell Results		Square Cell Results		Square Cell Results		Square Cell - Average Delta D			
		Eccentricity		Raw Contact Pressure <sup>(1)</sup>		Modified Contact Pressure <sup>(1)</sup>		Step 0 <sup>(2)</sup> - Step 9 <sup>(3)</sup>		Step 4 <sup>(4)</sup> - Step 9 <sup>(3)</sup>	
		NOP	SLB	NOP	SLB	NOP	SLB	NOP	SLB	NOP	SLB
-	in	in/in	in/in	psi	psi	psi	psi	in	in	in	in
F											
F											
F											
F											
D5											
D5											
D5											
D5											

a,c,e

Notes:  
 1. Accounts for expansion pressure and geometry.  
 2. See Section 6.2.5 H\* WCAP. Step 0 is the condition of the unit-cell model prior to any modifications for tube expansion, loading, etc.  
 3. See Section 6.2.5 H\* WCAP. Step 9 is the condition of the unit cell model after all loading conditions have been applied.  
 4. See Section 6.2.5 H\* WCAP. Step 4 is the initialized condition of the Unit Cell model after tube expansion has been simulated.

**Table RAI4-6  
Eccentricity, Bore Dilation and Contact Pressure from 3D FEA Model**

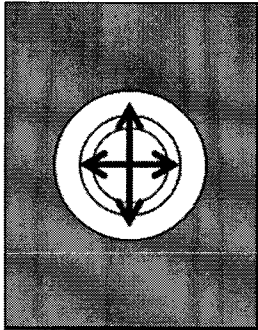
SG Model and Contact Pressure Reduction Model	Hstar Analysis		Hstar Analysis		Hstar Analysis - Avg. Δ D	
	Eccentricity		Avg. Contact Pressure		No Load to Operating	
	NOP	SLB	NOP	SLB	NOP	SLB
	in/in	in/in	psi	psi	in	in
F - Ref. 6-15						
Limiting Radius - F - Ref. 6-15						
D5 - Ref. 6-15						
D5 - White Paper						
Limiting Radius - D5 - Ref. 6-15						
Limiting Radius - D5 - White Paper						
F - Updated Model <sup>(1)</sup>						
D5 - Updated Model <sup>(1)</sup>						

a,c,e

(1): Updated Model Results based on estimates from approximate values in finite element analysis and do not reflect the result of a regression analysis.

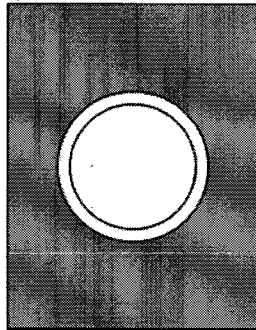
**Figure RAI4-2  
Unit Cell Model and Loading Sequence**

**(1)**



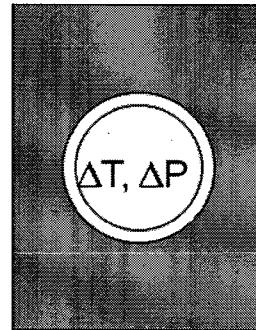
**Step 0**  
 $\Delta P = 0$   
 $\Delta T = 0$   
 Unexpanded Tube  
 $e = 0$   
 $e \text{ bar} = 0$

**(2)**



**Step 5**  
 $\Delta P = 0$   
 $\Delta T = 0$   
 Expanded Tube  
 $e = 0$   
 $e \text{ bar} = 0$

**(3)**



**Step 6-9**  
 $\Delta P > 0$   
 $\Delta T > 0$   
 Expanded Tube  
 $e > 0$   
 $e \text{ bar} > 0$

**Loading Steps:**

0. Initial Model
1. Initial Tube to TS gap
2. Pressurize tube to 16ksi
3. Pressurize tube to 28ksi
4. Release Pressure on Tube
5. Apply  $\Delta T^{(1)}$
6. Apply "E-bar"
7. Apply  $\Delta P = [ \quad ]^{a,c,e}$  psi
8. Apply  $\Delta P = [ \quad ]^{a,c,e}$  psi
9. Apply  $\Delta P = [ \quad ]^{a,c,e}$  psi

Notes: (1) The application of the unit cell model in support of Tables 6-18 and 6-19 does not include application of  $\Delta T$ .



**Figure RAI4-3**  
**Relationship between "E-bar" and  $\Delta D$ ; Model F**

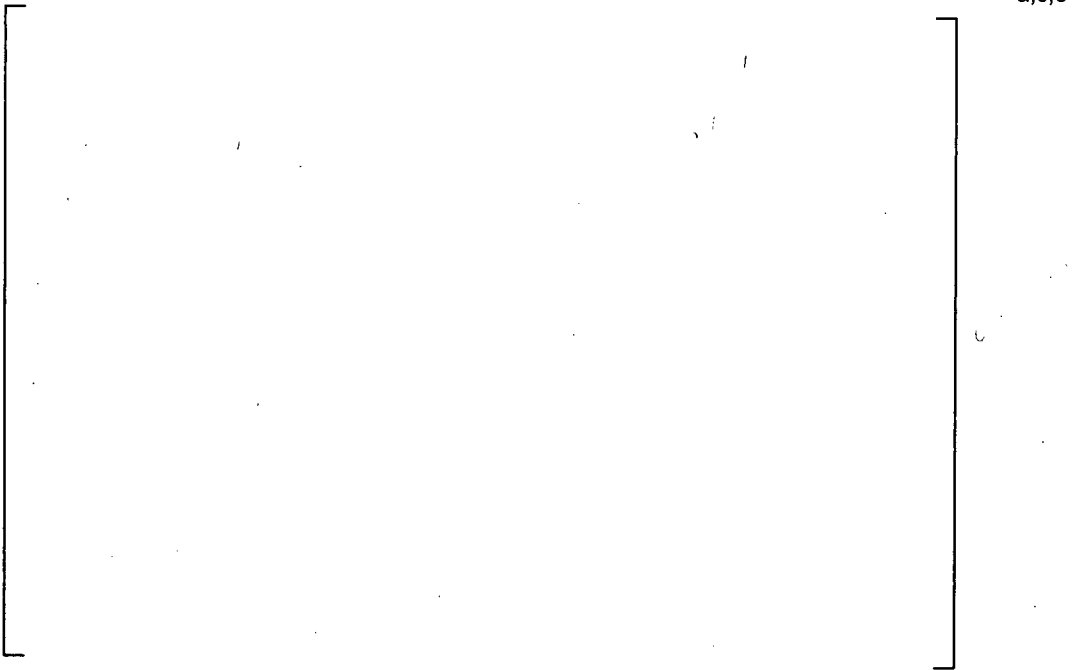


**Figure RAI4-4**  
**Relationship between "E-bar" and  $\Delta D$ ; Model D5**



**Figure RAI4-5**  
**Relationship between "E-bar" and Eccentricity "e"; Model F**



**Figure RAI4-6**  
**Relationship between "E-bar" and Eccentricity "e"; Model D5**



**Figure RAI4-7**  
**Relationship between "E-bar" and Contact Pressure; Model F**



**Figure RAI4-8**  
**Relationship between "E-bar" and Contact Pressure; Model D5**

## 2.0 Comparison of Slice Model and Unit Cell Model Results

***The basis for applying the correlation for scale factor outside an “eccentricity” range of between 1E-3 to 1E-4 inch in the calculation of contact pressure needs to be further explained. Values for displacements included in Table 6-18 (of WCAP-17071) suggest that contact pressure may be lost at displacement ranging between 1E-3 in to 1E-4 in.***

Response:

Interpretation of the displacements noted in Table 6-18 of the WCAP reports was clarified in the prior response, Section 1.3. The values noted in the column titled “Displacement Total” refer to the condition of the unit cell model after Step 4 of the loading sequence (See Figure RAI4-2). When the true reference condition (Step 0) for total displacement is considered, the values of total displacement are significantly larger as noted previously.

Westinghouse agrees that the derivation of the fit in Reference 6-15 is non-intuitive and limited in its application. However, the results of applying the fit described in reference 6-15 are acceptable relative to a best case finite element model (unit cell with thermal and  $\Delta P$  loading) for the reasons described below.

Westinghouse also agrees that the fit that describes the reduction in contact pressure for the steam line break condition in the Model D5 White Paper does not account for the reduction in contact pressure due to tube bore dilation in the same manner as the fit described in Reference 6-15. The results of using the fit described in Reference 6-15 also match the expected trend from a best case finite element model. See the response to b.4 below for more details.

A series of tubesheet tube bore eccentricities were applied to the tubesheet cell model and combined with different pressure and temperature loads. The average, maximum and minimum values of the tube-to-tubesheet (T/TS) contact pressures around the circumference of the tube were reported. The values of tubesheet relative displacement, pressure and temperature that were used in the analysis are summarized in the table below.

Input Conditions for Unit Cell Model (no correlation implied)		
$\bar{e}$	Internal Pressure	Temperature Difference
in	$\Delta P$ , psi	$\Delta T$ , °F <sub>a,c,e</sub>
0.00	[	]
2.0E-04	[	]
4.0E-04	[	]

Normal operating (NOP) conditions in the Model D5 and Model F steam generators are represented by a  $\Delta P$  of [ ]<sup>a,c,e</sup> psi and a  $\Delta T$  of [ ]<sup>a,c,e</sup> °F. Main steam line break (SLB) conditions in the Model D5 are represented by a  $\Delta P$  of [ ]<sup>a,c,e</sup> psi and a  $\Delta T$  of [ ]<sup>a,c,e</sup> °F. The value of  $\Delta P$  in the tubesheet cell can change as a function of elevation in the tubesheet due to the distribution of crevice pressure. The results of the study include the data for a depth ratio of 0.9 which is an elevation roughly 2 inches below the top of the tubesheet. The values of  $\Delta P$  represented in this study account for the region of interest near the top of the tubesheet where the maximum eccentricity in the tubesheet is expected and where the crevice fluid is transitioning from the crevice conditions to the secondary side fluid conditions. The region roughly 2 inches below the top of the tubesheet is also where a significant portion of the T/TS contact pressure develops so it is a good indicator of trends in the effect that different operating conditions have on the contact pressure.

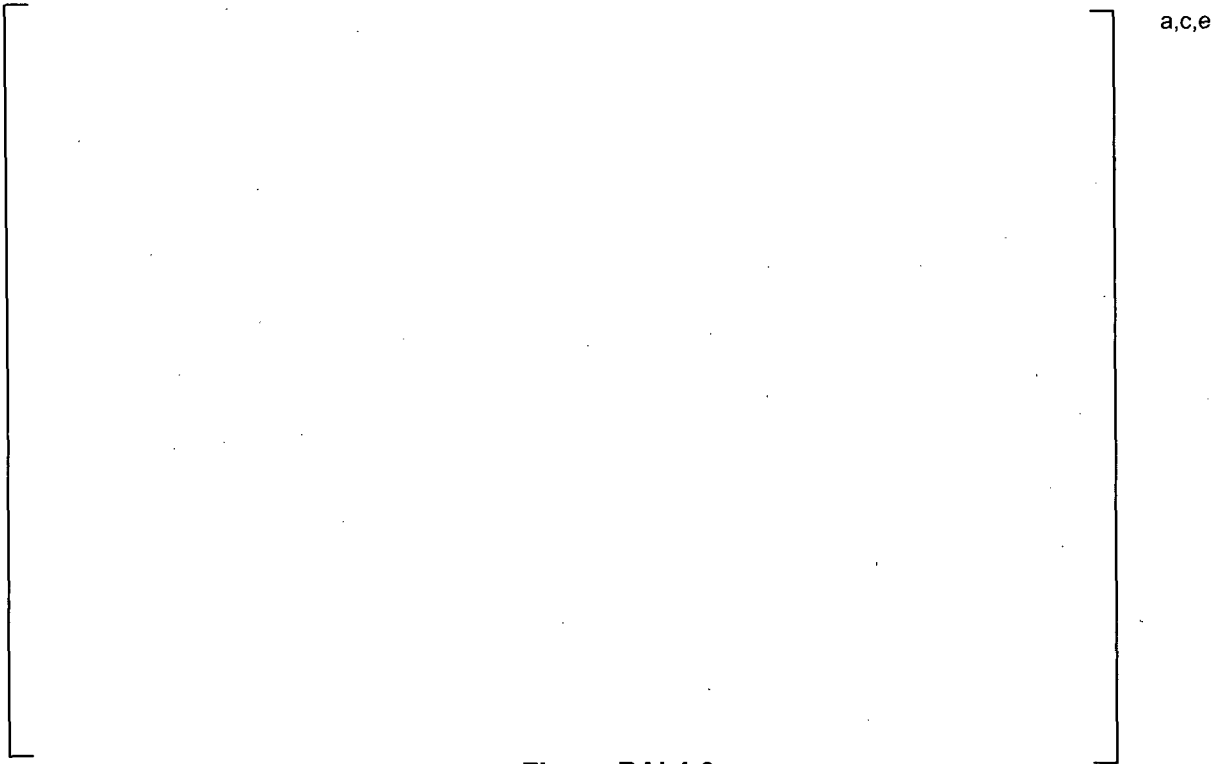
The original results in section 6.2.5 of WCAP-17071-P were used to verify that the reduction in T/TS contact pressure as a function of tubesheet tube bore eccentricity was appropriate for the Model F SG. The original relationship that is used to define the reduction in T/TS contact pressure as a function of eccentricity is described in section 6.3 of WCAP 17071-P and WCAP 17072-P. However, the result of applying the fit described in section 6.3 to the Model D5 SG during SLB was shown to be inconsistent with the expected trend from the more detailed analysis described in section 6.2.5. The results of section 6.2.5 were then used to define a new relationship between the reduction in T/TS contact pressure and tube bore eccentricity. This new relationship is described in the Model D5 White Paper (Reference 12). Figure RAI4-8 shows the result of applying the new relationship to the Model D5 SLB conditions (i.e., White Paper results, Reference 12) in comparison with the results from the old 3<sup>rd</sup> order polynomial relationship. Because the tubesheet temperature induced hole dilation, potentially the most significant factor in contact pressure reduction, was not considered in the Model D5 condition results, a third curve was added to the figure titled "Model D5 FEA trend." This curve represents the most accurate calculation of the contact pressure ratio.

Figure RAI4-9 shows the contact pressure ratio ( $PC_{SLB}/PC_{NOP}$ ) as a function of tubesheet relative displacement,  $E$ -bar. It is clear from Figure RAI4-9 that the results of using the old fit for the Model D5 SLB are inconsistent with the more detailed analysis. At SLB conditions, the tubesheet bore dilation is relatively larger than at NOP conditions due to the increased bending of the TS and decreased thermal expansion. Therefore, it is expected that the T/TS contact pressure ratio should increase by a factor of at least [ ]<sup>a,c,e</sup> (see Figure RAI4-9) when going from NOP to SLB. It is also expected that the tube to tubesheet contact pressure should decrease with increasing tube bore eccentricity. The  $H^*$  results using the old fit for the Model D5 clearly do not follow either expectation from the detailed analysis. However, when the new fit results are applied to the  $H^*$  calculation process the relationship between T/TS contact pressure in the Model D5 is much more reasonable and follows the expected trend from the more detailed analysis.

The Model F  $H^*$  contact pressure results, using the old fit, are well within the range predicted by the more detailed analysis in section 6.2.5 and the additional work described in this RAI response. See Figure RAI 4-10 below. This means that the old fit is appropriate to use for the

Model F NOP and SLB conditions and the NOP condition in the Model D5 SG. The results of using the fit described in Reference 6-15 match the expected trend from a best case finite element model for the NOP and SLB conditions for the Model F SGs and NOP conditions for the Model D5 SG.

To further address the concern that contact pressure may be lost at displacements ranging between 1E-3 in and 1E-4 in, the "Unit Cell" model is extensively discussed in Section 1.3 of this response above.



**Figure RAI 4-9**



**Figure RAI 4-10**

## 2.1 Calculation Basis for Contact Pressure Reduction Factors

***Provide the calculation basis for the upper and lower curves provided in Figure RAI 4-2***

Response:

The original figure RAI4-2, referred to in the question, is reproduced here as RAI4-10 to provide the foundation for the question and the response. Note that the scale of the y-axis has been corrected as discussed in the meeting on August 17, 2009.



**Figure RAI4-10 (original Figure RAI4-2)**

The upper curve in the figure above is based on the data from the following table:

Eccentricity ( $\Delta D_{max} - \Delta D_{min}$ ) (in)	Reduction in Contact Pressure (psi)(1)	Normalization Basis (psi)	Contact Pressure Reduction Factor(psi/psi)
0	0	1200	0
2E-4	[ ] <sup>a,c,e</sup> psi		[ ] <sup>a,c,e</sup>
4E-4	[ ] <sup>a,c,e</sup> psi		[ ] <sup>a,c,e</sup>
5E-4	[ ] <sup>a,c,e</sup> psi		[ ] <sup>a,c,e</sup>
6E-4	[ ] <sup>a,c,e</sup>		[ ] <sup>a,c,e</sup>
Notes: (1) Contact stress reductions are based on the values on Table RA14-3			

Referring to Table RAI 4-3, the contact pressure for a round tube bore hole is calculated to be [ ]<sup>a,c,e</sup> psi (Ratio = 1.0). The contact pressure for a tube bore hole that results in a contact pressure ratio reduction of [ ]<sup>a,c,e</sup> (Ratio = [ ]<sup>a,c,e</sup>), which corresponds to an eccentricity of 2E-4 inch, is [ ]<sup>a,c,e</sup> psi. The absolute reduction in contact pressure is [ ]<sup>a,c,e</sup> psi.

The total reduction in contact pressure using the new model is approximately [ ]<sup>a,c,e</sup> psi (see Figure 6-69 of WCAP-17072-P). To plot the absolute reduction in contact pressure of [ ]<sup>a,c,e</sup> psi for an eccentricity of 2E-4 on Figure RAI4-10, the value is normalized by the total reduction in contact pressure of [ ]<sup>a,c,e</sup> psi from the new method. This value represents a reduction in contact pressure of [ ]<sup>a,c,e</sup>.

Again, referring to Table RAI 4-3, the contact pressure for a round tube hole is calculated to be [ ]<sup>a,c,e</sup> psi. The contact pressure for a tube bore hole that results in a contact pressure ratio reduction of [ ]<sup>a,c,e</sup> (Ratio = [ ]<sup>a,c,e</sup>), which corresponds to be eccentricity of 4E-4 inch, is [ ]<sup>a,c,e</sup> psi. The absolute reduction in contact pressure is [ ]<sup>a,c,e</sup> psi.

Again, the total reduction in contact pressure using the new model is approximately [ ]<sup>a,c,e</sup> psi (see Figure 6-69 of WCAP-17072-P). To plot the absolute reduction in contact pressure of [ ]<sup>a,c,e</sup> psi for an eccentricity of 4E-4 on Figure RAI4-10, the value is normalized by the total reduction in contact pressure of [ ]<sup>a,c,e</sup> psi from the new method. This value represents a reduction in contact pressure of [ ]<sup>a,c,e</sup>.

The same calculation was completed for an eccentricity of 6E-4 in. The value for 5E-4 in is an interpolated value between 4 E-4 in and 6E-4 in.

The bottom curve in the figure above is generated using the 3<sup>rd</sup> order polynomial fit. The results are summarized in the following table:

E, eccentricity (in)	T/TS Contact Pressure Reduction (psi)	Normalized Contact Pressure Reduction
6.36E-07	[ ] <sup>a,c,e</sup>	[ ] <sup>a,c,e</sup>
5.53E-05	[ ] <sup>a,c,e</sup>	[ ] <sup>a,c,e</sup>
3.16E-04	[ ] <sup>a,c,e</sup>	[ ] <sup>a,c,e</sup>
5.69E-04	[ ] <sup>a,c,e</sup>	[ ] <sup>a,c,e</sup>
9.07E-04	[ ] <sup>a,c,e</sup>	[ ] <sup>a,c,e</sup>

**2.2 Conservatism of 3<sup>rd</sup> Order Polynomial Fit from WCAP Reference 6-15**

***Provide the basis for why the  $\Delta D_{hole}$  adjustment for contact pressure made using the old model remains conservative.***

Response:

The key conclusions from the comparison of the Reference 6-15 analysis, the WCAP results and the results of the square cell tubesheet model are:

- 1.) The fit described in Reference 6-15 of the H\* WCAP reports is conservative when applied to the NOP condition in both the Model D5 and Model F SG. The fit tends to underestimate the contact pressure during NOP by as much as [ ]<sup>a,c,e</sup> psi to [ ]<sup>a,c,e</sup> psi for the Model F SG and as much as [ ]<sup>a,c,e</sup> % for the Model D5 SG ([ ]<sup>a,c,e</sup> psi to [ ]<sup>a,c,e</sup> psi) (see Table RA14-6).
- 2.) The fit described in Reference 6-15 of the H\* WCAP reports is comparable when applied to the SLB condition in the Model F SG. The fit described in the Model D5 White Paper tends to over-estimate the contact pressure, by as much as [ ]<sup>a,c,e</sup> %, during SLB ([ ]<sup>a,c,e</sup> psi to [ ]<sup>a,c,e</sup> psi) because the White Paper does not fully account for the change in tube bore diameter during the transient.
- 3.) The fit described in Reference 6-15 of the H\* WCAP reports significantly under-estimates the contact pressure, by as much as [ ]<sup>a,c,e</sup> %, during the D5 SLB condition (from [ ]<sup>a,c,e</sup> psi to [ ]<sup>a,c,e</sup> psi).
- 4.) The square cell tubesheet finite element model shows an increase in contact pressure when going from NOP to SLB conditions in both the D5 and F SGs.

- 5.) Using the results from the square cell model to estimate the magnitude of the contact pressure reduction from the change in tube bore diameter calculated using the 3D finite element results from the lower SG tubesheet complex model show that the contact pressure still increases when going from NOP to SLB conditions in both the Model F and Model D5 SG.

The results of this analysis show that NOP contact pressures that define  $H^*$  in the Model F and Model D5 SG are conservative and that a more realistic model of contact pressure reduction as a function of tube bore deformation (including both dilation and eccentricity) would predict an increase in tube to tubesheet contact pressure at SLB conditions compared to NOP conditions.

(See also Section 2.3)

### 2.3 SLB vs. NOP Contact Pressures

***Provide an appropriate basis for demonstrating that joints tighten during a postulated SLB event. Why is it acceptable to compare the contact pressures calculated using the original model for NOP to the contact pressures calculated using the new model for SLB for the Model D5 SGs?***

Response:

Table RAI4-5 provides a summary of contact pressures between the tube and the tubesheet for various applied values of E-bar for the Model F and Model D5 SGs. Comparison of the eccentricity values calculated using the unit cell model (see Table RAI4-5) with the eccentricity values calculated from the 3D FEA model (see Table RAI4-1) shows that the eccentricities from both models are comparable. It is not reasonable to expect exact matches of numbers between the two models, however, the order of magnitude of the calculated eccentricities is the same. Given that the two structural models provide similar eccentricities, the unit cell model shows that for these eccentricities, positive contact pressure exists between the tubes and the tubesheet for the entire range of displacements considered. Further, the results show that the contact pressures at SLB conditions exceed those at NOP conditions (See Table RAI4-6). See also the discussion in Section 2.4 below.

## 2.4 Relative Conservatism of “Old” and “New” Fit

***If both old and new models are conservative, is there an appropriate basis to show the relative conservatism of the methods?***

Response:

As noted above in Section 1.3 of this response, tube bore dilation is a more significant factor in determining tube-to-tubesheet contact pressure at higher temperatures and the effect of eccentricity on contact pressure is reduced at higher temperatures. The methodology for addressing the effect of eccentricity on contact pressure discussed in Reference 6-15 and utilized in WCAP-17071-P, WCAP-17072-P, WCAP-17091-P and WCAP-17092-P reflects this fact and it, therefore, provides acceptably accurate contact pressure results at higher temperatures (i.e., for all conditions except the “colder” SLB condition). This includes NOP, SLB (higher temperature, > 400°F, and FLB, where appropriate).

Also, as noted in Section 1.3 of this report, the effect of eccentricity on contact pressure loss is a more significant factor at the lower SLB temperatures for the Model D5 SG, but tube bore dilation due to temperature and pressure needs to be considered (which was not addressed in the “new” method, a.k.a the White Paper method discussed in WCAP-17072-P or 17091-P). Moreover, the original 3rd order polynomial fit significantly over-predicts contact pressure loss during the “colder” Model D5 SLB transient (and Model 44F two loop plant SLB).

Therefore, a more detailed model for contact pressure during a postulated SLB was developed. Referring to Table RA14-6, it shows that contact pressure increases during a SLB event ([ ]<sup>a,c,e</sup> psi) relative to NOP ([ ]<sup>a,c,e</sup> psi) with primary and secondary side temperatures as low as 212°F when comparing contact pressures for NOP conditions for the unit cell to contact pressures for SLB for the unit cell.

Again, referring to Table RA14-6, it has been shown when comparing contact pressures for NOP conditions for the unit cell to contact pressures for SLB for the unit cell for the Model F SG (higher temperature SLB conditions), that contact pressure increases during a postulated SLB (from [ ]<sup>a,c,e</sup> psi at NOP to [ ]<sup>a,c,e</sup> psi at SLB).

### 3.0 Comparison of 3D FEA and Unit Cell Model Results

***The eccentricities included in Table RAI 4-4 appear larger than anticipated. Need to confirm that positive contact pressure exists around the entire circumference of the tube and state this clearly in the response.***

Response:

Comparison of the eccentricity values calculated using the unit cell model (see Table RAI4-5) with the eccentricity values calculated from the 3D FEA model (see Table RAI4-1) shows that the eccentricities from both models are comparable. It is not reasonable to expect exact matches of numbers between the two models, however, the order of magnitude of the eccentricities calculated is the same. Given that the two structural models provide similar eccentricities, the unit cell model shows that for these eccentricities, positive contact pressure exists between the tubes and the tubesheet for the entire range of displacements considered. Further, the results show that the contact pressures at SLB conditions exceed those at NOP conditions.

### 4.0 Additional Background Information For Key Questions and Issues

RAI#4 evolved in several stages, each stage building on the prior stage. Reference 10 provided additional questions to augment those that were provided by Reference 5. Responses were prepared and were discussed in a telephone conference on August 11, 2009. During this telephone conference, additional questions were raised as identified in the introduction of this document. The following are responses that were provided in response to Reference 10 that were discussed in the August 11, 2009 telephone conference. They are historical in nature and are provided to complete the record of information provided in response to the NRC request for additional information.

#### 4.1 Comparison of "Old and New" Relationship for Reduction in Contact Pressure and Eccentricity

***In Figure 2 of the White Paper, add a plot for original relationship between reductions in contact pressure and eccentricity as given in Reference 6-15 in the graph accompanying Table 6-3. Explain why this original relationship remains conservative in light of the new relationship. Explain the reasons for the differences between the curves.***

In order to superimpose the results of the "old" and "new" analyses for reduction in contact pressure related to eccentricity, the data for the "old" method must be normalized in the same fashion that Figure 2 has been normalized. The plot of contact pressure reduction included in

Figure 2 of the White Paper represents the total reduction in contact pressure associated with a given eccentricity. The information from Table 6-3 represents the ratio of the contact pressure calculated at a given eccentricity divided by the contact pressure calculated for a tubesheet bore with no eccentricity. For the new analysis, the total reduction in contact pressure for the eccentricities ( $D_{MAX} - D_{MIN}$ ) for a range of up to [ ]<sup>a,c,e</sup> inch is determined to be [ ]<sup>a,c,e</sup> psi. For the old analysis, the total reduction in contact pressure for eccentricities in the same range is calculated to be [ ]<sup>a,c,e</sup> psi. The normalization basis is the same for both curves on the figure.

Figure RAI4-11, showing the normalized results as discussed during the August 17, 2009 meeting, is provided below. (Figure RAI4-11 is the same as Figure RAI4-10 in Section 2.1 of this document, except that the values of the "Old Polynomial Results" have been corrected on Figure RAI4-10 by a factor of 2 as discussed in the August 17, 2009 meeting.) The curve labeled "Old" Model Results is based on the data from Table RAI4-3 (Table 6-2 of Reference 15 of the WCAP report). The curve labeled "New" Model reproduces Figure 2 in the White Paper (Reference 12). The curve labeled "D5 SLB Polynomial Fit" are the results when the eccentricity data and  $\Delta D_{hole}$  for the Model D5 SLB condition are applied directly to the polynomial fit, equation 6-8 in WCAP-17072-P and similar equation on page 6-85 in WCAP-17071-P. The latter curve is based on the maximum displacement conditions at the top of the tubesheet for the Model D5.

The curve labeled "Old Model Results" (top curve on Figure RAI4-11) is misleading relative to making an assessment of the conservatism of the new analysis method compared to the old analysis method. Unlike the new analysis method, which is only applied to the SLB case for the Model D5 SGs, the old analysis method has not been applied as a linear function as represented in the figure as the uppermost curve (solid squares). In reality, the old data fit (top curve on Figure RAI4-11), which is a 3rd order polynomial fit, when extrapolated significantly outside its supported data range (i.e., at temperatures either significantly above or below 500°F), provides physically unrealistic results as shown on Figure RAI4-11 (bottom curve,  $\Delta$ -symbols). The Model D5 SLB condition puts the tubesheet at a nearly uniform temperature of less than 300°F, which is far outside of the range for which the eccentricity relationship was developed in Reference 6-15 in the WCAP reports.

The original relationship remains conservative because it predicts greater reduction of tube to tubesheet contact pressure than the new method for all operating conditions. However, the original relationship is only valid when  $\Delta D_{min}$  and  $\Delta D_{max}$  are within [ ]<sup>a,c,e</sup> % and eccentricity is within [ ]<sup>a,c,e</sup> inch to [ ]<sup>a,c,e</sup> inch range, (i.e., the basis of the original fit).

The maximum tube bore distortions occur at the top of the tubesheet. The results from applying the old fit for the relationship versus the new fit for the relationship for the Model D5 SLB tubesheet displacements and contact pressures are shown in Table RAI4-7. The tube-to-tubesheet (T/TS) contact pressure result due to thermal expansion of the tube and the pressure expansion of the tube including the effect of the crevice pressure distribution, is the same in the both the "old" and "new" cases in the Table RAI4-7.

**Table RAI4-7  
Summary of Model D5 SLB Contact Pressure Results for  
Different Eccentricity Fit Relationships**

Model D5			T/Ts P <sub>CON</sub> Reduction		T/Ts P <sub>CON</sub>	
Condition	Value	Eccentricity	Old	New	Old	New
SLB	Avg					
SLB	Max					
SLB	Min					

a,c,e

The results in Section 6.2.4 of WCAP-17071-P and WCAP-17072-P show that the average expected tubesheet-tube-bore eccentricity is on the order of [ ]<sup>a,c,e</sup> inch. The results in Table RAI4-7 show that the old method of calculating the reduction in contact pressure due to tubesheet-tube-bore eccentricity and change in diameter is conservative for larger values of eccentricity and ΔD (predicts greater decrease in contact pressure) than the new fit. However, it is inappropriate to use the old method at smaller values of eccentricity and ΔD because it provides physically impossible results (see Table RAI4-7). For example, the “old” method predicts a larger decrease in contact pressure for a smaller eccentricity on the order of 10<sup>-7</sup> inch than for a larger eccentricity on the order of 10<sup>-3</sup> inch. The “new” method, by comparison, predicts a slightly positive increase in contact pressure for an eccentricity of 10<sup>-7</sup> inch and a large reduction in contact pressure for an eccentricity of 10<sup>-4</sup> inch or greater, a physically realistic result. The reason that the “old” method predicts such a different reduction in contact pressure for small values of eccentricity is that these small eccentricity values are well outside the range of the data upon which the “old” relationship was developed. However, when used within its intended range of eccentricities and tubesheet bore displacement, the “old” method provides valid and conservative results. The “new” method of calculating the reduction in T/Ts contact pressure is linear and directly accommodates small calculated values of eccentricity. It is also clear from the results in Table RAI4-7 that the results from the old method when used in its supported eccentricity range are highly conservative compared to the “new” method.



a,c,e

**Figure RAI4-11**  
**Original Figure RAI4-2 Discussed at the August 17, 2009 Meeting**

#### 4.2 Use of Both "Old" and "New" Fit

***When establishing whether contact pressure increases when going from normal operating to steam line break conditions, how can a valid and conservative comparison be made if the normal operating case is based on the original delta contact pressure versus eccentricity curve and the SLB case is based on the new curve?***

Response:

It is important to note that the new analysis method is only used for the SLB condition for the Model D5 steam generators. Comparison of contact pressures between the normal operating condition and the SLB condition is made for the Model F steam generators in the H\* fleet in WCAP-17071-P on a consistent basis.

It is Westinghouse's engineering judgment that the old methodology provides an accurate determination of contact pressures during normal operating conditions and postulated accident conditions (FLB and SLB) when peak temperatures range between [ ]<sup>a,c,e</sup> °F and eccentricities are between [ ]<sup>a,c,e</sup> inch and [ ]<sup>a,c,e</sup> inch and  $D_{max}$  and  $D_{min}$  are within [ ]<sup>a,c,e</sup> % of each other.

Application of the new method to calculate eccentricities and values of  $D_{max}$  and  $D_{min}$  that fall outside the above noted range provides conservative results because the plane strain model upon which it is based over-estimates the stiffness of the tube and tubesheet structure leading to lower contact pressure results as a function of eccentricity. The new method also excluded the effect of temperature and therefore, conservatively bounds the lower temperatures of the Model D5 SLB transient. The T/TS contact pressure results during SLB are still expected to bound the T/TS contact pressure results during NOP because, even though the tube bore eccentricity during SLB is generally greater than that during NOP, the overall growth of the tube bore during NOP is greater than that during SLB. Larger magnitudes of tube bore growth are directly related to decreasing tube-tubesheet contact pressure regardless of the value of calculated tube bore eccentricity.

It is appropriate to compare the Model D5 SLB contact pressure results from the "new" method to the Model D5 NOP results from the "old" method because each condition uses the appropriate fit to conservatively determine the reduction in T/TS contact pressure due to tube bore eccentricity and tube bore growth.

The sole purpose of the new methodology was to develop a more accurate way of calculating contact pressures during a postulated SLB for the Model D5 steam generators. The comparison provided in Figure 6-83 of WCAP-17072-P remains a valid comparison.

## 5.0 Part A (Original RAI#4)

**Reference 1, Page 6-69: In Section 6.2.5.3, it is concluded that the tube outside diameter and the tubesheet tube bore inside diameter always maintain contact in the predicted range of tubesheet displacements. However, for tubes with through-wall cracks at the  $H^*$  distance, there may be little or no net pressure acting on the tube for some distance above  $H^*$ . In Tables 6-18 and 6-19, the fourth increment in the step that occurs two steps prior to the last step suggests that there may be no contact between the tube and tubesheet, over a portion of the circumference, for a distance above  $H^*$ . Is the conclusion in 6.2.5.3 valid for the entire  $H^*$  distance, given the possibility that the tubes may contain through-wall cracks at that location?**

The following response to RAI#4 was included in Reference 11. The same response is included here to complete the record of information provided in regard to RAI#4 of References 5, 6 and 7.

Response:

The conclusions reached in Section 6.2.5.3 of WCAP-17071-P are valid for the entire  $H^*$  distance because of the following considerations:

1. The primary source of contact pressure between the tube and the tubesheet is differential thermal expansion between the tubes and the tubesheet. The analysis in Section 6.2.5.3 specifically excludes the effect of thermal expansion of the tube from the analysis. The tubesheet is assumed to deform due to the combination of pressure and thermal loads which produces the tube bore ovalization and leads to the displacements applied in this model. Only the residual effects from installation are considered for the tube in steps 1 through 5. The tube internal pressure applied in these steps only simulates the hydraulic expansion pressure to establish the initial conditions for the following step. The conditions assumed for this study are not possible during any operating condition in the steam generator but are conservative relative to actual SG conditions. (Note: Residual contact pressure is not used in the calculation of  $H^*$  values in Section 6. The residual effects of installation are included in the results of Section 6.2.5.3 so that the sensitivity of a strain hardened tube to tubesheet tube bore deformation can be studied.)
2. Step 5 on Tables 6-18 and 6-19 is not representative of any condition in the steam generator because it assumes that the tubesheet is at operating temperature with an applied primary-to-secondary pressure differential while the tubes remain at room temperature and are not pressurized. That is why Steps 1 through 5 are described as "initializing" steps in the process. It is physically impossible for these conditions to occur simultaneously in the same steam generator.

3. Because no pressure loading is applied to the tube in Step 5 of the analysis discussed in section 6.2.5, the results presented in Tables 6-18 and 6-19 are applicable regardless of whether, or not, a through-wall crack exists at the  $H^*$  location. The more representative case is Step 6 shown on Tables 6-18 and 6-19 in which tube internal pressure is included. For that case, the potential point of zero contact pressure is at an applied displacement a factor of 5 greater than for Step 5, and far in excess of what is reasonably predicted for the actual tubesheet deformation. The factor of 5 difference in required displacement to cause the contact pressure to reduce to zero more than adequately covers the postulated potential local reduction in crevice pressure due to a circumferential separation at the location of  $H^*$ . Recall also, that no thermal expansion of the tube is considered in this analysis.

It is also noted that tables 6-18 and 6-19 are the results of a sensitivity study that is not intended to represent the integrated calculation for  $H^*$ . The integrated  $H^*$  analysis is a complex process that combines the effects of several types of loading and deformation into an integrated estimate of the tube-to-tubesheet contact pressure. Therefore, it is not appropriate to consider a sensitivity study out of the context of the greater analysis. The integrated analysis presented in the complete Section 6 shows that for the combined case of the thermal effects, pressure effects, and tubesheet displacement there is tube-to-tubesheet contact pressure throughout the tubesheet.

It is acknowledged that the cut end of a tube is radially less stiff than a tube that is radially loaded at a point away from the tube end, and that the presumption of a tube sever at the  $H^*$  distance may represent the case of a tube end. The decreased tube-end stiffness is referred to as "compliance." In other words, a tube that is loaded at the cut end provides less resistance to the load than a tube with equal load applied a distance removed from the tube-end. Thus, conceptually, a local "end effect" could be expected to occur due to the increased compliance of the tube-end.

The calculation process for  $H^*$  shown in Figure 1-1 of the  $H^*$  WCAP reports and discussed in several places in the report notes that an adjustment is made to the initial prediction of  $H^*$  to account for the distributed crevice pressure referenced to the predicted  $H^*$  position. Thus, the greatest crevice pressure is always located at the final value of  $H^*$ . Increased tube compliance cannot result in a higher local crevice pressure than is already included in the analysis because, at the point of sever, the primary side pressure is the crevice pressure.

It may be postulated that the increased tube compliance results in reduced contact pressure because the net differential pressure across the tube wall is zero. At the tube-end, the current analysis already includes a zero differential pressure due to the adjustment process for distributed crevice pressure. Therefore, the net reduction in contact pressure would be limited to the axial length of the local effect and would further depend on the slope of the decrease in crevice pressure.

For the Model F and Model D5 SGs, the bounding value of isolation distance above the tube end is 0.6 inch based on classical solutions for the design of pressure vessels (Timoshenko).

The isolation distance is the generically applicable minimum separation distance from an applied load to a point of interest in order to safely assume that the load is in the far field relative to the point of interest. Specific structures and load cases may have different isolation distances but the classical result by Timoshenko for a pressure vessel will conservatively bound any specific cases. For this length, the slope of the contact pressure curve would have to decrease by a factor of at least  $[ ]^{a,c,e}$  before the value of  $H^*$  is affected by more than  $[ ]^{a,c,e}$  inch. If the tube is conservatively modeled as a center-loaded beam on an elastic foundation compared to an end-loaded beam on an elastic foundation, the resulting worst case change in structural compliance and the resulting contact pressure slope could be a factor of up to 2. Alternatively, similar analyses for the cross sections of curved beams suggest that the change in compliance of the structure could be as high as a factor of 6. Neither case approaches the factor of  $[ ]^{a,c,e}$  required based on classical pressure vessel analysis to impact the value of  $H^*$ ; therefore, no additional adjustments to  $H^*$  are necessary to address the potential end effects.

#### 6.0 Summary of the Response to RAI #4

A summary of the response to the original RAI# 4 and additional questions related to RAI 4 are provided below:

1. No additional adjustment to the value for  $H^*$  is necessary to address the potential for end effects. This is because the greatest crevice pressure is always located at the final value of  $H^*$ . At the  $H^*$  distance, the current analysis already includes a zero pressure differential due to the adjustment process for the distributed crevice pressure. Therefore, the net reduction in contact pressure would be limited to the axial length of the local effect and would further depend on the slope of the decrease in crevice pressure. It is judged that the slope of the contact pressure curve would not decrease at a rate such that the value of  $H^*$  would be affected.
2. Tube bore dilation is a more significant factor in determining tube-to-tubesheet contact pressure at higher temperatures and the effect of eccentricity on contact pressure is reduced at higher temperatures. The methodology for addressing the effect of eccentricity on contact pressure discussed in Reference 6-15 and utilized in WCAP-17071-P, WCAP-17072-P, WCAP-17091-P and WCAP-17092-P reflects this fact and, therefore, it provides acceptably accurate contact pressure results at higher temperatures (i.e., for all conditions except the "colder" SLB condition). This includes NOP, SLB (higher temperature, > 400°F, and FLB, where appropriate).
3. The results of using the fit described in Reference 6-15 match the expected trend from a best case finite element model for the NOP and SLB conditions for the Model F SGs and NOP conditions for the Model D5 SG.
4. The  $\Delta D$ s from the 3D FEA model are significantly less than the corresponding  $\Delta D$ s from the unit cell model from the unloaded to the fully loaded condition (i.e.,

from step 0 to step 9) for both NOP and SLB conditions. This leads to the conclusion that the unit cell model displacement results and contact pressure predictions conservatively represent the reference 3D FEA model results.

5. The eccentricities from the unit cell model are generally comparable to those from the 3D FEA model. A more exact comparison is difficult based on the available data; however, it is clear that the actual range of eccentricities from the 3D FEA model was adequately addressed by the unit cell model.
6. Based on items 4) and 5) which demonstrate the acceptability of the use of the unit cell model for benchmarking the 3-D FEA model, the method for calculating the reduction in contact pressure defined by the unit cell model, when adjusted for temperature effects, shows that SLB contact pressure is increased relative to normal operating conditions for the Model D5 steam generators.
7. It has also been shown when comparing contact pressures for NOP conditions for the unit cell to contact pressures for SLB for the unit cell for the Model F SG (higher temperature SLB conditions), that contact pressure increases during a postulated SLB.
8. Given that the two structural models provide similar eccentricities, the unit cell model shows that for these eccentricities, positive contact pressure exists between the tubes and the tubesheet for the entire range of displacements considered.

Based on the above, it is concluded that the NOP contact pressures that define  $H^*$  in the Model F and Model D5 SG are conservative and that a more realistic model of contact pressure reduction as a function of tube bore deformation (including both dilation and eccentricity) would predict positive contact pressure around the entire circumference of the tube and an increase in tube to tubesheet contact pressure at SLB conditions compared to NOP conditions.

The conclusions reached in the response to RAI#4 apply equally for the Model 44F and Model 51F SGs.

**References:**

1. L-2009-151, "Turkey Point Units 3 and 4, Docket Nos. 50-250 and 50-251, License Amendment Request No. 197 for H\*: Alternate Repair Criteria for Steam Generator Tubesheet Expansion Region," FPL, July 23, 2009.
2. 09-455, "Virginia Electric and Power Company (Dominion), Surry Power Station Units 1 and 2, Proposed License Amendment Request, Permanent Alternate Repair Criteria for Steam Generator Tube Repair for Units 1 and 2," Virginia Electric and Power Company, July 28, 2009.
3. E-mail from Jason Paige (NRC) to Bob Tomonto (FPL), "RAI Questions RE Turkey Point's H\* LAR," August 17, 2009.
4. E-mail from Karen Cotton (NRC) to Gary D. Miller (Generation -6), "Surry Clarifications Regarding H\* PARC," August 14, 2009.
5. WCAP-17091-P, "H\*: Alternate Repair Criteria for the Tubesheet Expansion Region in Steam Generators with Hydraulically Expanded Tubes (Model 44F)," Westinghouse Electric LLC, June 2009.
6. WCAP-17072-P, "H\*: Alternate Repair Criteria for the Tubesheet Expansion Region in Steam Generators with Hydraulically Expanded Tubes (Model 51F)," Westinghouse Electric LLC, June 2009.
7. Vogtle Electric Generating Plant, Units 1 and 2, Request for Additional Information Regarding Steam Generator Program (TAC Nos. ME1339 and ME1340)," United States Nuclear Regulatory Commission, July 10, 2009.
8. Vogtle Electric Generating Plant, Units 1 and 2, Request for Additional Information Regarding Steam Generator Program (TAC Nos. ME1339 and ME1340), United States Nuclear Regulatory Commission, August 5, 2009
9. LTR-SGMP-09-100, "Response to NRC Request for Additional Information on H\*; Model F and Model D5 Steam Generators," August 2009.
10. LTR-NRC-09-26, "LTR-SGMP-09-66 P-Attachment, "White Paper: Low Temperature Steam Line Break Contact Pressure and Local Tube Bore Deformation Analysis for H\* (Proprietary)," Westinghouse Electric Company LLC, May 13, 2009.
11. LTR-SGMP-09-109, "Response to NRC Request for Additional Information on H\*; RAI#4; Model F and Model D5 Steam Generators," Westinghouse Electric Company LLC, August 25, 2009.